**PONTIFÍCIA UNIVERSIDADE CATÓLICA**
DO RIO DE JANEIRO

**Fernando Vasconcelos da Senhora**

# Topology Optimization with Stress Constraints: an Aggregation-Free Approach

## DISSERTAÇÃO DE MESTRADO

Dissertation presented to the Programa de Pós-Graduação em Engenharia Mecânica of the Departamento de Engenharia Mecânica, PUC–Rio as partial fulfillment of the requirements for the degree of Mestre em Engenharia Mecânica.

Advisor     : Prof. Ivan Fábio Mota de Menezes
Co–Advisor:      Prof.  Glaucio H. Paulino

Rio de Janeiro
March 2017

**Fernando Vasconcelos da Senhora**

## Topology Optimization with Stress Constraints: an Aggregation-Free Approach

Dissertation presented to the Programa de Pós-Graduação em Engenharia Mecânica of the Departamento de Engenharia Mecânica do Centro Técnico Científico da PUC–Rio as partial fulfillment of the requirements for the degree of Mestre em Engenharia Mecânica. Approved by the undersigned Examination Committee.

**Prof. Ivan Fábio Mota de Menezes**
Advisor
Departamento de Engenharia Mecânica - PUC-Rio

**Prof. Glaucio H. Paulino**
Co–Advisor
Georgia Institute of Technology

**Prof. Emílio Carlos Nelli Silva**
Escola Politécnica da USP

**Prof. Antonio André Novotny**
Pesquisador no Laboratório Nacional de Computação Científica

**Prof. Anderson Pereira**
Departamento de Engenharia Mecânica - PUC-Rio

**Prof. Márcio da Silveira Carvalho**
Vice Dean of Graduate Studies
Centro Técnico Científico – PUC-Rio

Rio de Janeiro, March 23th, 2017

**Fernando Vasconcelos da Senhora**

The author graduated in Mechanical Engineering, with a minor in Mathematics, from Pontifícia Universidade Católica do Rio de Janeiro - PUC-Rio in 2014.

To my great-grandmother Sarita.

# Acknowledgments

Render unto Caesar the things that are Caesar's, and so here I try to redeem part of the debt that I have with everyone that helped me to fulfill this work. I know that this small acknowledgment doesn't even begin to compensate all of you, but if words have any value I hope you find a little comfort on these.

Goes without saying that this work would not be possible if it wasn't for prof. Ivan Fábio Mota de Menezes for whom I have nothing but a profound admiration.

I also would like to thank prof. Glaucio Paulino whose guidance is responsible for the quality of this dissertation. While on this matter I would like to thank Georgia Institute of Technology for receiving me as a guest researcher during the development of this dissertation.

Prof. Anderson Pereira also had a crucial role on this work. The implementation wouldn't be nearly as efficient if it wasn't for his help.

I am deeply grateful to PUC-Rio for giving me the opportunity to learn from remarkable professors, in special prof. Vera Lúcia Baltar, prof. Angela O. Nieckele, prof. Márcio Carvalho and prof. Carlos Tomei, from whom I acquired invaluable knowledge, I just hope to be worthy and do justice to your legacy.

I could not leave out from this acknowledgment the TECGRAF Institute where I learned everything I know about programming and for giving me the environment and the resources necessary to conclude this work.

I also would like to thank CNPq, and FAPERJ for the financial support, specially in this time of economic crisis and political unrest.

Last, but of course not least, I would like to thank my family whose affectioned deeds lead me to this point. My friends for making my days brighter and life more interesting. My colleagues Guilherme Barros and Hugo Bastos for the companionship and for always having time for a açaí break.

# Abstract

Senhora, Fernando Vasconcelos ; Menezes, Ivan Fábio Mota (Advisor); Paulino, Glaucio H. (Co-Advisor). **Topology Optimization with Stress Constraints: an Aggregation-Free Approach** . Rio de Janeiro, 2017. 104p. Dissertação de Mestrado — Departamento de Engenharia Mecânica, Pontifícia Universidade Católica do Rio de Janeiro.

Structural design methodologies were strongly influenced by the advent of computing. The advances in numerical analyses, such as the finite element method, and Computer Aided Design software have literally helped shape the engineering world as it is today. Structural optimization methods such as topology optimization aim to take the next step by letting the computer guide the design, in order to achieve new and more efficient designs. This approach has the potential to change the future of various industries, including aircraft, automobile, construction, etc. The introduction of stress constraints on traditional topology optimization allows for safer and more reliable solutions that will more closely resemble the final structure. The successful solution of this problem poses several conceptual and numerical difficulties. Thus this dissertation details the main issues of this problem and reviews the current techniques discussed in the literature including some critiques of their performance. The main contribution of this work is a novel technique based on the Augmented Lagrangian method that can efficiently handle a large number of constraints. In contrast to existing methods which are both problem- and mesh-dependent, the presented approach contains only a few parameters which need to be adjusted for each new case. In order to verify the technique's capabilities, a user friendly MATLAB code was developed that is both effective and robust. Several representative examples, including large-scale problems, are presented. Finally, the solutions obtained here, including some unexpected complications, are thoroughly discussed and suggestions for future work are also addressed.

# Keywords

Topology Optimization; Stress Constraint; Augmented Lagrangian; Singular Optima.

# Resumo

Senhora, Fernando Vasconcelos ; Menezes, Ivan Fábio Mota; Paulino, Glaucio H.. **Otimização Topológica com Restrições de Tensão: Uma Abordagem Livre de Agregação** . Rio de Janeiro, 2017. 104p. Dissertação de Mestrado — Departamento de Engenharia Mecânica, Pontifícia Universidade Católica do Rio de Janeiro.

As metodologias de projeto estrutural foram fortemente influenciadas pelo advento da computação. Os avanços nas áreas de análise numérica, como o método dos elementos finitos, e os softwares de Desenho Assistido por Computador, literalmente ajudaram a moldar o mundo como ele é hoje. Implementações computacionais das técnicas de otimização estrutural, como a otimização topológica, permitem a determinação das estruturas base, gerando uma grande quantidade de projetos novos, mais eficientes, com o potencial de mudar drasticamente o futuro das aeronaves, automóveis, edifícios, etc. Introduzir restrições de tensão na otimização topológica tradicional permite a obtenção de soluções mais seguras e confiáveis que se assemelhem mais à estrutura final. Contudo, isto não é uma tarefa trivial, apresentando várias dificuldades conceituais e numéricas. Nesta dissertação, as principais questões deste problema são discutidas e as técnicas presentes hoje na literatura são revisadas e criticadas quanto aos seus desempenhos. A principal contribuição deste trabalho é uma nova técnica baseada no Método do Lagrangiano Aumentado que lida eficientemente com um grande número de restrições. Em contraste com os métodos existentes, que são dependentes do problema e da malha, a abordagem proposta apresenta poucos parâmetros que precisam ser ajustados a cada novo caso. Para avaliar suas potencialidades, desenvolveu-se um código em MATLAB, eficaz e robusto. Diversos exemplos representativos, incluindo problemas de larga escala, são apresentados. Finalmente, as soluções obtidas, incluindo algumas complicações inesperadas, são discutidas detalhadamente e sugestões para trabalhos futuros são propostas.

## Palavras–chave

Otimização Topológica; Restrição de Tensão; Lagrangiana Aumentada; Ótimo Singular.

# Contents

# List of figures

# List of tables

*Problems worthy of attack prove their worth*
*by fighting back.*

**Piet Hein**, *Grooks 1.*

# 1
# Introduction

The majority of problems in engineering focus on the optimization of some aspect of a project. Be it minimizing the cost, or maximizing the performance, it all comes down to making the best use of the resources available. This point of view may not be the most practical way to find the solution but it can give some perspective on the importance of this kind of work.

Structural optimization is the field of study that seeks the optimal distribution of material based on some measure of performance.

For most of human history, structural design relied mostly on intuition and trial and error. It was only in the XIX century that the foundations for structure optimization were settled. Unfortunately, the difficulties in producing complex geometries limited the utility of such a field since the results are not always cost-effective for the industry. However, recent advances in manufacturing, in general, and in additive manufacturing, in particular, can overcome this barrier, clearing the way for new and more efficient designs.

This area of research has been particularly popular in the aerospace industry since reducing the weight of an aircraft can significantly decrease its fuel consumption. By simply changing material distribution, structural optimization allows for the design of lighter configurations without compromising its safety. This not only provides an economic advantage, but also follows the trend of environmental awareness, since it reduces the $CO_2$ emissions per passenger.

Topology optimization is a technique used by structural optimization and involves the determination of the number, location and shape of holes in the final design. The main objective of topology optimization is to find the best material distribution for a physical system. In other words, it is the technique of removing material while minimizing the detriment to a structure's performance. Quoting the engineer and architect Robert Le Ricolais:

> *"The art of structure is where to put the holes."*
> *Robert Le Ricolais, (1894 – 1977)*

## 1.1
## Motivation and Objective

The most important aspects of structure design are safety and reliability. There are a lot of ways a structure can fail: instability, corrosion, fatigue, temperature, etc. The main focus in mechanical sciences is the catastrophic failure that happens when the structure is not strong enough to support the load which it is subjected to. Quite a few failure criteria were developed throughout the years in order to predict when this might occur, and the majority of them based on stress and stress invariants.

The von Mises yield criterion states that plastic deformation begins when the second deviatoric stress invariant is greater than a certain material limit. Eventually, this can cause the structure to fracture or deform beyond the acceptable range. Therefore, it is natural to want to incorporate this safety requirement into the design process.

Computer aided design using topology optimization has a typical workflow displayed in Fig. 1.1. First, the structural domain is defined as well as the boundary conditions. This is the entry information for the topology optimization. The optimized solution then needs to be interpreted, generally an iso-surface is extracted over a cutoff density. This can be followed by a shape optimization to reduce eventual anomalies and high stresses. Finally, the most important part is the engineer's input and analysis that will lead to an actual feasible result.
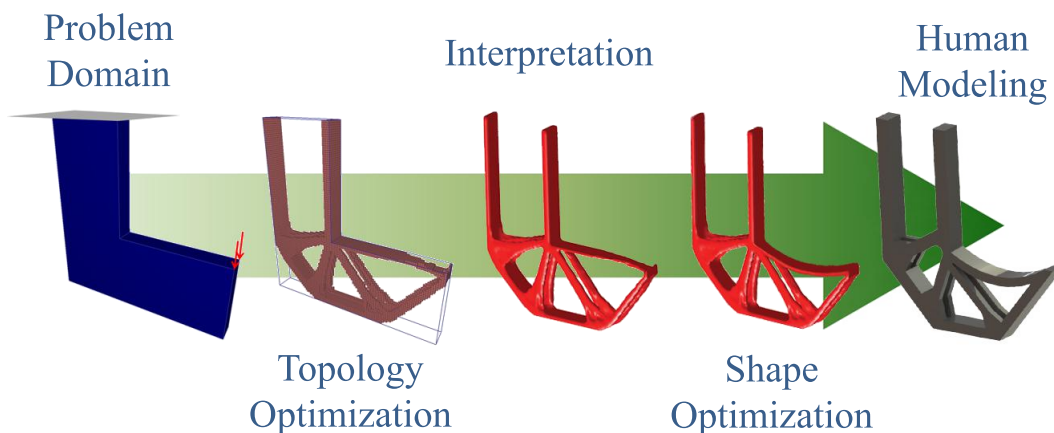


Figure 1.1: Typical topology optimization based computer aided design workflow.

Traditional topology optimization that focuses on minimizing the compliance can lead to solutions with stress concentrations that will fail under regular conditions of load. Consequently, the structure needs to be adapted,

which might demand far more work. The final design will be very different from the initial optimized concept and the outcome can be suboptimal.

The objective of this research is to incorporate stress constraints in the optimization process to ensure that the solutions will be close to a feasible structure, while also minimizing the adjustments that are needed to achieve a viable final design.

## 1.2
## Literature Review

Topology optimization with stress constraints is a challenging problem with several numerical complications. Among the many difficulties two stand out as the most troublesome and are the subject of most papers in the field: the local property of the stress and the singular optima.

The locality implies that a large number of stress evaluation points is necessary in order to ensure the integrity of the structure. This induces an equally large number of constraints, which demands a high computational cost, often making the problem impracticable (Duysinx & Bendsøe, 1998).

In order to treat these issues, some authors have resorted to a global measure of stress that is handled as the only constraint of the problem Yang & Chen (1996). Theoretically, this should be equivalent to constraining the maximum stress of the structure. Nonetheless the maximum function is not differentiable, and so it cannot satisfactorily be used with gradient-based optimization algorithms. A smooth approximation is then performed with the hope that it will mimic the maximum with enough precision to achieve the correct result. These are called aggregation techniques. Duysinx & Sigmund (1998), Holmberg *et al.* (2013b) and Kiyono *et al.* (2016) use the p-norm function, Yang & Chen (1996) uses the Kreisselmeier-Steinhauser function and obtain similar results. Le *et al.* (2009) proposes a correction for the p-norm that increases its consistency, but has a detrimental effect on the convergence of the optimization. In addition, aggregating the stress masks its local property which leads to suboptimal results. Le *et al.* (2009) and París *et al.* (2010) try to mitigate this problem by using regional clusters over which the aggregation is performed. However, this raises the question of how many clusters to use and how to define the distinct regions, which are not only problem-dependent but also mesh-dependent.

In contrast to aggregation, the Augmented Lagrangian method has also been adopted to deal with the large number of constraints. In this approach, the constraints are replaced by a penalization to the objective function that is adapted throughout the optimization process to achieve a feasible final

solution. Despite allowing a better interpretation of the constraints' locality, it requires progressive updates on the optimization parameters, which can be time-consuming. Pereira *et al.* (2004) and Emmendoerfer Jr. & Fancello (2014) use this technique and obtain fairly interesting results but does scarce comments on its efficiency.

Another less-explored option is the active-set method that only considers the constraints which are close to being violated. This raises a lot of concerns. It may not be viable for a large mesh, and by the end of the optimization, a large number of constraints might be active. The scalability of this approach is questionable. Guo *et al.* (2011), Duysinx & Bendsøe (1998) use this to solve small examples. Bruggi & Duysinx (2012) also uses an active-set method but introduces a compliance constraint and does a study on its effects. Later, Holmberg *et al.* (2013a) combined this idea with aggregation techniques and was able to improve its performance.

The other issue commonly denominated as singular optima was first reported by Sved & Ginos (1968) and later developed in Kirsch (1989, 1990). Rozvany (2001) does a very thorough historical review on the subject. Simply put, the optimum point is at a degenerated, disconnected region of the solution space and cannot be reached through traditional optimization methods. This happens because stress is a vanishing constraint, which basically means that the constraint is irrelevant when the optimization variable goes to zero. This kind of optimization problem is thoroughly discussed in Hoheisel (2009). A more detailed explanation can be seen in Section 3.5 of this work. In the author's opinion, this is the main challenge of this problem.

The most popular approach for dealing with this, has been to modify the constraints in order to include the degenerated optima of the solution space into the feasible region in a way that they can be easily achieved. Among the most popular modified constraints are the $\varepsilon$ relaxation (Cheng & Guo, 1997) and the q-p relaxation (Bruggi, 2008), from which several variations have been developed with similar concepts. However, one has to be careful when altering the constraints so as not to lose consistency with the physical reality. Otherwise, the solution found might not closely comply with the integrity requirements.

The damage approach proposed by Verbart *et al.* (2016a) naturally handles the locality and singular optima problems in an elegant manner. This formulation is based on the supposition that the material over the stress limit is damaged and thus, will contribute less to the overall stiffness. Further details are given in Subsection C. Although fairly efficient, it lacks consistency and the stress limit might not be strictly satisfied.

Most of the methods discussed so far have at least some numerical parameters that need to be predefined. These tend to be problem-dependent, or worse, mesh-dependent. Therefore, each new problem requires a step of empirical adjustment. The approaches used to handle the locality and singular optima greatly interfere with each other, increasing the difficulty of these issues even more. Verbart *et al.* (2016b) tries to unify aggregation and relaxation, and in doing so, reduces the number of numerical parameters needed.

In a different approach, Amstutz & Novotny (2010) obtains the topological derivative for plane stress linear elasticity which enable the authors to compose a shape functional that directs the optimization without using a conventional density base formulation.

All things considered, topology optimization with stress constraints is still an open problem. An efficient and robust solution that is appropriately scalable  is not found in literature .

## 1.3
## Outline

The remainder of this dissertation is organized as follows: Chapter 2 gives a brief overview on the topology optimization method. Chapter 3 is completely dedicated to stress constraints. It presents some of the issues of this specific problem as well as a few of the methods found in the literature to solve them. Chapter 4 is the main contribution of this work. It proposes a new, efficient method for solving the problem based on the Augmented Lagrangian formulation. In Chapter 5 several numerical examples demonstrating the robustness of this approach are shown. In addition, important considerations are made on the practical issues of stress constraints. Finally, Chapter 6 draws some conclusions and makes suggestion for future research.

# 2
# Formulation

This chapter presents a brief overview of the many aspects of the topology optimization method.

The first step in defining a specific problem is to determine the domain ($\Omega$) of the design. Figure 2.1 shows a representation of a general domain, where the area marked as $\omega$ defines the material region.
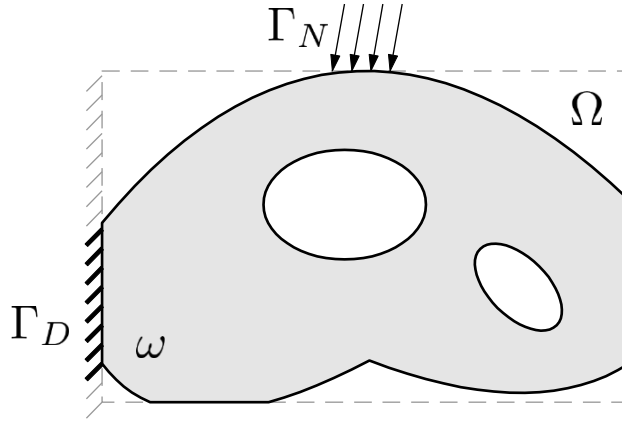
Figure 2.1: Design domain and boundary conditions. [Image from (Talischi *et al.*, 2012b)]

The general topology optimization problem is posed in Eq. (2.1), where $f(\omega)$ is the objective function, which is generally a measure of performance of the underlying structure. The functions $h_i(\omega)$ and $g_i(\omega)$ are the equality and inequality constraints, respectively, which can impose a physical, manufacturing, or other requirement that might be relevant. The design variable $\omega$ defines the material region inside the domain $\Omega$. The resulting material distribution will depend on the requirements.

$$
\begin{aligned}
&\underset{\omega \in \Omega}{\text{minimize}} && f(\omega) \\
&\text{subject to} && h_i(\omega) = 0 \\
& && g_i(\omega) \leqslant 0
\end{aligned}
\tag{2.1}
$$

The physics of the system is imposed as a set of equilibrium equations. Topology optimization has been used in a variety of problems, from fluid flow, to acoustic. Because this research focuses on structural integrity, the static linear elasticity model is applied.

Until this point the problem is seen as continuous and the structure's shape can vary freely inside the domain. Unfortunately, this formulation is not solvable with current methods and so it is necessary to discretize the domain for both the topology optimization and the equilibrium equations. While most work uses the same mesh to map the optimized structure and to find the physical response, this is not essential. In fact, Nguyen *et al.* (2010) explains the advantages of using separate discretizations for the analysis and the material distribution.

It is worth noting that any method of solving the equilibrium equations is valid. The finite element method (**FEM**) was used, as it is consolidated for the analysis of solid structures subjected to linear elasticity, which is the focus of this work.

## 2.1
## Quick Revision of Finite Elements

The Finite Elements Method (FEM) is a numerical approach for solving differential equations in an arbitrary given domain. In this case, the equations come from the static linear elastic modeling of solid materials. This model is derived from three main principles:

Newton's second law (Equilibrium of Forces):

$$\nabla \boldsymbol{\sigma} + \mathbf{f} = 0 \tag{2.2}$$

Strain-Displacement relation:

$$\varepsilon = \frac{1}{2}\left[ \nabla \mathbf{u} + (\nabla \mathbf{u})^T \right] \tag{2.3}$$

Constitutive equation (Hooke's Law):

$$\boldsymbol{\sigma} = \mathbf{C} : \boldsymbol{\varepsilon} \tag{2.4}$$

where $\boldsymbol{\sigma}$ is the Cauchy stress tensor, $\boldsymbol{\varepsilon}$ is the strain tensor, $\mathbf{f}$ are forces, $\mathbf{u}$ is the displacement vector and $\mathbf{C}$ is the constitutive stiffness tensor.

The principle of virtual displacement states that if a body is in equilibrium, for any small virtual perturbation of the displacements, the internal virtual work is equal to the external virtual work, i.e.:

$$\int_{\Omega} \overline{\boldsymbol{\varepsilon}} : \boldsymbol{\sigma} d\Omega - \int_{\Gamma} \overline{\mathbf{u}}^T \cdot \mathbf{f} d\Gamma - \mathbf{R} = 0 \tag{2.5}$$

here $\overline{\mathbf{u}}$ is the virtual displacement, and $\overline{\varepsilon}$ is the strain caused by it. $\mathbf{R}$ comprises the body forces that, in this particular case, are zero. Thus it will not appear in the subsequent derivations.

Now approximate $\mathbf{u}$ by a sum of piecewise linear functions. These functions are defined in elements with a local support:

Modified equation

$$\mathbf{u}(\mathbf{x}) \approx \sum_{i=1}^{M} U_i \mathbf{N}_i(\mathbf{x}) \tag{2.6}$$

$\mathbf{N}_i(\mathbf{x})$ is one at position $\mathbf{x}_i$ of the node $i$, and $\mathbf{N}_j(\mathbf{x})$ is zero at the node $\mathbf{x}_i$ for every $j \neq i$. Additionally, $\mathbf{N}_i(\mathbf{x})$ is null at every element that does not share the node $i$. Consequently, $\mathbf{u}(\mathbf{x}_i) = U_i$ for every node i and the problem is reduced to finding the $U_i$.

Using this approximation the gradient is:

Modified equation

$$\boldsymbol{\nabla}\mathbf{u}(\mathbf{x}) \approx \sum_{i=1}^{M} U_i \boldsymbol{\nabla}\mathbf{N}_i(\mathbf{x}) \tag{2.7}$$

Therefore, the strain can be written as:

$$\boldsymbol{\varepsilon} \approx \sum_{i=1}^{M} \frac{1}{2} \left[ U_i \boldsymbol{\nabla}\mathbf{N}_i(\mathbf{x}) + (U_i \boldsymbol{\nabla}\mathbf{N}_i(\mathbf{x}))^T \right] = \sum_{i=1}^{M} \frac{U_i}{2} \left[ \boldsymbol{\nabla}\mathbf{N}_i(\mathbf{x}) + (\boldsymbol{\nabla}\mathbf{N}_i(\mathbf{x}))^T \right]$$
$$\tag{2.8}$$

Renaming the term between brackets as:

$$\mathbf{B}_i(\mathbf{x}) = \frac{1}{2} \left[ \boldsymbol{\nabla}\mathbf{N}_i(\mathbf{x}) + (\boldsymbol{\nabla}\mathbf{N}_i(\mathbf{x}))^T \right] \tag{2.9}$$

This term $\mathbf{B}_i$ is called the displacement matrix. The strain can then be written in a simple expression:

$$\varepsilon \approx \sum_{i=1}^{M} U_i \mathbf{B}_i(\mathbf{x}) \tag{2.10}$$

Replacing Eq. (2.6) and (2.10) in Eq. (2.5):

$$\int_{\Omega} \sum_{i=1}^{M} \overline{U_i} \mathbf{B}_i(\mathbf{x}) : \mathbf{C} : \sum_{j=1}^{M} U_j \mathbf{B}_j(\mathbf{x}) d\Omega = \int_{\Gamma} \sum_{i=1}^{M} \overline{U_i} \mathbf{N}_i(\mathbf{x}) \cdot \mathbf{f} d\Gamma \tag{2.11}$$

Here again $\overline{U_i}$ are the virtual displacements. These can be chosen arbitrarily provided that they respect the prescribed displacements. If one chooses $l = 1..nNodes$, sets of $\left\{ \overline{U_i} \right\}_l$ as $\overline{U_i} = 1$ if $i = l$ and $\overline{U_i} = 0$ if $i \neq l$, one obtains a system of $l$ linear equations:

$$\int_{\Omega} \mathbf{B}_l(\mathbf{x}) : \mathbf{C} : \sum_{j=1}^{M} U_j \mathbf{B}_j(\mathbf{x}) d\Omega = \int_{\Gamma} \mathbf{N}_l(\mathbf{x}) \cdot \mathbf{f} d\Gamma \tag{2.12}$$

Expressing this system in matrix form, with $\mathbf{U} = (U_j)_{j=1}^{M}$, yields the familiar result:

$$\mathbf{KU} = \mathbf{F} \tag{2.13}$$

$$\mathbf{K}_{lj} = \int_{\Omega} \mathbf{B}_l(\mathbf{x}) : \mathbf{C} : \mathbf{B}_j(\mathbf{x}) d\Omega \tag{2.14}$$

$$\mathbf{F}_l = \int_{\Gamma} \mathbf{N}_l(\mathbf{x}) \cdot \mathbf{f} d\Gamma \tag{2.15}$$

There are considerably more details to the Finite Element Method than are displayed here, as this is not the main objective of this text. For further reading see Bathe (1996).

## 2.2
## Solid Isotropic Material with Penalization (SIMP)

The material distribution also needs a discrete representation. This is done by associating a design variable, denoted $\mathbf{z}$, to each element of the mesh, representing the structure. Its values can be one, which signifies

a material region, or zero: void. This combinatorial problem is especially troublesome, because it is non-linear, and the number of possible solutions rapidly exceeds the reasonable computational cost as the number of elements increases. Moreover, it is part of the set of NP-Hard problems and there isn't to this day an efficient method to solve it. In order to use gradient based optimizers, and, consequently, be able to greatly reduce the computational cost, a material interpolation with penalization formulation called SIMP (Bendsøe, 1989) is used. In this representation the design variables are allowed to vary continuously in the interval $[0, 1]$.

However, elements with variables between zero and one have a weak physical meaning in traditional design, since the intermediate values don't have a material counterpart. Furthermore, when dealing with composite material design, it is possible to develop a formulation in such a way that these rational values represent fractions in the composition. But this is not the focus of this work. In order to eliminate this "gray" regions on the final structure, a penalization function is used to correlate the designs variables with the element density and stiffness. With $\rho$ being the density and $E$ being the material interpolation stiffness function:

$$\rho(\mathbf{z}) = \mathbf{z} \tag{2.16}$$

$$E(\mathbf{z}) = \epsilon + \rho(\mathbf{z})^p (1 - \epsilon) \tag{2.17}$$

$\epsilon$ is the Erzat stiffness, a small value to avoid numerical instability while solving the equilibrium equations. $p$ is a penalization factor greater than one, and as the limit $p \to \infty$ is achieved the discrete problem is reattained.

The material interpolation stiffness function multiplies the constitutive matrix in the equilibrium equation, and so the penalization makes the intermediate values of $\mathbf{z}$ contribute less to the overall stiffness of the structure than the density. This leads to a solution close to a 0 or 1 design.

$$\mathbf{C}_E(E) = E(\mathbf{z})\mathbf{C} \tag{2.18}$$

$$\mathbf{K}_{lj} = \int_\Omega \mathbf{B}_l(\mathbf{x}) : E_j(\mathbf{z})\mathbf{C}\mathbf{B}_j(\mathbf{x})d\Omega \tag{2.19}$$

where the subscript $j$ in $E_j(\mathbf{z})$ links each displacement matrix $\mathbf{B}_j$ with its respective interpolated constitutive matrix.

Alternative formulations for material distribution have been developed using frontier tracking techniques such as level-set (van Dijk *et al.*, 2013) and phase-field (Takezawa *et al.*, 2010). Such methods have their own features and are not elaborated in this work.

## 2.3
## Regularization Techniques

The physical phenomenon of interest is continuous in the length scale of relevance, as the material region is modeled macroscopically as a continuous media. Unfortunately, it is not possible for most cases to obtain a continuous solution with the knowledge available today. For this reason the domain is discretized in a finite set of points in which a approximated solution is obtained. The basis for this technique is the hypothesis that the discrete domain can model its continuous counterpart well enough if a suitable distribution of points is chosen as such the solution in between them has a predictable behavior. This foments the intuition that a finer set of points would indulge a more accurate solution.

However, this is not always the case for some numerical methods with mesh size-dependent models. Mesh dependency is the effect that the choice of discretization has on the solution. This anomaly is undesirable since the modeling of a physical phenomenon cannot depend on the choice of spatial representation.

A conventional density based material representation in topology optimization suffer from this ailment as the minimum size of structural artifacts (holes, beams, etc) able to be represented is restricted by the size of the elements used in the mesh. As the mesh gets refined, the set of admissible solutions changes because thiner details are able to increase stiffness/weight ratio of the results. Eventually this leads to the representation of the material microstructure which is not the objective of traditional structural optimization.

Furthermore, it is worth noting that there are manufacturing limits on the size of the details that one is able to produce. This means that small holes and thin trusses may not be constructible.

Another matter of interest is the infamous checkerboard problem ( Fig. 2.2 ) that can appear in meshes where elements have the same hinge connections as they do in regular square elements in 2D, due to the overestimation of this pattern's stiffness. Obviously, these are not valid structures and should not be in the final solution.
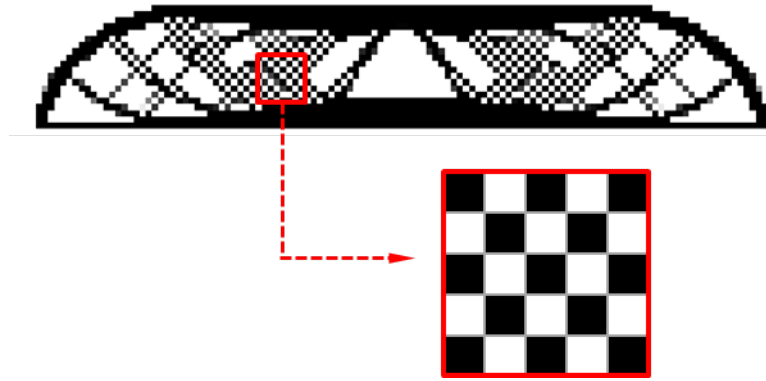
Figure 2.2: Checkerboard pattern arising in the solution of the topology optimization problem.

Several works in the literature deal with these issues, and three main techniques stand out: perimeter control, gradient restriction, and filtering.

### 2.3.1
### Perimeter Control

Perimeter control (Haber *et al.*, 1996) introduces constraints in the optimization problems that limit the total perimeter of the final structure. Increasing the number of holes also increases the total perimeter of the design, and so this results in a solution with fewer small-scale details. However, as this is a global constraint, it is still possible to have local problematic regions. Moreover, the numerical approximation of the perimeter can be influenced by the mesh. This is especially true for regular elements.

The determination of the limit for the total perimeter is not trivial and has to be done empiracally. This value heavily influences the solution which makes this technique very problematic for pratical use.

### 2.3.2
### Gradient Restriction

Gradient restriction (Petersson & Sigmund, 1998) introduces a constraint in the local density variation, producing a smooth distribution of material.This means that density of an element must be cointaned in a limited range from the density of its neighboor. An advantage of this is that it allows direct control of the minimum length scale, as one can choose the variation limit based on the size of the elements. Unfortunately, this introduces a large number of constraints which severely slow down the optimization process.

### 2.3.3
### Filtering Techniques

Filtering techniques (Bourdin, 2001) allows for a local control on the material distribution and ensures a smooth transition of the density field. The method consists of defining a map that correlates the design variables with the element densities. Choosing this mapping wisely, one can naturally eliminate distributions with abrupt changes in density from the solution space. Most traditional filters used consist of a convolution of the design variables with a smooth function $S(x, \overline{x})$, causing the density distribution to inherit this smoothness, i.e.:

$$\rho_i(\boldsymbol{z}) = \frac{\int_\Omega S(\boldsymbol{x}, \overline{\boldsymbol{x}}_i) z(\boldsymbol{x}) d\boldsymbol{x}}{\int_\Omega S(\boldsymbol{x}, \overline{\boldsymbol{x}}_i) d\boldsymbol{x}} \qquad (2.20)$$

where $\rho(z)$ is the density, $x$ are the domain's space coordinates, and $\overline{x}_i$ is the location of the $i - th$ design variable. The integral on the denominator normalizes the value of this functional.

This function is chosen to be local in the sense that is null in all domain except for a small continuous region. The most common choice for $S(x, \overline{x})$ is the linear hat kernel. This function has its maximum in $\overline{x}$, and it decreases linearly in region $r_{min} > |x - \overline{x}|$ until it reaches zero in $r_{min} = |x - \overline{x}|$ and is zero everywhere else. It has this name because its 2D plot resembles a conical party hat as displayed in Fig 2.3. Simplifying it:

$$S(\overline{x}_j, \overline{x}_i) = max\left(1 - \frac{|\overline{x}_i - \overline{x}_j|}{r}, 0\right) \qquad (2.21)$$
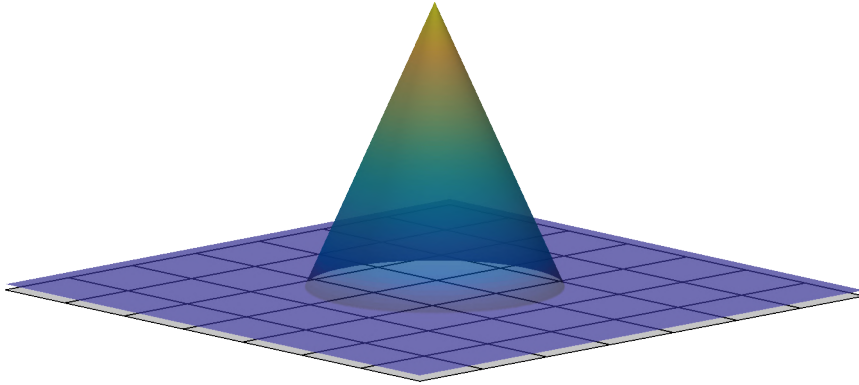


Figure 2.3: 2D representation of the linear hat kernel.

In the discrete form considering that the design variable is located at the centroid of the element this translates to:

$$\rho_i(z) = \frac{\sum_{j=1}^{nElem} max\left(1 - \frac{|\overline{x}_i - \overline{x}_j|}{r}, 0\right) z_j}{\sum_{l=1}^{nElem} max\left(1 - \frac{|\overline{x}_i - \overline{x}_l|}{r}, 0\right)} \tag{2.22}$$

This can be written in matrix form as:

$$\rho_i(z) = P_{ij}z_j \tag{2.23}$$

with:

$$P_{ij} = \frac{max\left(1 - \frac{|\overline{x}_i - \overline{x}_j|}{r}, 0\right)}{\sum_{l=1}^{nElem} max\left(1 - \frac{|\overline{x}_i - \overline{x}_l|}{r}, 0\right)} \tag{2.24}$$

Alternatively, it is possible to use a polynomial instead of a linear function, which translates to Eq. (2.25), with the power coefficient "$s$". This diminishes the influence of the more distant elements as can be seen in Fig. 2.4, facilitating more abrupt changes in densities, and thus, better defined material boundaries.

$$S(x, \overline{x}_i) = max\left[\left(1 - \frac{|\overline{x}_i - \overline{x}_j|}{r}\right)^s, 0\right] \tag{2.25}$$

## 2.4
## Polygonal Elements

The use of polygonal elements presents some advantages over the Q4 and other regular counterparts. First and more obvious, it can be used on complex domains and provide a good approximation without the need for advanced meshing techniques as are seen in Fig. 2.5. Moreover, it naturally avoids the well-known checkerboard and one-node connection problems.

A more subtle matter is that structured meshes tend to have preferential directions. So, the geometry of the final solution may be dependent on the geometry of the mesh. This type of mesh dependency can lead to suboptimal
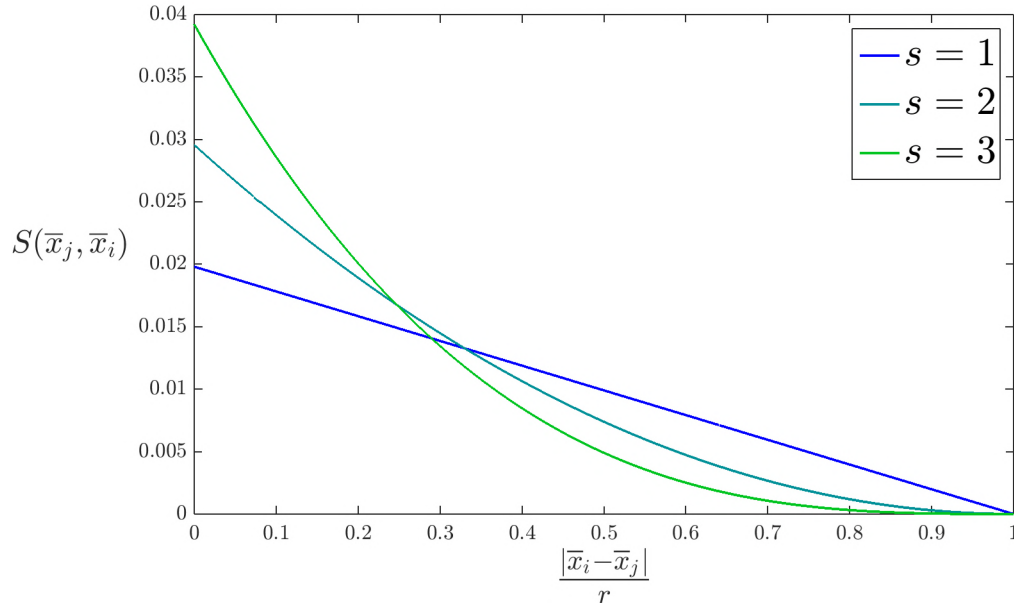
Figure 2.4: Regularization function for different values of $s$.
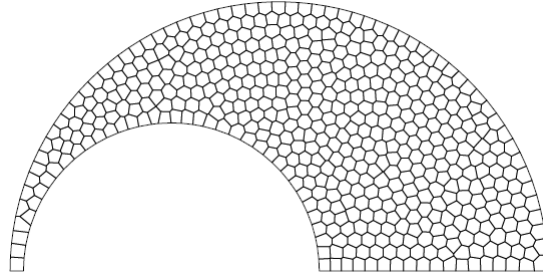


Figure 2.5: Polygonal mesh over curved geometry.

designs in topology optimization. Unstructured meshes tend to be a better representation for isotropic domains.

From the finite elements point of view this type of discretization leads to higher precision in the solution of linear elastic problems and are stable with respect to the Babuska-Brezzi condition (Pereira *et al.*, 2016).

On the other hand, good unstructured meshes are harder to generate. The ones used in this paper are created using Voronoi diagrams and Loyd iterations as described in Talischi *et al.* (2012a).

For a more detailed discussion on the use of polygonal elements for topology optimization, the reader must refer to Talischi *et al.* (2010, 2012b,a).

# 3
# Stress Constraints

Stress is a troublesome constraint with several numerical and conceptual difficulties, making this a  interesting problem. In this chapter the main complications of this constraint as well as the most relevant ways to deal with them (as found in the literature) are discussed.

## 3.1
## Optimization Problem

This thesis focus on a specific problem of topology optimization, the minimization of the structure's weight subjected to a stress constraint with a linear elastic model. Simply speaking, it seeks to find the lightest structure able to withstand the load applied.

The mathematical statement of the optimization problem is:

$$\underset{\mathbf{z}}{\text{minimize}} \quad M(\mathbf{z}) = \frac{\sum_{i}^{nElem} m_i(\mathbf{z})v_i}{\sum_{i}^{nElem} v_i}$$

$$\text{subject to} \quad g_j(\mathbf{z}) = \frac{\sigma_j^{VM}(\mathbf{z})}{\sigma_{lim}} - 1 \leqslant 0 \qquad j = 1 \cdots nStress$$

$$0 \leqslant z_i \leqslant 1 \qquad\qquad i = 1, ..., nElem$$

$$\text{with} \qquad \mathbf{K}(\mathbf{z})\mathbf{U} = \mathbf{F}$$

(3.1)

here $m_i(\mathbf{z})$ is the normalized weight per volume of the element "$i$" which depends on the optimization variable $\mathbf{z}$ and varies in the interval $[0, 1]$, $\sigma_j^{VM}$ is a measure of stress to be defined later, and $\sigma_{lim}$ is a limit value for this stress, $v_i$ is the volume (in the 2D case the area) of the element $i$ and dividing by the sum of $v_i$ normalizes the values of $M(\mathbf{z})$ to the interval $[0, 1]$. The nested formulation (Christensen & Klarbring, 2008) is used as the equilibrium equations are not set as constraints of the problem, but are implicitly imposed as the stress depends on the displacements.

The stress is evaluated in a finite set of points $j = 1 \cdots nStress$ that need not to be related to the finite element's or the topology optimization's mesh.

These points need, however, to be dense enough to guarantee the integrity of the final structure. Due to the local nature of stress, this leads to a high number of evaluation points. The *max* is taken over all the $j$ stresses.

The issues with the stress constraints are discussed thoroughly in this Chapter.

## 3.2
## Objective Function

Most of the papers impose a identity relation between the density $\rho(\mathbf{z})$ and the weight $m(\rho(\mathbf{z}))$. However, this is not a requirement and one can benefit from penalizing this relation in a similar manner as one does with the material interpolation stiffness function.

This can be done through a power weight relation with a factor $0 \leqslant \beta \leqslant 1$ (Fig. 3.1):

$$m(\rho) = \rho^{\beta} \tag{3.2}$$
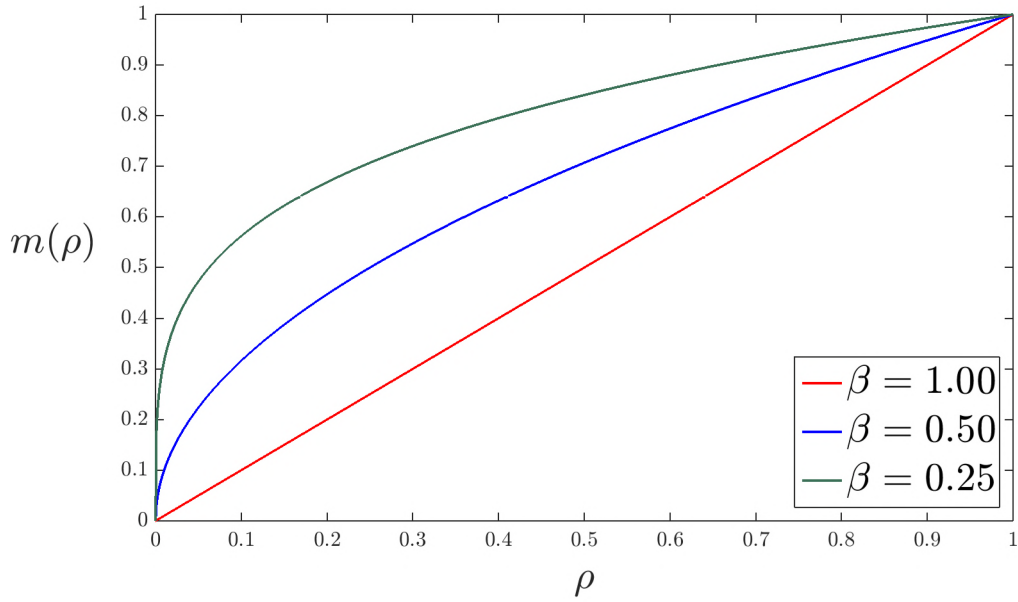


Figure 3.1: Power weight relations for different values of $\beta$.

Alternatively, the exponential weight relation with a factor $\beta \geqslant 0$ presents some similar properties (Fig. 3.2):

$$m(\rho) = 1 - e^{-\beta\rho} + \rho e^{-\beta} \tag{3.3}$$
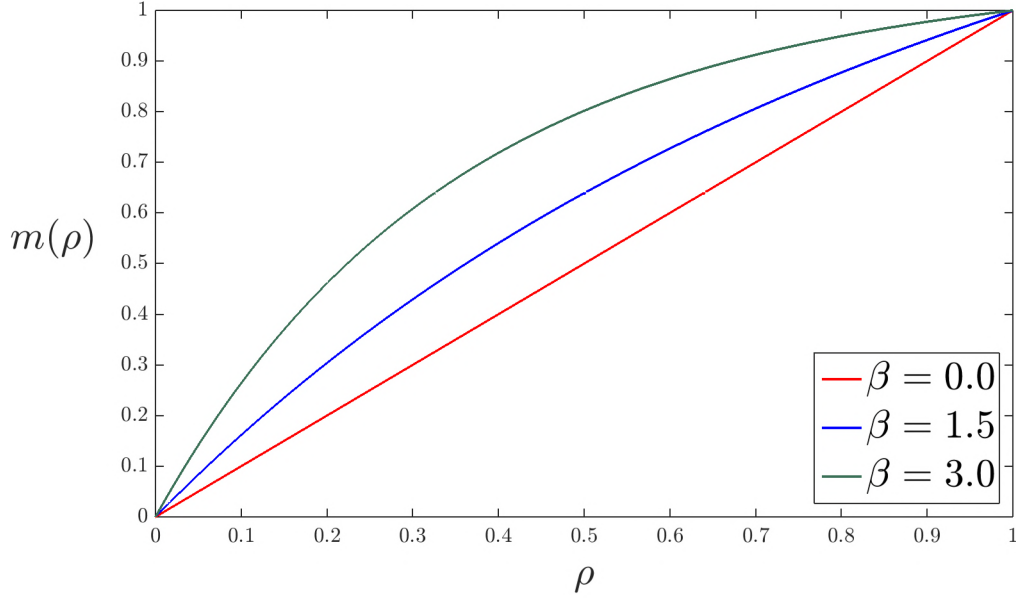
Figure 3.2: Exponential weight relations for different values of $\beta$.

Both of the proposed penalization guarantee the monotonic increasing property of the total weight function.

## 3.3
## Stress Definition

Traditional macroscopic stress can be obtained from the strain on the material following Eq. (2.4) repeated here:

$$\boldsymbol{\sigma} = \mathbf{C} : \boldsymbol{\varepsilon}$$

These quantities can be approximated through the use of the finite element method as described in Section 2.1:

$$\hat{\boldsymbol{\sigma}} = \mathbf{C}_E(E) : \sum_{j=1}^{M} \mathbf{B}_j U_j = E\mathbf{C} : \sum_{j=1}^{M} \mathbf{B}_j U_j \tag{3.4}$$

where $E$ is the material interpolation stiffness function defined in Section 2.2.

A careful analysis of Eq. (3.4) shows that the stiffness is proportional to $\rho^p$ while the nodal displacements $\mathbf{U}$ are proportional to $\rho^{-p}$. As a matter of fact, this definition of $\hat{\sigma}$ is invariant through the scaling of $\rho$.

In order to better grasp what is happening imagine that we analyze a single element from a larger mesh, fixing the density everywhere except for the

element of interest. To simplify the calculations the effect that the rest of mesh has on the subject is substitute by equivalent forces. This example is described in Fig. 3.3.
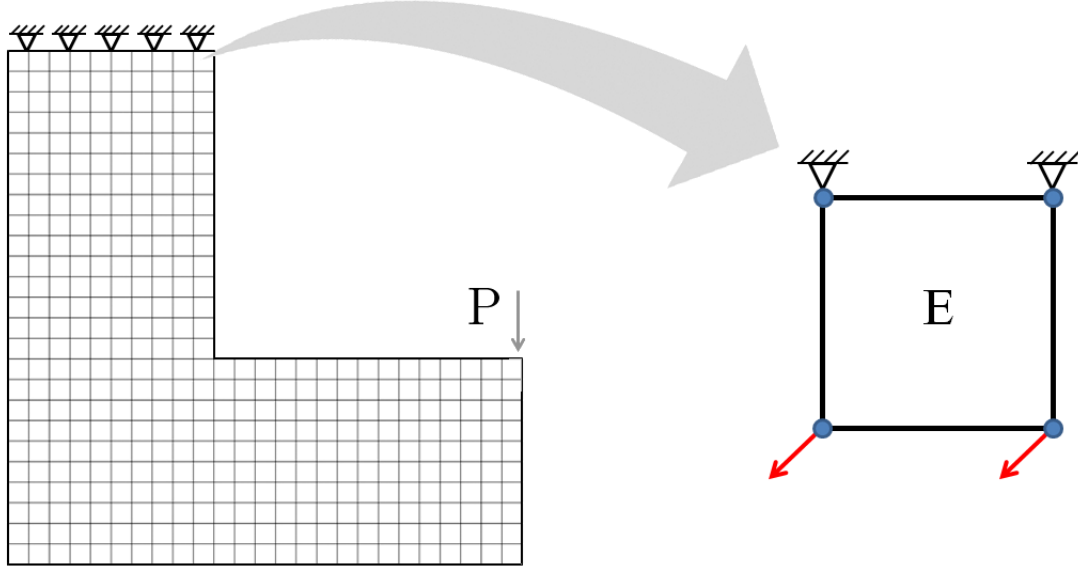


Figure 3.3: Single element Example.

The displacement at the free the nodes can be computed as:

$$\mathbf{k}(E)\mathbf{U} = E\mathbf{k}_0\mathbf{U} = \mathbf{f} \tag{3.5}$$

where $k(E)$ is the element stiffness matrix of the free degrees of freedom that is a function of the elements density through the material interpolation function $E$, $k_0$ is the same matrix for $E = 1$, $\mathbf{f}$ is the applied force vector. The displacement is then:

$$\mathbf{U} = \frac{1}{E}\mathbf{k}_0^{-1}\mathbf{f} \tag{3.6}$$

As the prescribed degrees of freedom are zero, it is possible to make the variable $E$ explicit:

$$\mathbf{U} = \frac{1}{E}\mathbf{U}_0 \tag{3.7}$$

$\mathbf{U}_0 = \mathbf{k}_0^{-1}\mathbf{f}$ are the displacements in the case of $E = 1$. Substituting $\mathbf{U}$ in the expression for $\hat{\sigma}$:

$$\hat{\boldsymbol{\sigma}} = E\mathbf{C} : \sum_{j=1}^{M} \mathbf{B}_j U_j = E\mathbf{C} : \sum_{j=1}^{M} \mathbf{B}_j \frac{(U_0)_j}{E} = \mathbf{C} : \sum_{j=1}^{M} \mathbf{B}_j (U_0)_j \qquad (3.8)$$

In other words, the macroscopic stress in the element does not depend directly on the design variable of that element. Thus, it does not have an appropriate behavior for topology optimization.

For this reason it is common practice to use an altered version of the microscopic stress in a composite porous media proposed by Duysinx & Bendsøe (1998). To satisfy this, the stress must be inversely proportional to the density and be finite as it approaches zero. One of simplest formulations for this is:

$$\hat{\boldsymbol{\sigma}} = \frac{E}{\rho^q}\mathbf{C} : \sum_{j=1}^{M} \mathbf{B}_j U_j = \frac{\epsilon + \rho^p(1-\epsilon)}{\rho^q}\mathbf{C} : \sum_{j=1}^{M} \mathbf{B}_j U_j \approx \rho^{(p-q)}\mathbf{C} : \sum_{j=1}^{M} \mathbf{B}_j U_j \quad (3.9)$$

The only plausible choice of $q$ is then $q = p$. In this formulation the stress does not depend directly on $E$ and it is simply:

$$\boldsymbol{\sigma} = \mathbf{C} : \sum_{j=1}^{M} \mathbf{B}_j U_j \qquad (3.10)$$

### 3.3.1
### Von Mises Stress

The Von Mises stress is defined as the square root of three times the second invariant of deviator stress tensor. It is extensively used as a failure criterion for materials with similar behavior in tension and compression. It is therefore used in this dissertation for the stress constraints. The deviator stress tensor can be defined as:

$$\overline{\boldsymbol{\sigma}} = \boldsymbol{\sigma} - \frac{tr(\boldsymbol{\sigma})}{3}\boldsymbol{\delta} \qquad (3.11)$$

in which $\boldsymbol{\delta}$ is the Kronecker delta and $tr()$ is the trace of the tensor. The Von Mises stress then can be calculated through Eq. (3.12).

$$\sigma^{VM} = \sqrt{\frac{3}{2}tr(\overline{\boldsymbol{\sigma}}^2)} = \sqrt{\frac{3}{2}\left[tr(\boldsymbol{\sigma}^2) - \frac{1}{3}tr(\boldsymbol{\sigma})^2\right]} \qquad (3.12)$$

## 3.4
## Stress Locality

As stated before, the number of stress evaluation points must be dense in the domain in order to guarantee structural integrity. It is desirable that the maximum stress on all of these points stays below a certain value. This translates to a large number of constraint which greatly increases the computational cost not only for the optimization algorithm but also for the computation of the sensitivities necessary for gradient based methods.

As a response to this, two main techniques with vastly different theoretical consequences have been taken.One of them is to use a global measure that in some way represents all the constraints. This leads to the several aggregation techniques in the contemporary literature. The other possibility is to use an approach, such as penalization methods, to reduce the cost of applying a large number of constraints but to consider each constraint independently.

### 3.4.1
### Aggregation Techniques

It is easy to see that the optimization problem (3.1) and the one in (3.13) are equivalent in the sense that they have the same solution and the same feasible space. However, as one uses a gradient based algorithm for the optimization, it is extremely prejudicial to have the maximum function in the formulation, as it is not differentiable, in the usual sense, in possibly infinite many points.

$$\begin{aligned}
\underset{\mathbf{z}}{\text{minimize}} \quad & M(\mathbf{z}) = \frac{\sum_i^{nElem} m_i(\mathbf{z})v_i}{\sum_i^{nElem} v_i} \\[2em]
\text{subject to} \quad & G(\mathbf{z}) = \frac{max(\sigma_j^{VM}(\mathbf{z}))}{\sigma_{lim}} - 1 \leqslant 0 \qquad j = 1\cdots nStress \\[1em]
& 0 \leqslant z_i \leqslant 1 \qquad\qquad\qquad\quad i = 1,...,nElem \\[1em]
\text{with} \quad & \mathbf{K}(\mathbf{z})\mathbf{U} = \mathbf{F}
\end{aligned} \qquad (3.13)$$

Aggregation Techniques have been very popular in recent years due to their simplicity and the idea is to approximate the maximum by a smooth

function . This greatly reduces the computational cost both in the optimization algorithm and in the computation of the sensitivities with the adjoint method.

### P-norm, P-mean and KS-function

The most popular aggregation functions are defined below:

$$\text{P-norm}: G(\mathbf{x}, p) = \left[ \sum_{i=1}^{n} (x_i)^p \right]^{(1/p)} \tag{3.14}$$

Used in (Holmberg *et al.*, 2013b; Kiyono *et al.*, 2016).

$$\text{P-mean}: G(\mathbf{x}, p) = \left[ \sum_{i=1}^{n} \frac{(x_i)^p}{n} \right]^{(1/p)} \tag{3.15}$$

Used in (Duysinx & Sigmund, 1998; Le *et al.*, 2009).

$$\text{KS-function}: G(\mathbf{x}, p) = \frac{1}{p} ln \left[ \sum_{i=1}^{n} e^{x_i p} \right] \tag{3.16}$$

Used in (Yang & Chen, 1996).

In all three equations $p$ is an adjustable parameter, with the property that $\lim_{p \to \infty} G(\mathbf{x}, p) = max(\mathbf{x})$. Generally, a higher value of $p$ translates to a better approximation of the maximum function, however, its increase can be detrimental due to numerical instability. This means that the choice of this parameter has to be a mid-term, high enough to achieve a decent accuracy but not so much as to disrupt the convergence of the optimization algorithm. Typical values are set between 2 and 32.

The behavior of all of this functions is similar. However the P-norm and the KS-function tend to overestimate the maximum, while the P-mean is a underestimation. The KS-function on the contrary of the other two can be used with negative values.

The use of one global constraint to represent all stresses in the domain can be troublesome, especially when the number of evaluations are large and there are zones of much higher stress, such as geometrical singularities. The quality of the approximation depends not only on the value of $p$ but also on

the number of variables $n$ (see Eq. (3.14),(3.15), (3.16)) and the variance of their values. As $n$ increases, the quality of approximation rapidly degenerates, which is of great concern, since generally, for topology optimization, one has to use fine meshes and a high number of stress evaluation points. Moreover, it is desirable that the method be stable over mesh refinement. This is hard to achieve with aggregation, because this inherently increases the value of $n$ hence the solution deteriorates as the mesh is refined. To complicate matters further, the number of elements necessary for 3D cases is extremely high. This coarse approximation can lead to suboptimal design and large regions of unnecessary material with low stress.

**Regional Clustering**

Regional clustering is an idea very commonly used with aggregation techniques. It consists of dividing the original domain in regions and applying aggregation individually over each region. This can better capture the local property of the stress and enhances the quality of approximation, as it reduces the number of variables in each aggregation. These clusters are then introduced in the optimization problem as separate constraints, i.e.:

$$
\begin{aligned}
\underset{\mathbf{z}}{\text{minimize}} \quad & M(\mathbf{z}) = \sum_{i}^{nElem} m_i(\mathbf{z})v_i \\
\text{subject to} \quad & G\left(\Omega_1\right) - \sigma_{lim} \leqslant 0 \\
& G\left(\Omega_2\right) - \sigma_{lim} \leqslant 0 \\
& \quad \vdots \\
& G\left(\Omega_m\right) - \sigma_{lim} \leqslant 0 \\
& 0 \leqslant \mathbf{z} \leqslant 1 \\
\text{with} \quad & \mathbf{KU} = \mathbf{F}
\end{aligned}
\tag{3.17}
$$

where $\Omega_m$ are the clusters that group the stress evaluations and $m$ is their number.

This raises the question of how to divide the domains in such regions. A number of answers have been given in literature but none are conclusive. Dividing solely on spatial proximity is ineffective. This will generate preferential directions for the structural artifacts, because of the spatial discontinuity of the imposed constraints.

The most conventional way of defining a cluster is adaptively based on stress. This means that the members of a cluster change based on their value.

There are two main rules to do this, suppose $m$ is the number of clusters and $n$ the number of stress evaluations:

- Even Distribution (Le *et al.*, 2009): The stresses are organized in decreasing order and the $m$ highest values belong to a different cluster, doing the same for the $m$ second highest and so on.

- Order Distribution (Holmberg *et al.*, 2013b): The stresses are organized in decreasing order and the first $n/m$ evaluations go to the first cluster, and the $n/m$ evaluations that follow go to the second cluster and so on.

To clarify these methods, imagine an example with 9 stress evaluations:

$$\sigma_1 \geqslant \sigma_2 \geqslant \sigma_3 \geqslant \sigma_4 \geqslant \sigma_5 \geqslant \sigma_6 \geqslant \sigma_7 \geqslant \sigma_8 \geqslant \sigma_9 \tag{3.18}$$

Suppose that we want to divide them in three clusters $\Omega_m$, the result would be:

Even Distribution:  $\Omega_1 = \{\sigma_1, \sigma_4, \sigma_7\}, \quad \Omega_2 = \{\sigma_2, \sigma_5, \sigma_8\}, \quad \Omega_3 = \{\sigma_3, \sigma_6, \sigma_9\}$

Order Distribution:  $\Omega_1 = \{\sigma_1, \sigma_2, \sigma_3\}, \quad \Omega_2 = \{\sigma_4, \sigma_5, \sigma_6\}, \quad \Omega_3 = \{\sigma_7, \sigma_8, \sigma_9\}$

Each cluster generated by an even distribution has a similar value of $g(\mathbf{x})$ while the order distribution generates clusters with very different values of $g(\mathbf{x})$, however, the member of a single cluster are similar to the other members of that same cluster. The best approach depends on which function is chosen for the aggregation.

It is important to notice that the optimization problem changes each time the clusters are reorganized. This can lead to a slower convergence specifically with traditional algorithms. Thus, some authors perform the cluster composition once every 5, 10 or even 20 iterations. However, Holmberg *et al.* (2013b) affirms that the best performance is obtained if the reclustering is done at each iteration.

The efficiency and precision of clustering has been improved by Holmberg *et al.* (2013a), using an active-set type approach, which performs the clustering only over the points where the stress is above or close to the limit. This greatly reduces the number of variables over which the aggregation is done, ensuring a better approximation of the max function because it disregards points of low stress that are of little relevance to the problem. However, this increases the

discontinuity of the constraints and has to be done carefully so it doesn't slow down the optimization.

Another matter that merits our attention is the optimal number of clusters for a specific problem. Each additional cluster increases the computational cost because of the higher complexity of the optimization problem with the extra constraint. Hence, it is desirable to use the smallest number of clusters possible. Furthermore, Le *et al.* (2009) reports that an increase in the number of clusters does not necessarily lead to a better design due to numerical reasons. However the number of subdivisions is not only problem dependent but also mesh dependent and so far very little success was obtained in determining, a priori, their necessary number.

### 3.4.2
### Penalty Methods

The use of penalty methods can greatly reduce the expenditure associated with the large number of constraints while at the same time providing a more consistent model than the aggregation techniques.

This Section is just a brief introduction to these methods. For further knowledge the reader can refer to Nocedal & Wright (2006) and Bertsekas (1996).

Suppose that we have the following optimization problem:

$$
\begin{aligned}
\underset{x}{\text{minimize}} \quad & f(x) \\
\text{subject to} \quad & g_i(x) = 0 \qquad\qquad i = 1...n
\end{aligned}
\tag{3.19}
$$

The idea is to transform it into a equivalent unconstrained problem:

$$
\underset{x}{\text{minimize}} \quad J(x) = f(x) + \sum_{i=1}^{n} I_i(g_i(x))
\tag{3.20}
$$

where $I_i$ are penalization functions based on the constraints. The appropriate choice of $I_i$ ensures that the solutions of (3.20) are also solutions of (3.19). This transformation allows us to use unconstrained optimization algorithms to solve the problem. Ideally, the penalization functions would be such that:

$$
I_i(g_i(x)) = \begin{cases} 0, & \text{if} \quad g_i(x) = 0 \\ \infty, & \text{otherwise} \end{cases}
\tag{3.21}
$$

It is easy to see that this would guarantee the same solution for the original and the modified problem. Unfortunately, the discontinuity of this function renders it unsuitable for traditional gradient-based optimization. So, it is desirable to have a continuous function that behaves similarly to Eq. (3.21).

**Quadratic Penalization Method**

Historically, the first algorithm developed with this idea was the quadratic penalization method, in which the penalization function $I_i$ was defined as:

$$I_i(g_i(x)) = \frac{\mu}{2}(g_i(x))^2 \tag{3.22}$$

where $\mu$ is a numerical parameter that has to be adjusted for the constraint. A large value for $\mu$ ensures a better feasibility of the solution as it increases the cost of violating the constraint, but at the same time, increases the steepness of this function. And, again, this can make the convergence of gradient based algorithms troublesome. In order to mitigate this, the quadratic penalization method gradually increases the value of $\mu$ solving a sequence of $k$ subproblems, using the $k$ problems solution as a initial guess for the $k+1$. In the limit $k \to \infty$, $\mu^k \to \infty$ and the condition in Eq. (3.21) is obtained, i.e.:

$$\underset{x}{\text{minimize}} \quad J^k(x, \mu^k) = f(x) + \sum_{i=1}^{n} \frac{\mu^k}{2}(g_i(x))^2 \tag{3.23}$$

$$\mu^{k+1} = \beta\mu^k \qquad \beta > 1 \tag{3.24}$$

The choice of $\beta$, responsible for the update of $\mu$, can be very problem dependent. A high value of this parameter intuitively would lead to a faster convergence to a feasible solution, however a severe update could also mean a drastical change of the subproblem $k$ to $k+1$ compromising the optimization. A modest update on the other hand might demand a massive number of subproblems to achieve feasibility. In the end what dictates the measure of $\beta$ is not only the problem as well as the initial guess of each iteration.

Defining the Lagrangian of the original problem (3.19) with the appropriate Lagrange multipliers $\lambda_i^*$ as:

$$L(x) = f(x) + \sum_{i=1}^{n} \lambda_i^* g_i(x) \tag{3.25}$$

The KKT optimality conditions (assuming a well-behaved problem) states that the gradient of the Lagrangian at the optimum point $x^*$ with the appropriate Lagrange multipliers be equal to zero:

$$\boldsymbol{\nabla} L(x) = \boldsymbol{\nabla} f(x^*) + \sum_{i=1}^{n} \lambda_i^* \boldsymbol{\nabla} g_i(x^*) = \mathbf{0} \tag{3.26}$$

At the same time, at the optimum $x^k$ of the approximated problem (3.23):

$$\nabla J^k(x^k, \mu^k) = \nabla f(x^k) + \sum_{i=1}^{n} (\mu^k g_i(x^k)) \nabla g_i(x^k) = 0 \tag{3.27}$$

Supposing that $x^k \approx x^*$ as $k \to \infty$, it is possible to make the following approximations:

$$\nabla f(x^*) + \sum_{i=1}^{n} \lambda_i^* \nabla g_i(x^*) = \nabla f(x^k) + \sum_{i=1}^{n} (\mu^k g_i(x^k)) \nabla g_i(x^k) \tag{3.28}$$

$$\lambda_i^* \nabla g_i(x^*) \approx (\mu^k g_i(x^k)) \nabla g_i(x^k) \tag{3.29}$$

$$\lambda_i^* \approx (\mu^k g_i(x^k)) \qquad\qquad g_i(x^k) \propto \frac{\lambda_i^*}{\mu^k} \tag{3.30}$$

The last equation gives us a  insight. At the optimum point $x^*$, the constraints must be $g_i(x^*) = 0$. As they are proportional to $\dfrac{\lambda_i^*}{\mu^k}$ for every constraint which the Lagrange multiplier $\lambda_i^*$ is different from zero $\mu_k$ must tend to infinity. In practical terms there is always a numerical tolerance for the constraint and $\mu^k$ must be just large enough. However, because the increment on $\mu^k$ has to be done gradually, it can take a considerable time to achieve such value.

## Augmented Lagrangian

The Augmented Lagrangian is a penalization technique of constrained optimization. It is an efficient way to deal with a large number of constraints and it is based on the Lagrangian multipliers. Its formulation was an improvement on the original quadratic penalization method. It introduces the following penalization function:

$$I_i(g_i(x)) = \lambda_i g_i(x) + \frac{\mu}{2}(g_i(x))^2 \tag{3.31}$$

in which $\lambda_i$ is a numerical parameter determined iteratively, and $\mu$ is analogous to the quadratic penalization. Once again, a sequence of $k$ subproblems that converge to the original one, are solved and the solutions $x^k$ tend to the optimum point of the original problem.

At the optimum point $x^k$ similar to Eq. (3.27):

$$\nabla J^k(x^k, \mu^k, \lambda^k) = \nabla f(x^k) + \sum_{i=1}^{n} \left[\lambda_i^k + \mu^k g_i(x^k)\right] \nabla g_i(x^k) = 0 \tag{3.32}$$

Making the same suppositions as before that $x^k \approx x^*$ as $k \to \infty$ and comparing it with Eq. (3.26):

$$\nabla f(x^*) + \sum_{i=1}^{n} \lambda_i^* \nabla g_i(x^*) = \nabla f(x^k) + \sum_{i=1}^{n} \left[\lambda_i^k + \mu^k g_i(x^k)\right] \nabla g_i(x^k) \tag{3.33}$$

$$\lambda_i^* \nabla g_i(x^*) \approx \left[\lambda_i^k + \mu^k g_i(x^k)\right] \nabla g_i(x^k) \tag{3.34}$$

$$\lambda_i^* \approx \left[\lambda_i^k + \mu^k g_i(x^k)\right] \qquad\qquad g_i(x^k) \propto \frac{\lambda_i^* - \lambda_i^k}{\mu^k} \tag{3.35}$$

Equation (3.35) gives us a good estimative to update the value of $\lambda_i^{k+1} = max(\lambda_i^k + \mu^k g_i(x^k), 0)$, remembering that the Lagrangian multipliers are always positive. Also notice that the convergence of $g_i(x^k) \to 0$ is reached much more quickly with $\lambda_i^k \to \lambda_i^*$. The final scheme is then:

$$\underset{x}{\text{minimize}} \quad J^k(x, \mu^k) = f(x) + \sum_{i=1}^{n} \left[\lambda_i g_i(x) + \frac{\mu}{2}(g_i(x))^2\right] \tag{3.36}$$

$$\lambda_i^{k+1} = max(\lambda_i^k + \mu^k g_i(x^k), 0) \qquad \mu^{k+1} = \beta\mu^k \qquad \beta > 1 \qquad (3.37)$$

The descriptions above are just the main ideas of the Augmented Lagrangian method. Several variations exist in literature that present some advantage for specific problems, but all of them are based on the formulation presented here.

Furthermore the "$k$" subproblems are simple approximations and the advantages of solving them exactly are questionable, as it provides little extra precision on the real problem solution and increases the computational cost. It is thus common practice to have a small limit for the maximum number of iterations of the optimization of these subproblems.

### Slack Variables and Inequality Constraints

The careful reader will have noticed by now that the above formulation only works for equality constraints. However, there is a clever way to extend this method for inequality constraints with only a few modifications.

The formulation can be transformed to handle inequality constraints with the use of slack variables "$s$" in the optimization problem:

$$h_i(x, s_i) = g_i(x) + s_i = 0 \qquad\qquad 0 \leqslant s_i \qquad (3.38)$$

$g_i$ are the inequality constraints. The $s_i$ are now optimization variables of the modified problem:

$$\begin{aligned}
\underset{x,s_1,...,s_n}{\text{minimize}} \quad & f(x) \\
\text{subject to} \quad & h_i(x, s_i) = g_i(x) + s_i = 0 \qquad i = 1...n \\
& 0 \leqslant s_i \qquad\qquad\qquad\qquad i = 1...n
\end{aligned} \qquad (3.39)$$

The Augmented Lagrangian for the above problem is:

$$\underset{x,s_1,...,s_n}{\text{minimize}} \quad J^k(x, s_1, ..., s_n) = f(x) + \sum_{i=1}^{n}\left[\lambda_i(g_i(x) + s_i) + \frac{\mu}{2}(g_i(x) + s_i)^2\right]$$

$$\text{subject to} \quad 0 \leqslant s_i \qquad\qquad i = 1...n$$

$$(3.40)$$

The bound constraints are not removed from the problem, as they are easy to handle in most optimization algorithms. The minimization of

$J^k(x, s_1, ..., s_n, \mu^k, \boldsymbol{\lambda}^k)$ with respect to $s_1, ..., s_n$ can be done explicitly for each fixed $x$ by solving problem (3.41) for every $s_i$.

$$\underset{s_i}{\text{minimize}} \quad \left[ \lambda_i(g_i(x) + s_i) + \frac{\mu}{2}(g_i(x) + s_i)^2 \right] \tag{3.41}$$
$$\text{subject to} \quad 0 \leqslant s_i$$

Deriving the objective function and setting it to zero:

$$\frac{d}{ds_i} \left[ \lambda_i(g_i(x) + s_i) + \frac{\mu}{2}(g_i(x) + s_i)^2 \right] = \lambda_i^k + \mu^k(g_i(x) + s_i) = 0 \tag{3.42}$$

$$s_i = - \left( \frac{\lambda_i^k}{\mu^k} + g_i(x) \right) \tag{3.43}$$

However, because of the bound constraint, the actual solution to the optimization problem is:

$$s_i = max \left[ 0, - \left( \frac{\lambda_i^k}{\mu^k} + g_i(x) \right) \right] \tag{3.44}$$

From this, it is possible to explicitly obtain the value of $h(x)$:

$$h_i(x) = g_i(x) + max \left[ 0, - \left( \frac{\lambda_i^k}{\mu^k} + g_i(x) \right) \right] = max \left[ g_i(x), -\frac{\lambda_i^k}{\mu^k} \right] \tag{3.45}$$

From the equations above, we conclude that the slack variables $s_i$ need not to be numerically computed and that it is possible to use the Augmented Lagrangian Method with inequality constraints.

## 3.5
## Singular Optima

The singular optima was first observed by Sved & Ginos (1968) and later developed by Kirsch in Kirsch (1989, 1990). This kind of numerical issue arises as a consequence of the choice to use the microscopic stress as a base measure in the formulation, for which the value of stress in void regions is not null. This is not physically accurate since the stress needs a material media to propagate.

It is reasonable to say that the stress constraint does not have meaning when the density reaches zero, which makes it a vanishing constraint (Hoheisel, 2009) and degenerates the optimization problem. In practical terms, the global optima lies in a disconnected subspace of the solution domain that cannot be reached through traditional gradient-based optimization algorithms.

### 3.5.1
### Kirsch three bar truss

One classical example which illustrates this issue is the Kirsch three truss problem introduced by Kirsch (1990) and described in Fig.3.4. The optimization variables represent the cross section area of the bars and as the area of a bar decreases, its stress increases. If the area reaches zero, the stress becomes singular and has no physical meaning since a bar with zero area is inexistent. The mathematical statement of the problem is described in Eq. (3.46).



Parameters:

$L_i = L = 1$ for $i = 1, 2, 3$

$E_i = E = 1$ for $i = 1, 2, 3$

$\rho_1 = 4, \rho_2 = \rho_3 = 0.5$

$\sigma_{\lim} = 20$
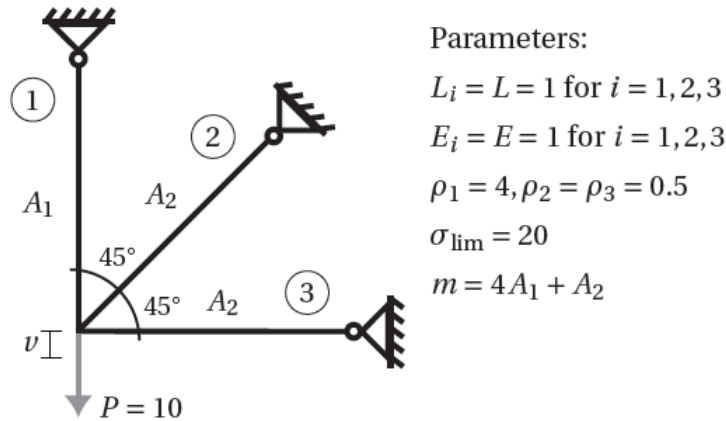
$m = 4A_1 + A_2$

Figure 3.4: Kirsch three bar truss problem. Image from Verbart *et al.* (2016a).

$$\begin{aligned}
\underset{\mathbf{z}}{\text{minimize}} \quad & M(\mathbf{z}) = 4A_1 + A_2 \\
\text{subject to} \quad & g_1(A_1, A_2) = \frac{\sigma_1}{20} - 1 \leqslant 0 \\
& g_2(A_1, A_2) = \frac{\sigma_2}{20} - 1 \leqslant 0 \\
& g_3(A_1, A_2) = \frac{\sigma_3}{20} - 1 \leqslant 0 \\
& 0 \leqslant A_1, A_2 \\
\text{with} \quad & \mathbf{K}(A_1, A_2)\sigma = \mathbf{F}
\end{aligned} \tag{3.46}$$

The solution space of the problem above is represented in Fig. 3.5. From this image one might think that the first constraint dominates the problem

and the traditional feasible region with its apparent global optimum is as it is represented in Fig. 3.6. However, the constraint $g_1$ has no meaning when $A_1 = 0$ and therefore it must vanish for a physically consistent formulation. This leads us to consider an extended version of the feasible region in which the $g_1$ constraint is irrelevant at the $A_2$ axis where $A_1$ is zero. This extended feasible region is represented in Fig. 3.7 along with the actual global optimum.
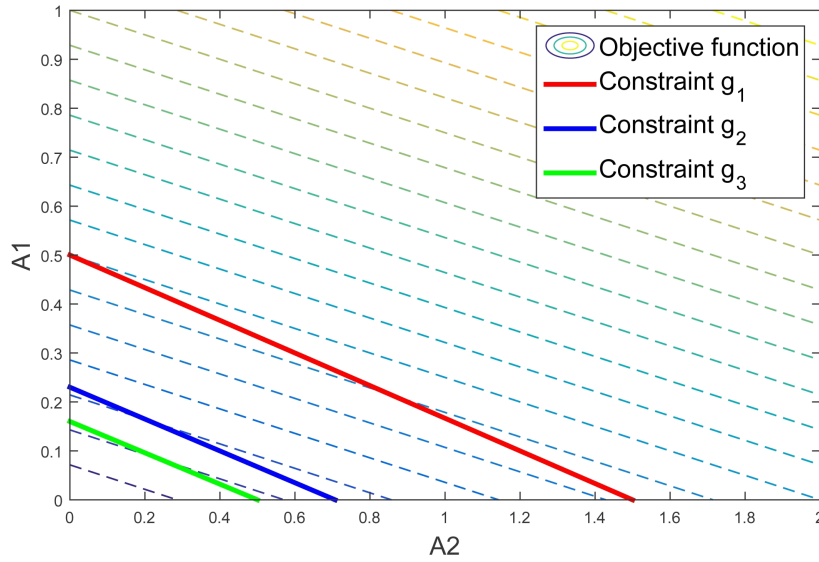


Figure 3.5: Solution Space of the Kirsch three bar truss.
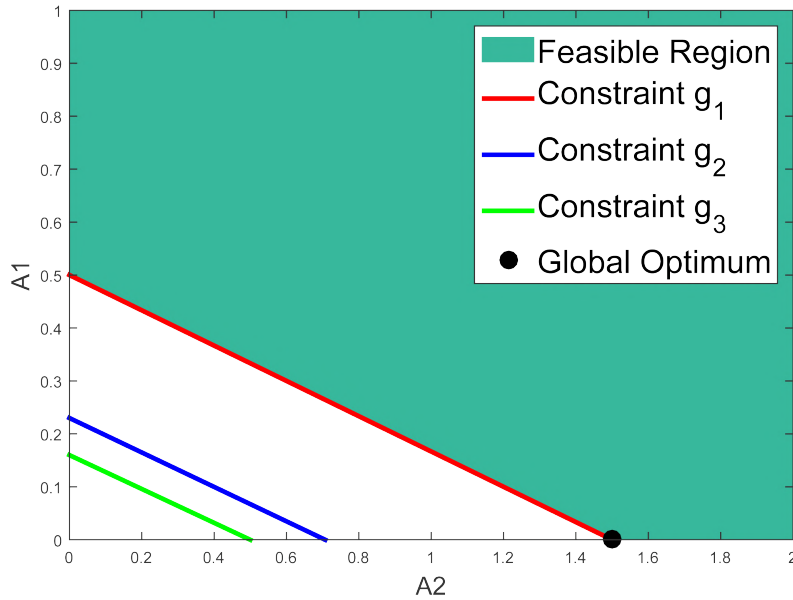


Figure 3.6: Kirsch three bar truss traditional feasible regions.
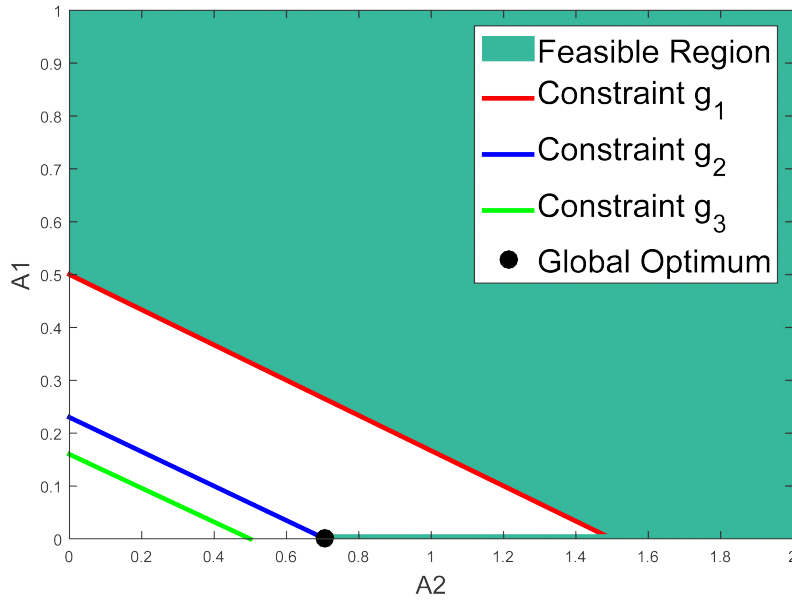
Figure 3.7: Kirsch three bar truss extended feasible regions.

In contrast to most of the literature, the difficulty in achieving the optimum point is not based on the fact that the region in which it is contained has a lower dimension than the rest of the domain. A slight change on the constraint, described in Eq. (3.47), allows us to include the degenerated region without increasing its dimensionality or changing the extended feasible region. The problem with this altered constraint was solved directly using both the MMA algorithm (Svanberg, 1987) and the MATLAB fmincon function with the "interior-point" option. The paths to convergence of the algorithms are shown in Fig. 3.8.

$$A_i \left( \frac{\sigma_i}{\sigma_{lim}} - 1 \right) \leqslant 0 \tag{3.47}$$
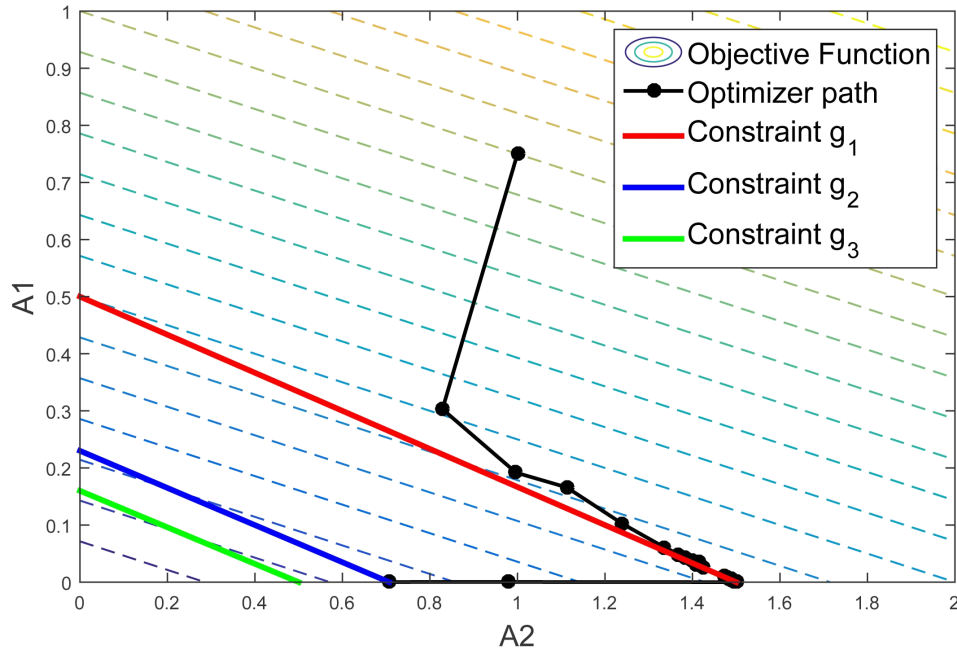
3.8(a): fmincon
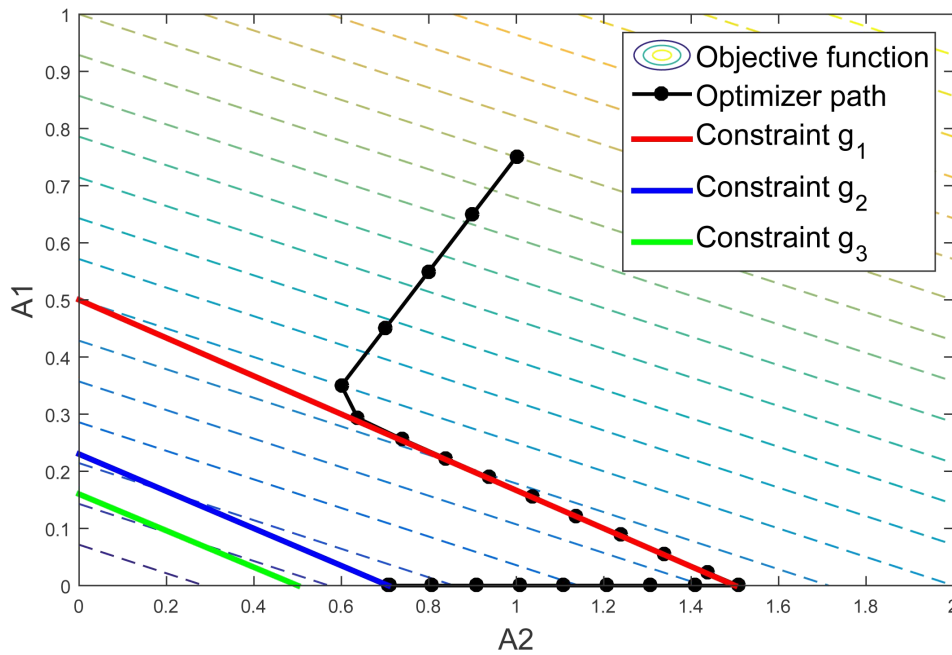


3.8(b): MMA

Figure 3.8: Solution of the Kirsch three bar truss with modified constraints using (a) the fmincon function of MATLAB and (b) the MMA.

### 3.5.2
### Diagonal Square Problem and Disconnected Regions

The real issue with vanishing stress constraints is much more complicated. In order to explain it, the author provides another example that is much more closely related to the topology optimization problem. The domain is a 2 by 2

square with a mesh of 4 regular Q4 elements. Two of those elements have fixed density of 1 and the other two are the design variables, $Z_1$ and $Z_2$. The load and support regions can be seen in Fig. 3.9 represented by a red arrow and blue triangles, respectively.



$$\begin{cases} L = 2m \\ P = (0.1, -0.1)N \\ E_0 = 1Pa \\ \upsilon = 0.3 \\ \sigma_{lim} = 1Pa \end{cases}$$
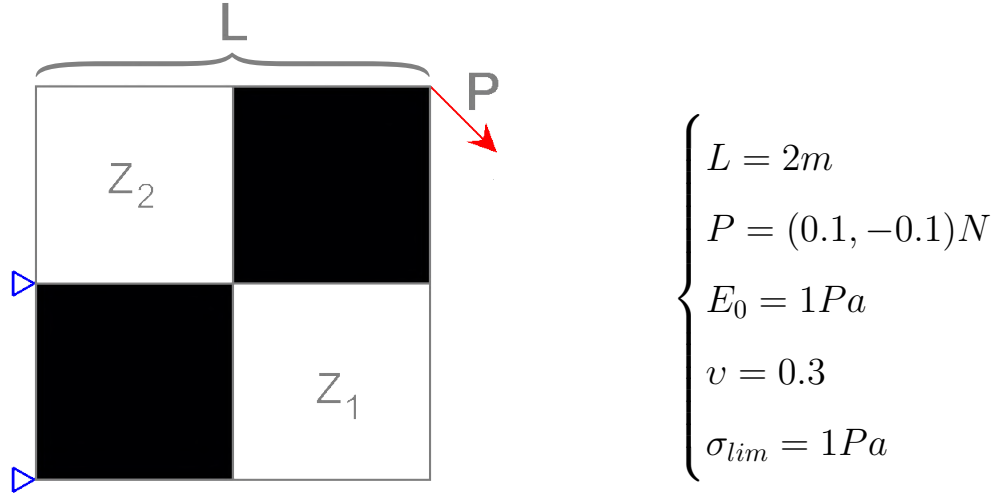
Figure 3.9: Diagonal Square problem.

The mathematical statement of the optimization problem is shown in Eq. (3.48), where $\sigma_1$ and $\sigma_2$ are evaluated at the centroid of the elements. There is no filtering applied so the density and the design variables are equivalent.

$$\begin{aligned} \underset{Z_1, Z_2}{\text{minimize}} \quad & M = Z_1 + Z_2 \\ \text{subject to} \quad & \frac{\sigma_1}{\sigma_{lim}} - 1 \leqslant 0 \\ & \frac{\sigma_2}{\sigma_{lim}} - 1 \leqslant 0 \\ & 0 \leqslant Z_1 \leqslant 1 \\ & 0 \leqslant Z_2 \leqslant 1 \\ \text{with} \quad & \mathbf{K}(Z_1, Z_2)\mathbf{U} = \mathbf{F} \end{aligned} \qquad (3.48)$$

The solution space of this problem is shown in Fig. 3.10. The traditional feasible domain is quite simple and the global optimum is readily apparent. However, in the same manner as before, it is necessary to disregard the constraints of the elements with zero density. In contrast to the previous case, there is now two degenerated regions added this way and both of them are disconnected from the main feasible space (Fig. 3.11 ). This separation absolutely prevents traditional gradient-based optimization algorithms from reaching these regions where, once more, the global optimum is present. It is

also worth noting that there is a distinct local optimum that is very similar to the global optimum.

Figure 3.10: Traditional feasible region.



Figure 3.11: Extended feasible region.

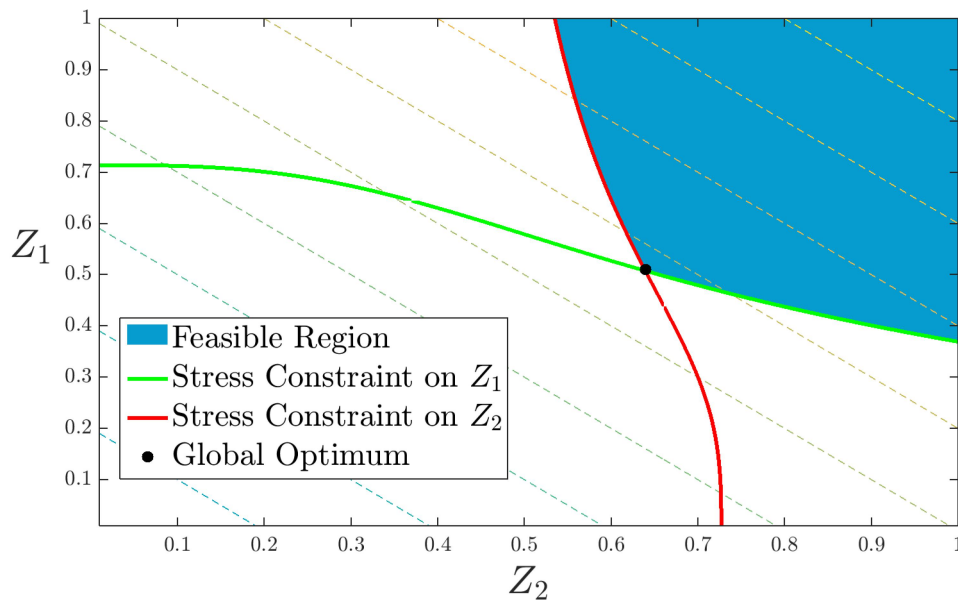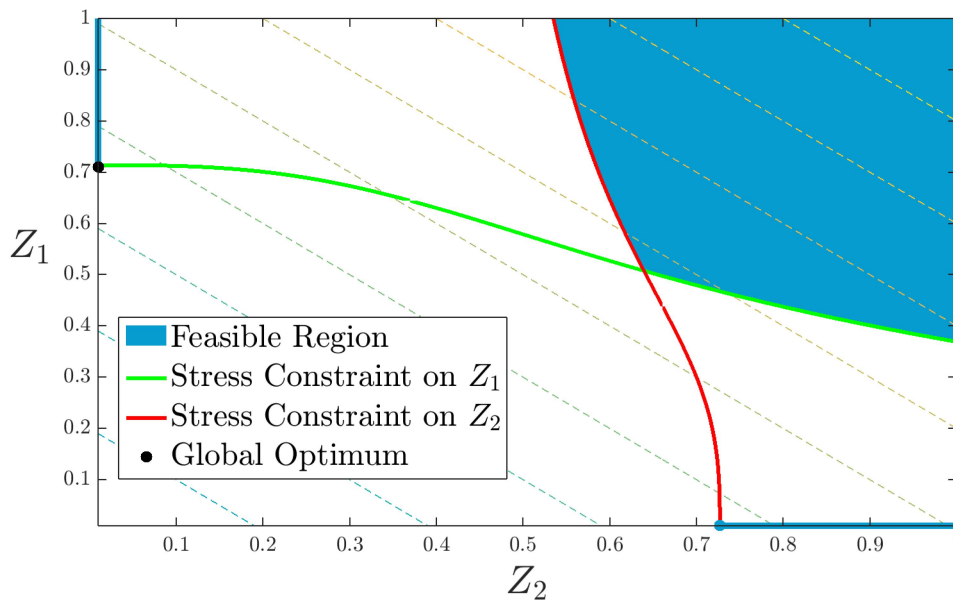The disconnected property of the solution space is, in the author's opinion, the main difficulty of the stress-constrained topology optimization. To the best of the author's knowledge , there is still no efficient way to solve this kind of problem exactly in large scale.

Nonetheless, several heuristic methods have been developed that can find an approximated solution. The basic idea to overcome this issue is to modify the constraint to obtain a continuous function that is null at zero density and is still able to recover the usual stress value.

### 3.5.3
### $\varepsilon$ relaxation

The $\varepsilon$ relaxation was first proposed by Cheng & Guo (1997) when dealing with truss optimization. It was later used successfully with the 2D topology optimization problem. It expands the region of the minimum by introducing a tolerance $\varepsilon$ on the constraint:

$$g(z) = \frac{\sigma^{VM}}{\sigma_{lim}} - 1 - \frac{\varepsilon}{\rho} \leqslant 0 \qquad (3.49)$$

For any $\varepsilon > 0$ the constraint (3.49) is eventually satisfied for a small enough $\rho$. As $\varepsilon \to 0$ the original constraint is obtained. It is common practice to start with a moderately high value for $\varepsilon$ and gradually decrease it in a continuous manner as to re-obtain the original constraint. However, Stolpe & Svanberg (2001) proved that this method is flawed, because the global optimum might not vary continuously with $\varepsilon$.

Another numerical matter that demands attention is the equivalence of constraints (3.49) and (3.50). Although this holds for optimization algorithms that strictly satisfy the constraints at each step, this is not true for the algorithms that allows some degree of constraint violation throughout the optimization, such as the Augmented Lagrangian method. For the latter, the value of the constraint in the unfeasible regions is crucial for the optimization. This can be seen in Fig. 3.12.

$$g(z) = \rho \left( \frac{\sigma^{VM}}{\sigma_{lim}} - 1 \right) - \varepsilon \leqslant 0 \qquad (3.50)$$
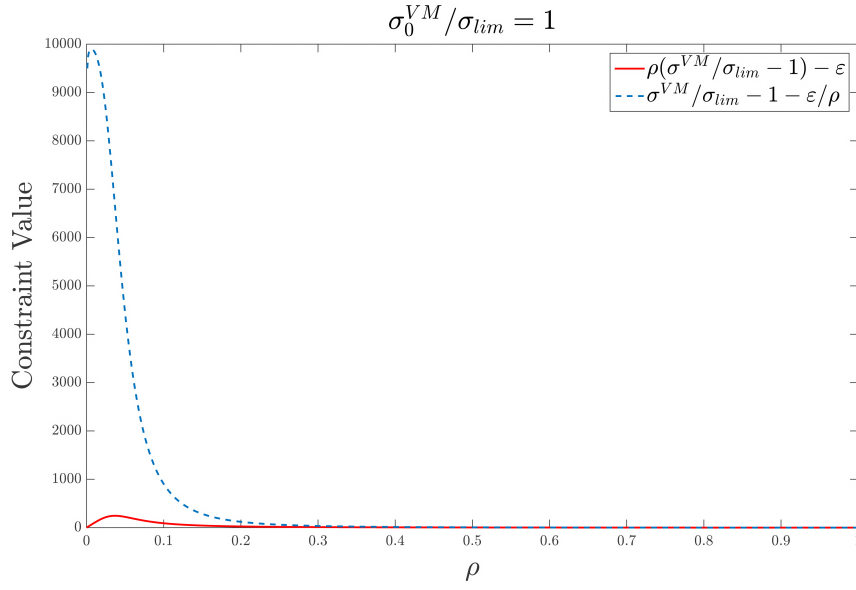
Figure 3.12: Different formulations of $\varepsilon$ relaxation.

In this plot $\varepsilon = 0.5$ and $\boldsymbol{\sigma}^{VM}$ are replaced by a simplified model (See Chapter 4 of this work).

**Diagonal Square Verification**

It is interesting to see what this relaxation does to the feasible region of the Diagonal Problem defined in Subsection 3.5.2. Figures 3.13 and 3.14 show how the constraints vary with the values of $\varepsilon$ as $\varepsilon \to 0$ the original constraint is obtained.
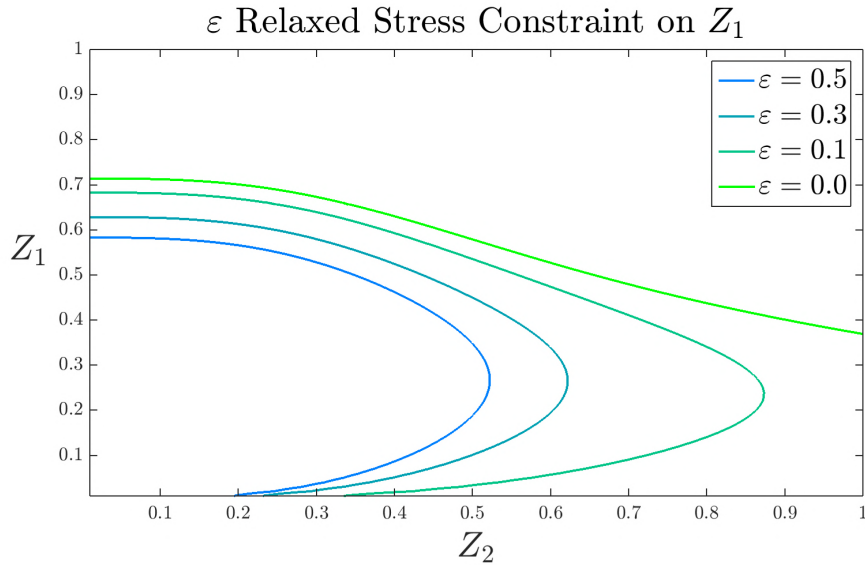


Figure 3.13: $Z_1$ Stress constraint of the diagonal square problem using $\varepsilon$ relaxation and different values of $\varepsilon$.

Figure 3.14: $Z_2$ Stress constraint of the diagonal square problem using $\varepsilon$ relaxation and different values of $\varepsilon$.

### 3.5.4
### q-p relaxation

This relaxation was proposed by Bruggi (2008) and is based on the definition of stress described in Section 3.3. The basic idea is to choose $q < p$ in Eq. (3.9). This way the stress is proportional to:

$$\sigma \approx \rho^{p-q} CB\hat{U} \tag{3.51}$$

This nullifies the stress when $\rho = 0$, which is more physically accurate. On the other hand if $\rho = 1$, meaning that the element is in a material region, the stress regains its traditional value. For intermediate densities, however, there is a loss in consistency and originally the literature proposed this as simple numerical tweak. The Von Mises stress using this formulation is:

$$\sigma_{qp}^{VM} = \sqrt{\sigma^T V \sigma} = \rho^{p-q}\sqrt{(CB_{el}\hat{U})^T V CB_{el}\hat{U}} = \rho^{p-q}\sigma^{VM} \tag{3.52}$$

The constraints are directly derived from $\sigma_{qp}^{VM}$ and vanish as $\rho = 0$. Consequently, the necessary regions are included as feasible, i.e.:

$$g(z) = \frac{\sigma_{qp}^{VM}}{\sigma_{lim}} - 1 = \rho^{p-q}\frac{\sigma^{VM}}{\sigma_{lim}} - 1 \leqslant 0 \tag{3.53}$$

**Diagonal Square Verification**

The q-p relaxation has a similar effect to that of the $\varepsilon$ relaxation on the feasible region of the Diagonal Problem defined in Subsection 3.5.2. Figures 3.15 and 3.16 show how the constraints vary with the values of $q - p$. As $(q - p) \to 0$ the original constraint is obtained.



Figure 3.15: $Z_1$ Stress constraint of the diagonal square problem using qp relaxation and different values of $q - p$.
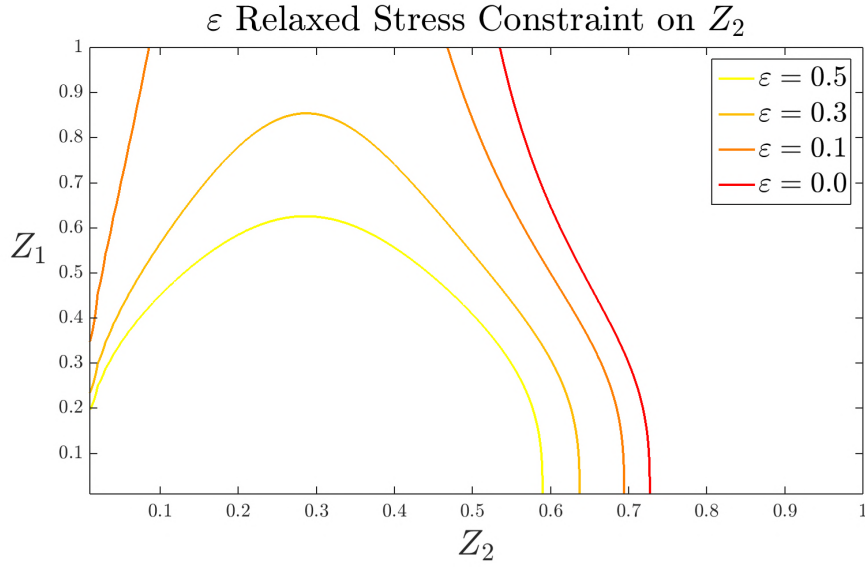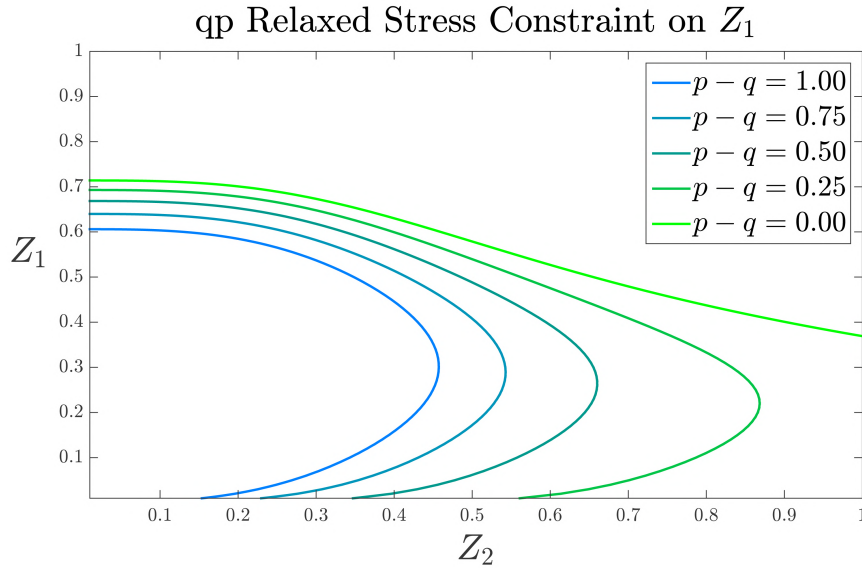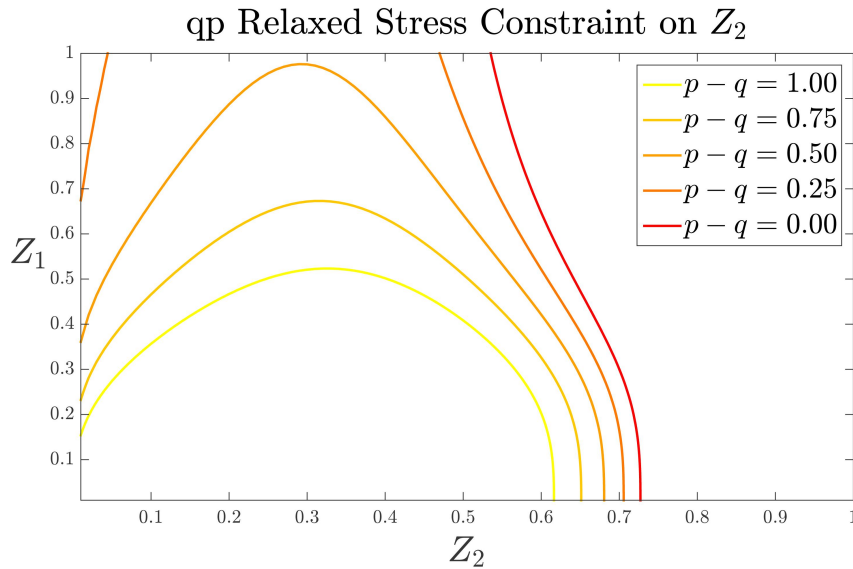


Figure 3.16: $Z_2$ Stress constraint of the diagonal square problem using qp relaxation and different values of $q - p$.

## 3.6
## Stress Measure

Although the definition of stress presented in Section 3.3 has some consistency for topology optimization, it still presents some practical problems, such as the fact that it has a non-null value for regions without any material. The interpretation of these values is dubious at best. Stress in a void has little physical meaning. To demonstrate this issue, imagine the following configuration of the diagonal square problem and its respective stress map:
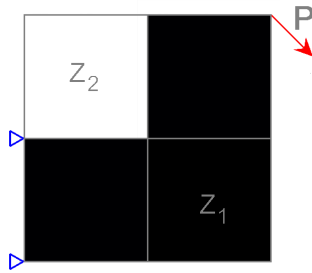


3.17(a): Density Configuration          3.17(b): Stress Map
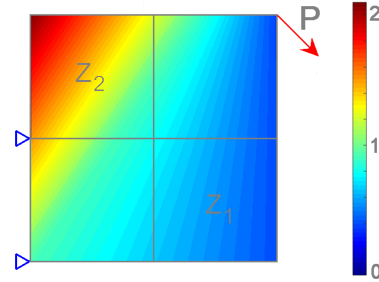
It is apparent that the higher stress is situated at the element with zero density, and the stress on the structure is below $\sigma_{lim} = 1$. Therefore, this would be a feasible solution. However, the stress analyses would not show this, because the maximum stress of the domain is above the admissible range. One could choose to disconsider the stress in the elements with a density close to zero. This would lead to a discontinuous measure which is used by some engineers. It is also important to note that the stress is not ill-defined only in regions of zero density. If one strives to manufacture the final design, it will be hard to come up with a configuration that correctly represents the values between zero and one. Even with penalization and other techniques to eliminate intermediate values, these values will still, to some extent, be present. Consequently, some form of post-processing has to be done to the solution of the topology optimization. For this reason the stress of the gray regions is not so meaningful. Following this train of thought, the qp relaxed stress became very popular as an alternative measure. It is zero when $\rho = 0$ and it regains its traditional value when $\rho = 1$. In addition, it reduces the relevance of the stress in the transition zones.

# 4
# Proposed Formulation

This chapter presents the formulation proposed by the author and it is also the main contribution of this dissertation. It is based on the Augmented Lagrangian method and uses a local adaptation to properly handle the vanishing constraints.

Let's first analyze the stress constraint using the same approach as in Section 3.3. We will consider the single element problem showed again in Fig. 4.1.
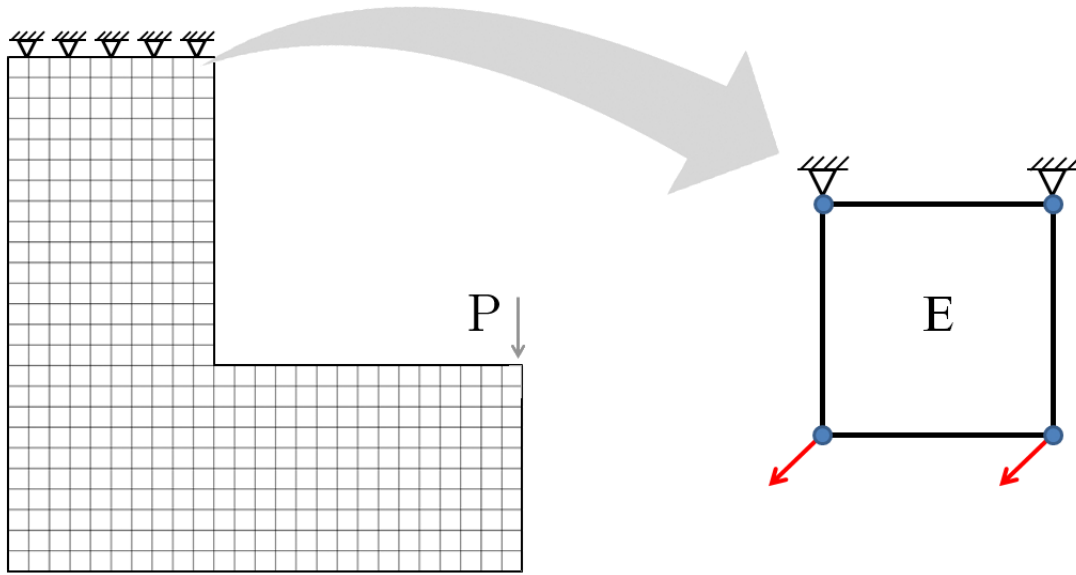
Figure 4.1: Single element Example.

The microscopic stress can be calculated as:

$$\boldsymbol{\sigma} = \mathbf{C} : \sum_{j=1}^{M} \mathbf{B}_j U_j = \frac{1}{E} \mathbf{C} : \sum_{j=1}^{M} \mathbf{B}_j (U_0)_j \qquad (4.1)$$

The computation of the Von Mises stress as described in Eq. (3.12), is given as:

$$\sigma^{VM} = \sqrt{\boldsymbol{\sigma}^T \mathbf{V} \boldsymbol{\sigma}} = \frac{1}{E}\sqrt{(\boldsymbol{\sigma}_0)^T \mathbf{V} \boldsymbol{\sigma}_0} \qquad (4.2)$$

with:

$$\boldsymbol{\sigma}_0 = \mathbf{C} : \sum_{j=1}^{M} \mathbf{B}_j (U_0)_j \qquad (4.3)$$

Notice that the term in the square root does not depend directly on the design variables and so it is possible to define $\sigma_0^{VM}$ as the Von Mises stress of the element with density equal to 1 (Eq. (4.4)). This value depends only on the variables that characterize the problem ($P$, $L$, $E_0$, $\nu$, etc ), i.e.:

$$\sigma_0^{VM} = \sqrt{(\sigma_0)^T V \sigma_0} \qquad (4.4)$$

Therefore, we can get a simplified expression for the stress:

$$\sigma^{VM}(E) = \frac{1}{E}\sigma_0^{VM} \qquad (4.5)$$

Remembering that:

$$E = \epsilon + \rho^p(1 - \epsilon) \qquad (4.6)$$

it is possible to estimate the stress with respect to $\sigma_0^{VM}$ and $\rho$. Let's evaluate the different relaxations of the stress constraints and how they behave. The penalization factor $p = 3$ will be chosen for the reasons described in Chapter 2, Subsection B of this work.

- – Original Constraint: $\sigma^{VM}/\sigma_{lim} - 1 \leqslant 0$
- – q-p Relaxation: $\rho^{0.5}\sigma^{VM}/\sigma_{lim} - 1 \leqslant 0$
- – $\varepsilon$ Relaxation: $\sigma^{VM}/\sigma_{lim} - 1 - \varepsilon/\rho \leqslant 0$
- – Vanishing Constraint: $\rho(\sigma^{VM}/\sigma_{lim} - 1) \leqslant 0$

The disconnected feasible regions discussed in Section 3.5 become apparent as the "hills" presented in the Fig. 4.2. A gradient-based optimization algorithm handling the constraints strictly throughout the steps would be restricted to zones where the plots are below zero. Figure 4.3 shows these regions

more clearly. It is easy to understand that the solution would be stuck in the area next to one and it would not be able to reach zero.
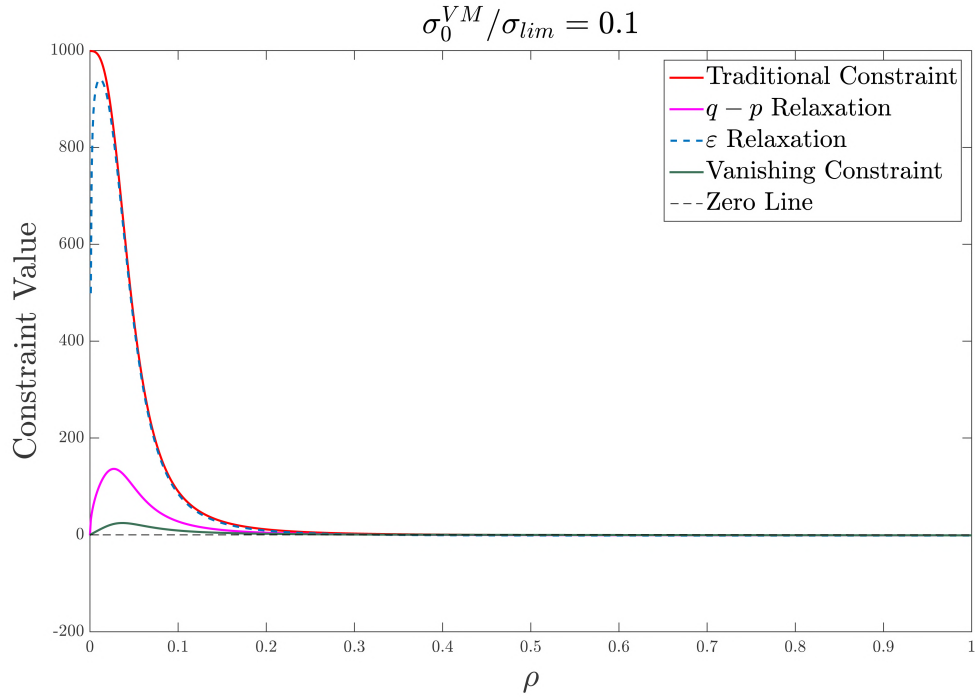


Figure 4.2: Behavior of different variations of the stress constraint with $\rho$ and $\sigma_0^{VM}/\sigma_{lim} = 0.1$.
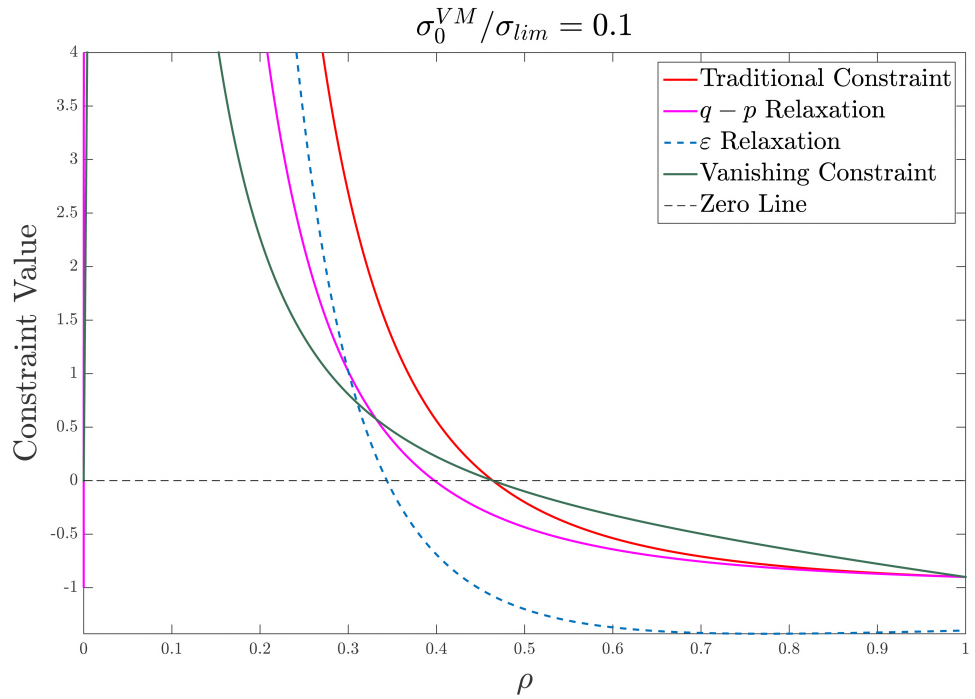


Figure 4.3: Plots of Fig. 4.2 with the vertical axis limited for a better view.

The Augmented Lagrangian method, however, does not impose direct constraints on the problem and in fact only ensures constraint satisfaction on the final solution. The penalization term is defined as:

$$I(\rho) = \lambda \left[ max(g(\rho), -\lambda/\mu) \right] + \frac{\mu}{2} \left[ max(g(\rho), -\lambda/\mu) \right]^2 \tag{4.7}$$

where $g(\rho)$ is the constraint function. Choosing initial values $\lambda = 0.001$ and $\mu = 0.001$, it is possible to compute the penalization for the various constraints displayed so far.

Besides the penalization, the Augmented Lagrangian method has another term related to the objective function of the original problem, in this case it is the total weight. This plot is no longer a constraint and the algorithms are not restricted to the intervals below zero, however most of them don't take steps towards directions of increasing value. The weight contribution of this single element would be $m(\rho)$ and so the objective function of the subproblem is described in Eq. (4.8). Figure 4.6 shows the plot for the exponential weight relation described in Section 3.2.

$$J(\rho, \mu, \lambda) = m(\rho) + \lambda \left[ max(g(\rho), -\lambda/\mu) \right] + \frac{\mu}{2} \left[ max(g(\rho), -\lambda/\mu) \right]^2 \tag{4.8}$$
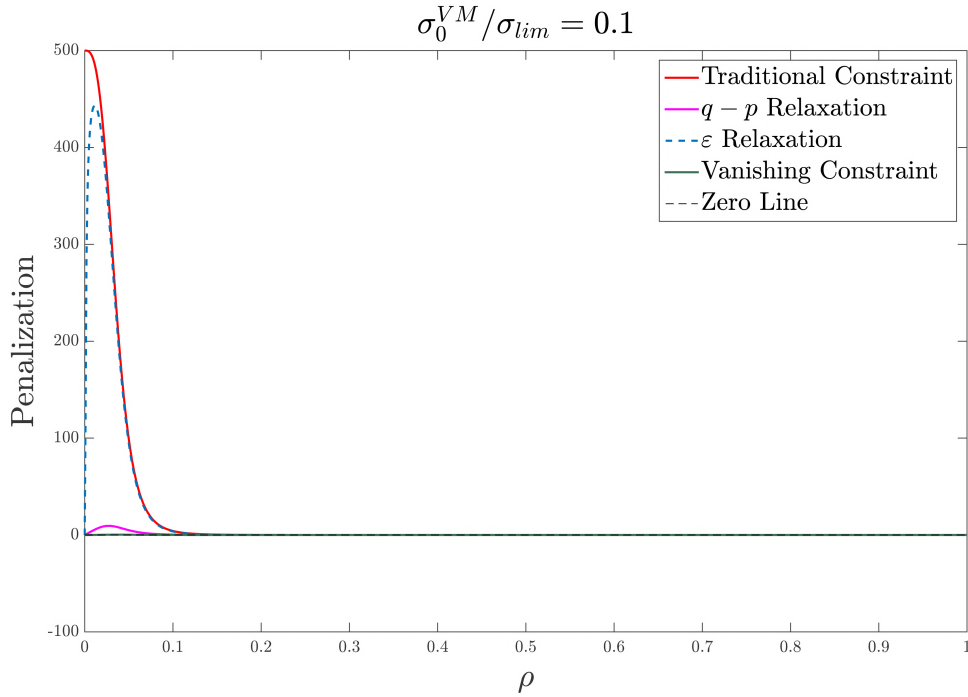


Figure 4.4: Plots of the penalization of the Augmented Lagrangian for different stress constraints.

$$\sigma_0^{VM}/\sigma_{lim} = 0.1$$
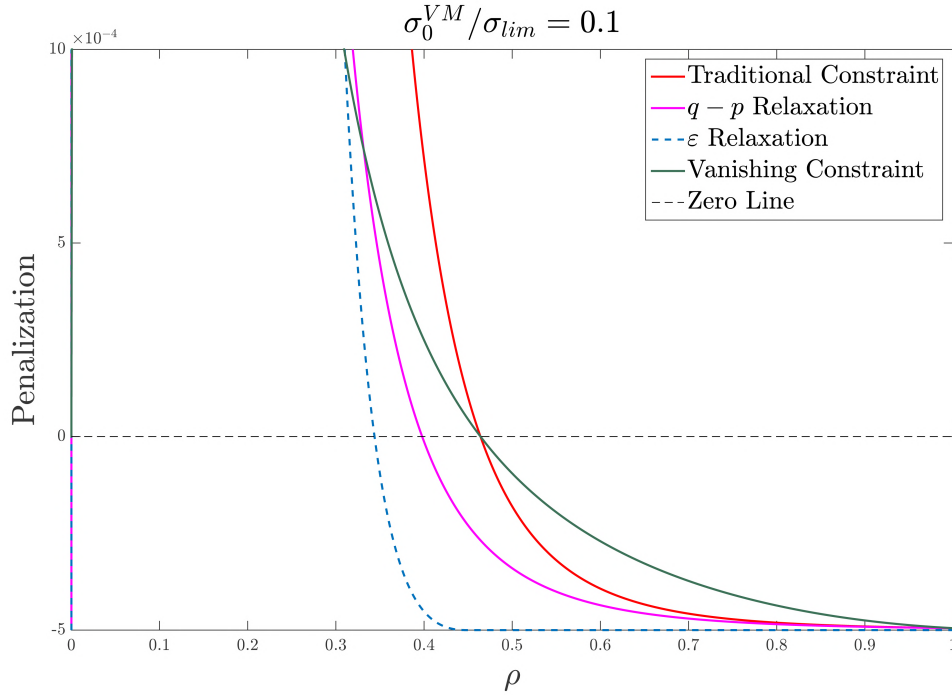
Figure 4.5: Plots of Fig. 4.4 with the y axis limited for a better view.

$$\sigma_0^{VM}/\sigma_{lim} = 0.1$$
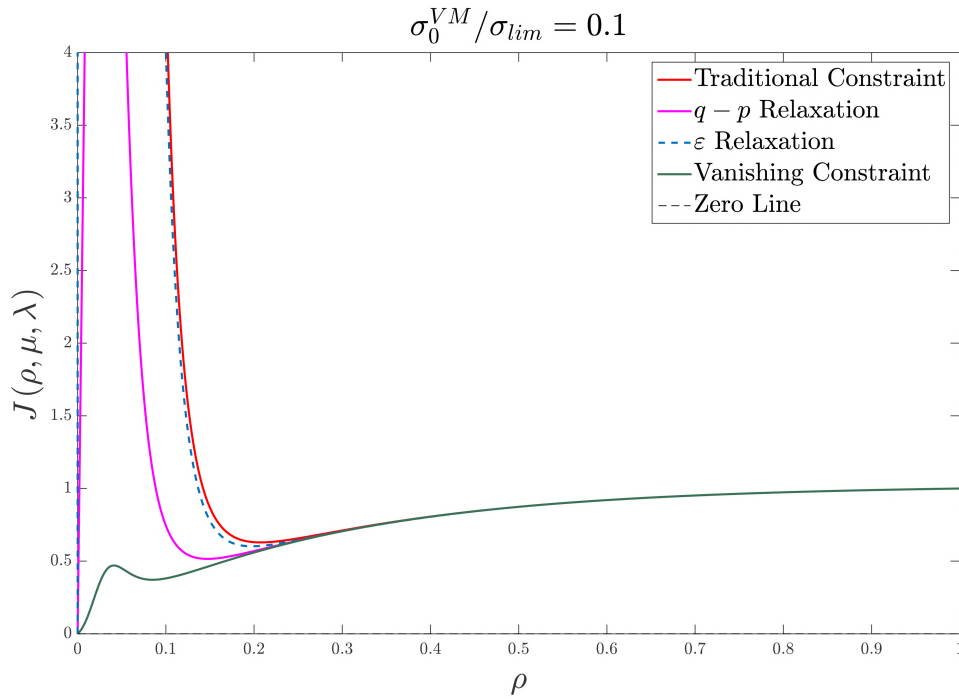
Figure 4.6: Objective Function of the Augmented Lagrangian method.

Considering an initial guess of $\rho = 0.5$, and that the optimization algorithm is only capable of going downhill, it still wouldn't be possible to reach zero density. To overcome this, one could try to adjust $\mu$ and/or $\lambda$ to reduce the effect of the constraints. This was the first attempt made, which leads to

several numerical difficulties, as the stress is a highly nonlinear function. Yet the weight is a monotonic well behaved function and so multiplying it by a factor $\gamma$ preserves its nice properties. Setting $\gamma = 4$ yields to a promissory result displayed in Fig. 4.7. Not only it is now possible to reach zero using vanishing constraints, but the function is also much more steep, which enables a faster convergence. Of course, this is just another way of diminishing the relevance of the constraint.

$$J(\rho, \mu, \lambda, \gamma) = \gamma m(\rho) + \lambda \left[ max(g(\rho), -\lambda/\mu) \right] + \frac{\mu}{2} \left[ max(g(\rho), -\lambda/\mu) \right]^2 \quad (4.9)$$
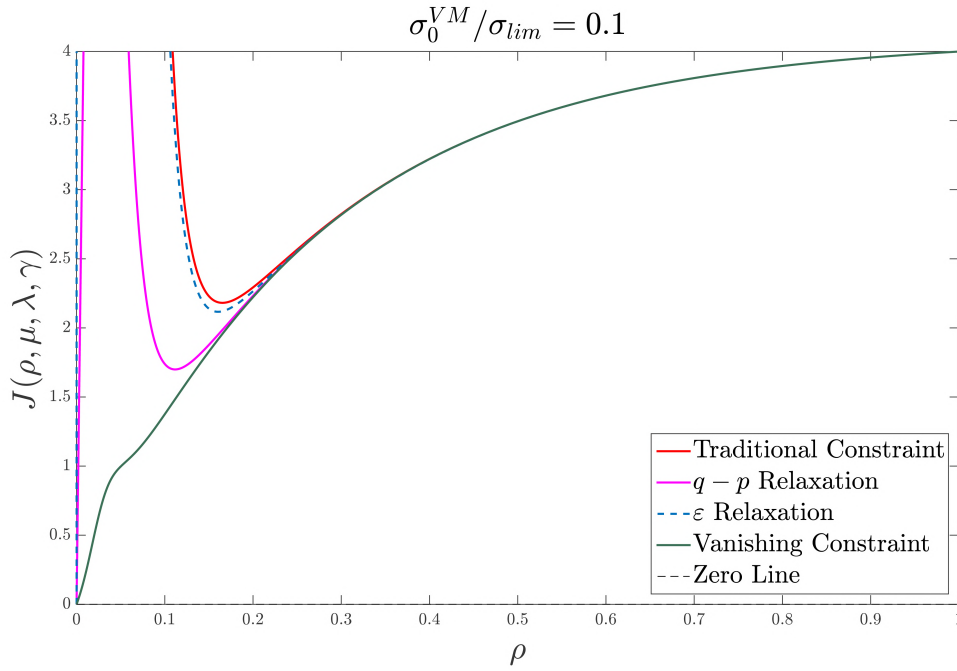


Figure 4.7: Objective Function of the Augmented Lagrangian method with the $\gamma$ parameter.

On the other hand if the constraint is violated, and it should have density $\rho_{el} = 1$, the increase of the Lagrangian Multipliers will lead to this solution. Figure 4.8, shows this tendency for the vanishing constraint. Setting $\gamma = 0$, however, leads to this solution immediately (see fig. 4.9). Ultimately lowering $\gamma_{el}$ and increasing $\lambda_{el}$ is done simultaneously .
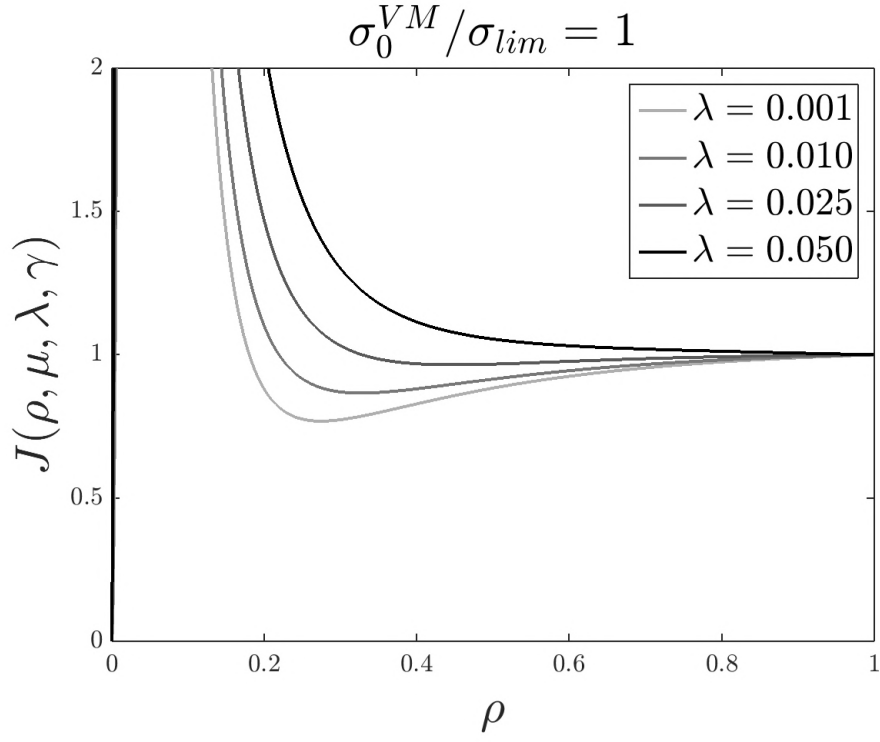
Figure 4.8: Augmented Lagrangian with $\mu = 0.001$ and $\gamma_{el} = 1$ for various values of $\lambda$ using the vanishing constraint.
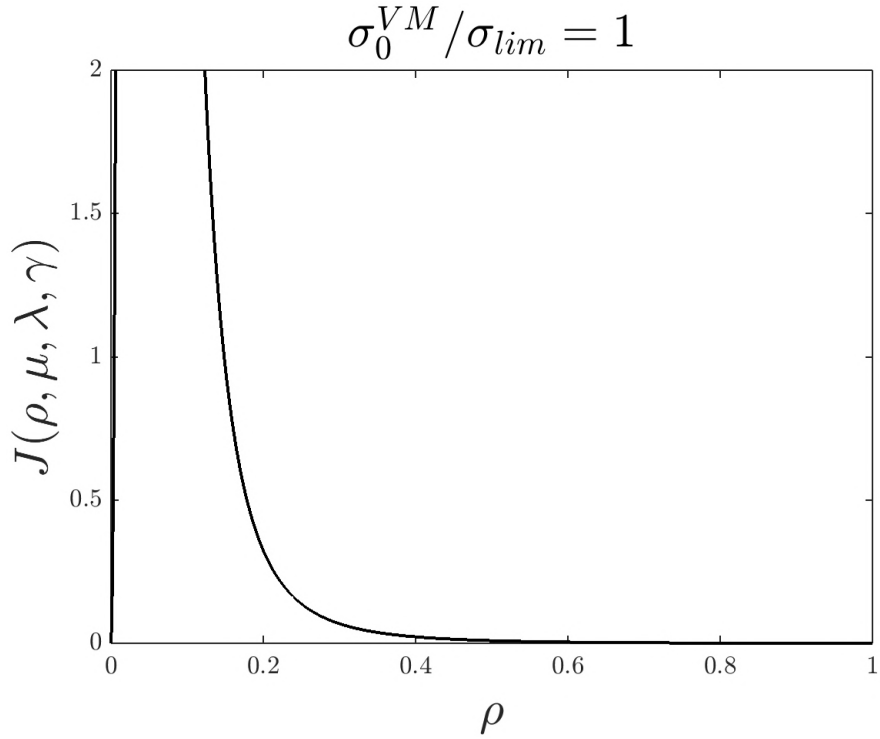


Figure 4.9: Augmented Lagrangian with $\lambda_{el} = 0.001$, $\mu = 0.001$ and $\gamma_{el} = 0$ using the vanishing constraint.

Of course, Eq. (4.2) is an oversimplification of the stress. In a larger case, the forces acting on a element are a function of the densities of other elements as well as its own, which makes the analyses much more difficult. However, this elementary model gives the idea to use an adaptive $\gamma$ for each element. Unfortunately, as one does not know a priori, which elements must have density one or zero, the adaptation has to be done heuristically using some estimative of stress. The stress measure defined in Section 3.6 is used for this purpose. The adjustment of this parameter is done at the same time as the update of the Lagrangian Multipliers, following this equation:

$$
\gamma_i^{k+1} = \begin{cases} max(a_1\gamma_i^k + b_1, \gamma_l), & \text{if} \quad \rho_i^{0.5}\dfrac{\sigma_i^{VM}}{\sigma_{lim}} > 1.01 \\[3ex] min(a_2\gamma_i^k + b_2, \gamma_u), & otherwise \end{cases} \tag{4.10}
$$

where $\gamma_l$ and $\gamma_u$ are lower and upper limits for $\gamma$, respectively. The variables $a_1$, $a_2$, $b_1$, $b_2$ are constant throughout the optimization and the determination of their values is explained in Appendix A.

The version of the constraint used is a piecewise variation of the vanishing constraint, i.e.:

$$
g_i(\rho) = \begin{cases} \rho_i^3(\sigma_i - 1)^2 & \text{if} \quad \sigma > 1 \\ 0, & otherwise \end{cases} \tag{4.11}
$$

This is now an equality constraint with continuity $C^1$ in zero, which is very helpful for numerical convergence. This constraint penalizes more severely higher stress and is more moderate for stresses closer to the limit.

In order to speed up convergence, when the average step size is lower than a tolerance, the parameters $\mu$ and $\gamma_u$ are updated to increase the influence of the constraints. The iterations stop when the average size of the step is lower than this tolerance, and the maximum stress measure is within an admissible range.

The full algorithm is depicted in the scheme below:

---

**Algorithm 1** Gamma Formulation

---

1: **procedure** GAMMA ADAPTATION
2:     $z^1$=initial guess
3:     $\lambda^1 = 0.01$
4:     $\mu^1 = 0.1$
5:     $\gamma^1 = 0$
6:     step_size=1
7:     $k = 1$
8:     **while** step_size>tol & $\max(\sigma)>\sigma_{tol}$ **do**
9:         minimize $J^k(z,\mu^k,\lambda^k,\gamma^k)$, starting at $z^k$
10:         $z^{k+1} \overset{z}{=}$ solution to the minimization of $J^k$
11:         Compute $\sigma^{VM}$ with $z^{k+1}$
12:         $\lambda^{k+1} = max\left[\lambda^k + \mu^k g(z^k), 0\right]$
13:         $\gamma^{k+1} =$ update following Eq. (4.10)
14:         step_size=sum($|z^k - z^{k+1}|$)/nElem     /∗ Size of the step $k+1$
15:         **if** step_size $<$ tol **then**
16:             $\mu^{k+1} = 1.05\mu^k$
17:             $\gamma_u = 0.95\gamma_u$
18:         **else**
19:             $\mu^{k+1} = \mu^k$
20:         **end if**
21:         $k = k + 1$
22:     **end while**
23: **end procedure**

---

The meaning of the word "minimize" in line number 9 of the algorithm must be considered very loosely. As stated in Subsection 3.4.2, the advantage of finding an actual local minimum for the subproblem $k$ is questionable, as it requires considerable computational time. An approximated solution is good enough to improve the values of $\lambda$ and $\gamma$, therefore a rather low limit on the maximum number of iterations for these cases is set. This procedure of "minimization" was done mostly through the MMA algorithm (Svanberg, 1987).

The optimization is stopped when a certain degree of stagnation is achieved and the constraints are satisfied to an admissible range. The choice of stagnation over the KKT conditions as stopping criteria is due to the bound constraints on the optimization problem. A final design close to a 0 or 1 solution means a large number of bound constrains active for which the appropriate

value for the KKT multipliers is not given by the optimization algorithm of choice. The admissible range for stress is defined for numerical reasons and is described as $\sigma_{tol}$ in the algorithm.

## 4.1
## Augmented Lagrangian Correction and Mesh Invariance

The progress in feasibility in the Augmented Lagrangian method is only obtained through the minimization of the objective function. The optimization is then an equilibrium between the satisfaction of the stress constraints and the reduction of total weight. This balance is controlled by the factors $\mu$ and $\lambda$.

As the mesh is refined, the total number of constraints increases (if one keeps the rule of one evaluation of stress per element). This shifts the equilibrium towards the satisfaction of constraints and can lead to suboptimal designs. In order to overcome this problem, it is necessary to lower the values of $\mu$ and $\lambda$.

Another idea is to calibrate the initial values of $\mu$ and $\lambda$ for a certain number $N$ of elements and use a ratio to adjust the relevance of the constraint. In other words, to use a correction factor $\eta$, given as:

$$\eta = \frac{N}{\text{Number of Constraints}} \tag{4.12}$$

$$J(z) = f(z) + \eta \sum_{i=1}^{n} I_i(g_i(z)) \tag{4.13}$$

The correction factor $\eta$ is then used to multiply the penalization as shown in Eq. (4.13), and the parameters $\mu$ and $\lambda$ do not need to be adjusted for each mesh. This approach has proved to be valid not only for mesh refinement/coarsening but also for different problems with arbitrary domains.

## 4.2
## Well posedness of the problem and a single element definition

Despite being a complicated problem with several local minimums, any relaxation that allows the elements' densities to achieve zero, guarantees an analytical solution to the problem that is fairly easy to describe. Setting all the design variables to zero minimizes the objective function, and it is a feasible point, because the relaxed constraints are satisfied by elements with zero density. This is a rather odd result, which indicates that the best structure

is no structure at all. This trivial solution is merely the result of the inability of the numerical model to represent the real, physical world. It must, therefore, be excluded as a viable solution.

One (simple) way to achieve this is to fix a single (load bearing) element to have a density of one. The solution for a non-degenerated problem with all zeros will cause high stresses in this fixed element, thus excluding this type of solutions from the admissible set. This causes the problem to become physically better posed.

## 4.3
## Sensitivity Analysis

The formulation proposed is intended to be used with a gradient-based optimizer and so it is necessary to compute the first order derivative of the gamma Augmented Lagrangian, displayed in Eq. (4.14), with respect to the optimization variables $\mathbf{z}$. The Einstein's tensor notation is used where repeated index are summed over.

$$J(\mathbf{z}, \mu, \boldsymbol{\lambda}, \boldsymbol{\gamma}) = M(\mathbf{z}, \boldsymbol{\gamma}) + \sum_{i=1}^{nConst} \left\{ \lambda_i g_i(\mathbf{z}) + \frac{\mu}{2} \left[ g_i(\mathbf{z}) \right]^2 \right\} \qquad (4.14)$$

in which $nConst$ is the total number of constraints. The derivation of the gradient can be separated in two parts, one relative to the objective function and the other, to the penalization term:

$$\frac{d}{d\mathbf{z}} J(\mathbf{z}, \mu, \boldsymbol{\lambda}, \boldsymbol{\gamma}) = \frac{d}{d\mathbf{z}} M(\mathbf{z}, \boldsymbol{\gamma}) + \sum_{i=1}^{nConst} \frac{d}{d\mathbf{z}} \left\{ \lambda_i g_i(\mathbf{z}) + \frac{\mu}{2} \left[ g_i(\mathbf{z}) \right]^2 \right\} \qquad (4.15)$$

## 4.3.1
## Total Weight

The derivative of the total Weight $M(\mathbf{z}, \boldsymbol{\gamma})$ is quite simple:

$$\frac{d}{dz_j} M(\mathbf{z}, \boldsymbol{\gamma}) = \sum_{i=1}^{nElem} \gamma_i v_i \frac{d}{dz_j} m_i(\rho_i(\mathbf{z})) = \sum_{i=1}^{nElem} \gamma_i v_i \frac{d \left[ m_i(\rho_i(\mathbf{z})) \right]}{d\rho_i(\mathbf{z})} \frac{d\rho_i(\mathbf{z})}{dz_j} \qquad (4.16)$$

Here the exponential weight relation for $m_i(\rho_i(\mathbf{z}))$ is used. It is defined in Eq. (3.3), hence:

$$\frac{d\left[m_i(\rho_i(\mathbf{z}))\right]}{d\rho_i(\mathbf{z})} = \beta e^{-\beta \rho_i(\mathbf{z})} + e^{-\beta} \tag{4.17}$$

On the other hand, $\rho_i(\mathbf{z}) = P_{ij} z_j$, where $P_{ij}$ is the regularization filter matrix described in Section 2.3, and:

$$\frac{d\rho_i(\mathbf{z})}{dz_j} = \frac{d}{dz_j} P_{ij} z_j = P_{ij} \tag{4.18}$$

Resuming:

$$\frac{d}{dz_j} M(\mathbf{z}, \boldsymbol{\gamma}) = \sum_{i=1}^{nElem} \gamma_i v_i \left[ \beta e^{-\beta \rho_i(\mathbf{z})} + e^{-\beta} \right] P_{ij} \tag{4.19}$$

### 4.3.2
### Penalization Term

The penalization term is more complicated and it will require several steps:

$$\sum_{i=1}^{nConst} \frac{d}{d\mathbf{z}} \left\{ \lambda_i g_i(\mathbf{z}) + \frac{\mu}{2} \left[ g_i(\mathbf{z}) \right]^2 \right\} = \sum_{i=1}^{nConst} \left\{ \lambda_i + \mu g_i(\mathbf{z}) \right\} \frac{d}{d\mathbf{z}} g_i(\mathbf{z}) \tag{4.20}$$

The constraint $g_i(\mathbf{z})$, is depicted in Eq. (4.11). If $\sigma_i^{VM} < \sigma_{lim}$ then:

$$\frac{d}{d\mathbf{z}} g_i(\mathbf{z}) = 0 \tag{4.21}$$

Otherwise:

$$\frac{d}{d\mathbf{z}} g_i(\mathbf{z}) = \frac{d}{d\mathbf{z}} \left[ \rho_i^3 (\sigma_i^{VM} - 1)^2 \right] = \frac{d\left[\rho_i^3\right]}{d\mathbf{z}} (\sigma_i - 1)^2 + \rho_i^3 \frac{d\left[(\sigma_i^{VM} - 1)^2\right]}{d\mathbf{z}} \tag{4.22}$$

$$\frac{d}{d\mathbf{z}} g_i(\mathbf{z}) = \begin{cases} 0 & \text{if } \sigma_i^{VM} < \sigma_{lim} \\ \frac{d}{d\mathbf{z}} \left[ \rho_i^3 (\sigma_i^{VM} - 1)^2 \right] & \text{otherwise} \end{cases} \tag{4.23}$$

$$\frac{d\left[\rho_i^3\right]}{dz_j} = 3\rho_j^2 P_{ji} \tag{4.24}$$

$$\frac{d\left[(\sigma_i - 1)^2\right]}{dz_j} = 2(\sigma_i - 1)\frac{d\left[\sigma_i^{VM}\right]}{dz_j} \tag{4.25}$$

The hardest and most computationally expensive part is to compute $\frac{d\left[\sigma_i^{VM}\right]}{dz_j}$, i.e.:

$$\frac{d\left[\sigma_i^{VM}\right]}{dz_j} = \frac{d\left[\sigma_i^{VM}\right]}{d\sigma_l}\frac{d\left[\sigma_l\right]}{dz_j} \tag{4.26}$$

$$\frac{d\left[\sigma_i^{VM}\right]}{d\sigma_l} = \frac{3}{4\sigma_i^{VM}}\left[2\boldsymbol{\sigma}_l - \frac{2}{3}tr(\boldsymbol{\sigma}_l)\boldsymbol{\delta}\right] \tag{4.27}$$

To understand the expression above see Eq. (3.12) and note that $\frac{d[tr(\boldsymbol{\sigma})]}{d\boldsymbol{\sigma}} = \boldsymbol{\delta}$. This is equation is quite long so the term $\frac{d\left[\sigma_i^{VM}\right]}{d\sigma_l}$ will be carried out for simplicity.

$$\frac{d\left[\sigma_l\right]}{dz_j} = \frac{d\left[\sigma_l\right]}{dU_p}\frac{d\left[U_p\right]}{dz_j} \tag{4.28}$$

$$\frac{d\left[\sigma_l\right]}{dU_p} = \mathbf{C} : \mathbf{B}_p \tag{4.29}$$

The expression above comes from Eqs. (2.10) and (2.4). Again for simplicity the term $\frac{d\left[\sigma_l\right]}{dU_p}$ is carried out instead of the above deduction. Summarizing so far for the derivation of $\sigma$:

$$\sum_{i=1}^{nConst} \left\{\lambda_i + \mu g_i(\mathbf{z})\right\} 2\rho_i^3(\sigma_i - 1)\frac{d\left[\sigma_i^{VM}\right]}{d\sigma_l}\frac{d\left[\sigma_l\right]}{dU_p}\frac{d\left[U_p\right]}{dz_j} \tag{4.30}$$

The computation of $\frac{d\left[U_p\right]}{dz_j}$ is rather expensive, but it is possible to circumvent that using the adjoint method. We must start with the equilibrium

equations:

$$K_{qp}U_p - f_q = 0$$

$$\frac{d}{dz_j}\left(K_{qp}U_p - f_q\right) = \frac{d\left[K_{qp}\right]}{dz_j}U_p + K_{qp}\frac{d\left[U_p\right]}{dz_j} = 0$$

and noticing that:

$$\xi_q\left(\frac{d\left[K_{qp}\right]}{dz_j}U_p + K_{qp}\frac{d\left[U_p\right]}{dz_j}\right) = 0 \tag{4.31}$$

can be added to the Eq. (4.30) without modifying it. Here $\xi_i$ is the adjoint variable:

$$\sum_{i=1}^{nConst}\left\{\lambda_i + \mu g_i(\mathbf{z})\right\}2\rho_i^3(\sigma_i-1)\frac{d\left[\sigma_i^{VM}\right]}{d\sigma_l}\frac{d\left[\sigma_l\right]}{dU_p}\frac{d\left[U_p\right]}{dz_j} + \xi_q\left(\frac{d\left[K_{qp}\right]}{dz_j}U_p + K_{qp}\frac{d\left[U_p\right]}{dz_j}\right) \tag{4.32}$$

Collecting the terms with $\dfrac{d\left[U_p\right]}{dz_j}$:

$$\left\{\sum_{i=1}^{nConst}\left\{\lambda_i + \mu g_i(\mathbf{z})\right\}2\rho_i^3(\sigma_i-1)\frac{d\left[\sigma_i^{VM}\right]}{d\sigma_l}\frac{d\left[\sigma_l\right]}{dU_p} + \xi_q K_{qp}\right\}\frac{d\left[U_p\right]}{dz_j} + \xi_q\frac{d\left[K_{qp}\right]}{dz_j}U_p \tag{4.33}$$

The trick now is to define $\xi_q$ in order to have:

$$\sum_{i=1}^{nConst}\left\{\lambda_i + \mu g_i(\mathbf{z})\right\}2\rho_i^3(\sigma_i-1)\frac{d\left[\sigma_i^{VM}\right]}{d\sigma_l}\frac{d\left[\sigma_l\right]}{dU_p} + \xi_q K_{qp} = 0 \tag{4.34}$$

$$\xi_q K_{qp} = -\sum_{i=1}^{nConst}\left\{\lambda_i + \mu g_i(\mathbf{z})\right\}2\rho_i^3(\sigma_i-1)\frac{d\left[\sigma_i^{VM}\right]}{d\sigma_l}\frac{d\left[\sigma_l\right]}{dU_p} \tag{4.35}$$

Noticing that $K_{ip} = K_{pi}$, and defining $\widehat{f}_p$ as:

$$\widehat{f}_p = -\sum_{i=1}^{nConst} \left\{\lambda_i + \mu g_i(\mathbf{z})\right\} 2\rho_i^3(\sigma_i - 1)\frac{d\left[\sigma_i^{VM}\right]}{d\sigma_l}\frac{d\left[\sigma_l\right]}{dU_p} \tag{4.36}$$

$$K_{pq}\xi_q = \widehat{f}_p \tag{4.37}$$

That way $\xi_q$ can be obtained solving the linear system with only one right-hand side. In contrast, using direct differentiation would require the solution of the linear system for "$nConst$" right-hand sides. Equation (4.33) breaks down to:

$$\xi_q\frac{d\left[K_{qp}\right]}{dz_j}U_p = \xi_q\frac{d\left[K_{qp}\right]}{dE_q}\frac{d\left[E_q\right]}{d\rho_q}\frac{d\left[\rho_q\right]}{dz_j}U_p \tag{4.38}$$

The whole penalization differentiation term is then:

$$\sum_{i=1}^{nConst}\frac{d}{d\mathbf{z}}\left\{\lambda_i g_i(\mathbf{z}) + \frac{\mu}{2}\left[g_i(\mathbf{z})\right]^2\right\} = \xi_q\frac{d\left[K_{qp}\right]}{d\mathbf{z}}U_p + \sum_{i=1}^{nConst}\left\{\lambda_i + \mu g_i(\mathbf{z})\right\}3\rho_j^2 P_{ji}(\sigma_i^{VM}-1)^2 \tag{4.39}$$

# 5
# Numerical Results

This Chapter presents the numerical results obtained with the proposed method (described in Chapter 4) through a MATLAB implementation. Some problems are used as examples to address concerns over the results, while others are merely expositions and demonstrate the robustness of the method.

The MMA algorithm was used for the optimization and its adjustable parameters setting is displayed in Table 5.1. The parameters control how conservative the algorithm is and significantly influence on the results. For more information on those see Svanberg (1987).

Table 5.1: MMA adjustable parameters setting

| MMA Parameters | | |
|---|---|---|
| Parameter | Description | Value |
| asyinit | Asymptote Control | 0.2 |
| asyinc | Asymptote Control | 1.2 |
| asydec | Asymptote Control | 0.7 |
| move | Move Limit | 0.3 |

Table 5.2 shows the initial values for $\mu$, $\lambda$ and $\gamma$ as well as other numerical settings. The values are used for all examples unless stated otherwise. Plane stress is considered for all the 2D cases presented.

Table 5.2: General numerical setting for the proposed method.

| Topology Optimization Parameters | | |
|---|---|---|
| Parameter | Description | Value |
| $\mu$ | Penalization factor | 0.1 |
| $\lambda$ | Lagrangian Multiplier | 0.01 |
| $\gamma$ | Proposed Factor | 0.0 |
| $\sigma_{tol}$ | Stress Tolerance | $1.1\sigma_{lim}$ |
| p | SIMP Penalization | 3 |
| $\beta$ | Weight Penalization | 3 |
| $\mathbf{z}_{ini}$ | Initial Guess | 0.5 |
| $\epsilon$ | Erzats Stiffness | $10^{-4}$ |

A tolerance of 10% over the stress limit is set. Theoretically it is possible to obtain a solution with $\sigma_{tol} = \sigma_{lim}$, however this makes the problem slightly instable, due to numerical reasons, which can degenerate the solution. Furthermore, tolerances as low as 1% were achieved. Regardless, this is of little significance as the result still needs to be interpreted to reach a manufacturable structure. This process of interpretation can severely alter the stress analyses and so a slight relaxation on the stress measure is not so detrimental. What is important is that there is a clear control over this allowable range.

The only numerical parameter from the proposed method that needs to be adjusted for the different mesh sizes is the tolerance for the minimum step for the stagnation condition that halts the optimization. This is probably because the finer meshes also need finer adjustments of the design variables in order to satisfy the stress tolerance. However, it seems to follow the heuristic Eq. (5.1) used in all the examples shown.

$$tol = min\left[c\left(\frac{1}{nElem}\right)^{0.5}, 0.01\right] \tag{5.1}$$

in which "$c$" is a constant that has value $c = 0.2$ for 2D cases and $c = 1.0$ for 3D.

## 5.1 L-Beam

The first problem analyzed is the L-Beam displayed in Fig. 5.1. The L-Beam is considered a benchmark problem for stress-constrained topology optimization because of its sharp corner, which generates a stress singularity. This causes the results of the compliance minimization and stress constraint to be much different. The physical parameters used for this problem are displayed in table 5.3.

Table 5.3: Physical parameter for the L-Beam problem.

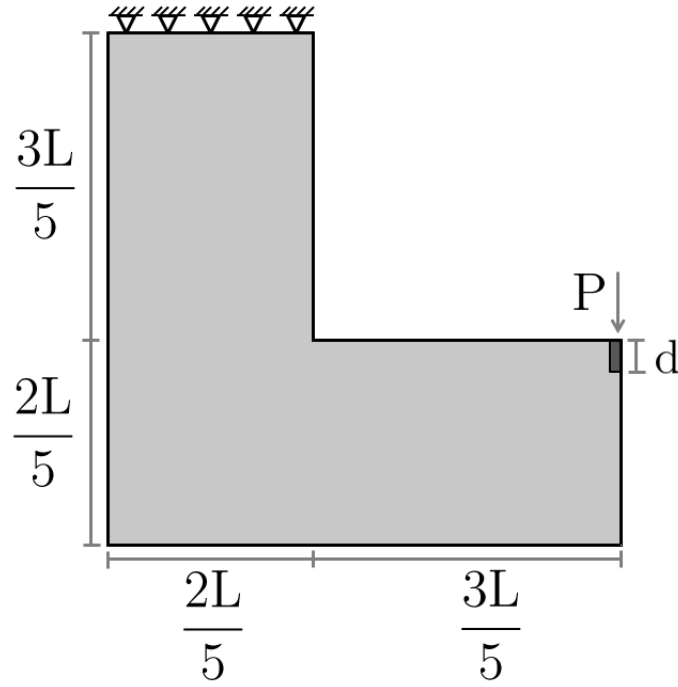| Physical Parameters | | |
|---|---|---|
| Parameter | Description | Value |
| $E_0$ | Young´s Modulus | 1 Pa |
| $\upsilon$ | Poisson Ratio | 0.3 |
| $\sigma_{lim}$ | Stress Limit | 42 Pa |
| L | Characteristic Length | 1 m |
| t | Thickness | 1 m |
| P | Load | 1 N |
| d | Load Distribution | 0.06 m |
| r | Filter Radius | 0.015 m |

Figure 5.1: L-Beam Domain and boundary conditions.

Figure 5.2 shows the results for a polygonal mesh with 16380. The mesh was generated using the `PolyMesher` implementation described in Talischi *et al.* (2012a) and is based on Voronoi diagrams and Loyd iterations.

Figures 5.3, 5.4, 5.5 and 5.6 show the results for regular Q4 element meshes with $6,400$ , $16,384$ , $160,000$ and $1,000,000$ elements and a filter power of $s = 1$, $s = 1$, $s = 2$ and $s = 4$, respectively. The reason behind the different filter powers is explained in Subsection 5.2.1.
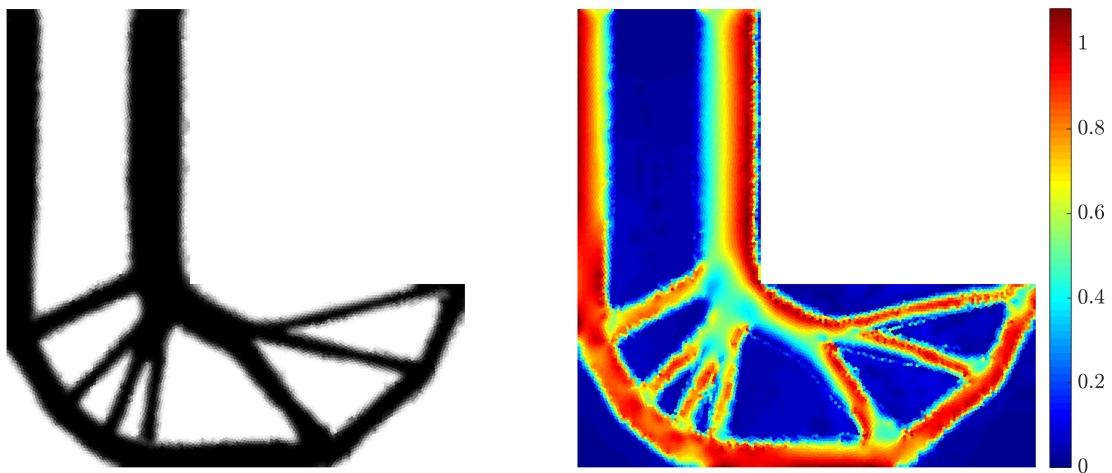


Figure 5.2: Result for a mesh of 16380 polygonal Elements and filter power $s = 1$. The final volume is 44% of the total volume.
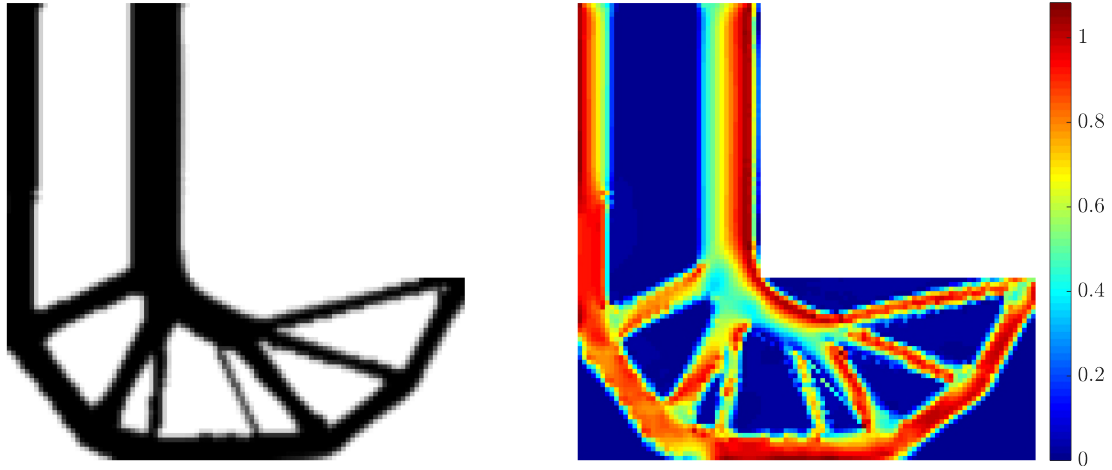
Figure 5.3: Result for a mesh of 6400 Q4 Elements and filter power $s = 1$. The final volume is 42% of the total volume.
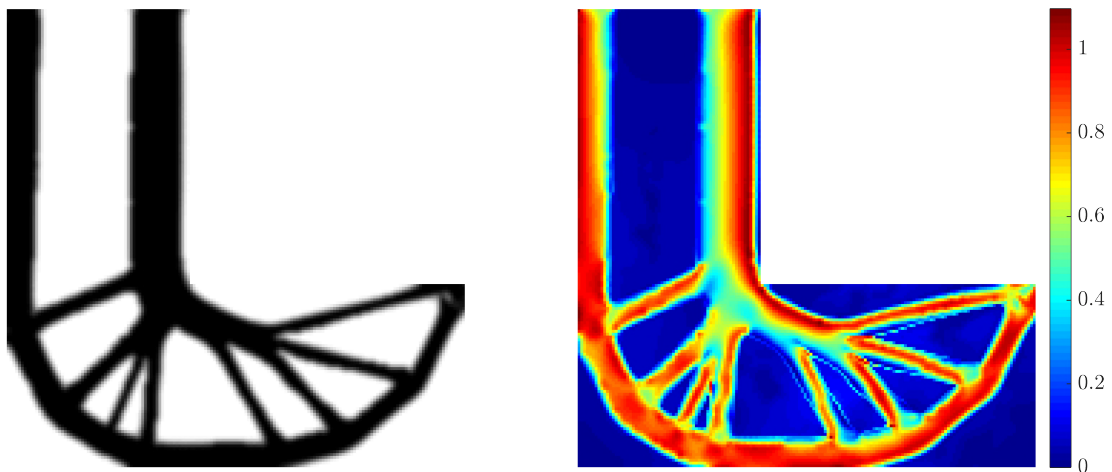


Figure 5.4: Result for a mesh of 16384 Q4 Elements and filter power $s = 1$. The final volume is 43% of the total volume.
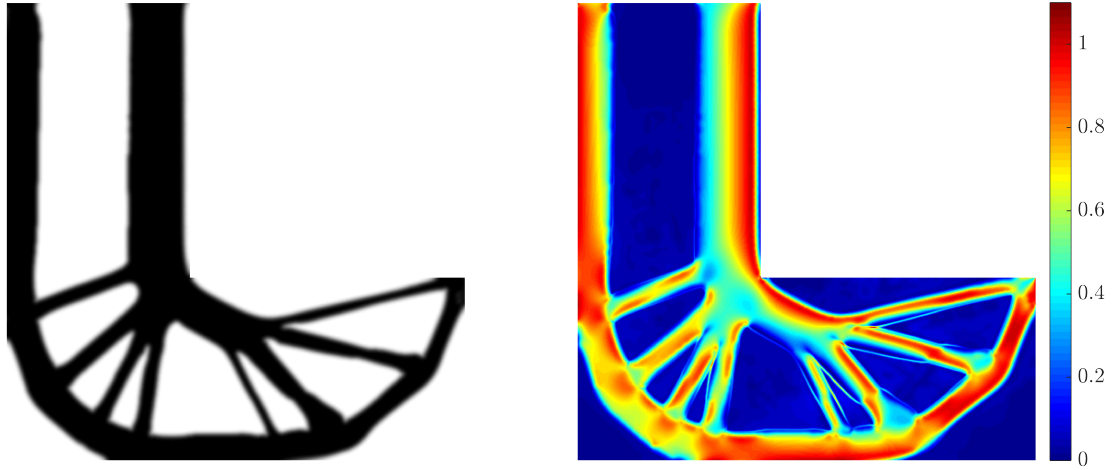
Figure 5.5: Result for a mesh of 160000 Q4 Elements and filter power $s = 2$. The final volume is 45% of the total volume.
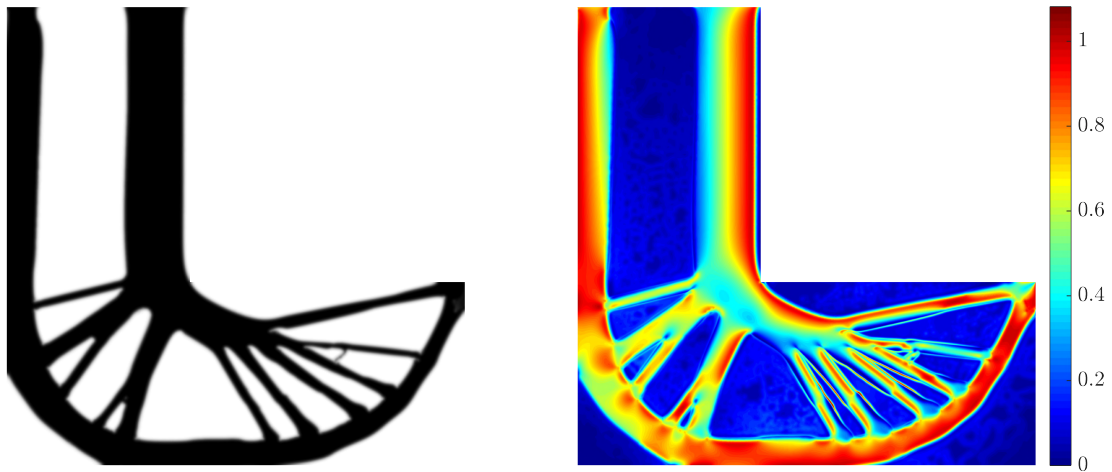


Figure 5.6: Result for a mesh of 1000000 Q4 Elements and filter power $s = 4$. The final volume is 46% of the total volume.

The results shown here clearly avoid the stress concentration of the sharp corner and lead to a more viable structure. Nevertheless, they do not converge with mesh refinement, which might be caused by the need to use different filters. The apparent tendency is an increase in final volume with the number of elements. This is expected since it also enhances the capability of the mesh in capturing the underlying stress.

## 5.2
## Considerations on mesh Refinement

It is desirable that the solution of the topology optimization problem do not depend on the discretization used. Thus, it should remain reasonably

constant under mesh refinement. As stated in Section 2.3, some authors have shown that techniques like Filtering can guarantee mesh convergence for the compliance minimization formulation. However, the stress constraint problem presents other subtle characteristics that hamper this.

One of the issues is that the stress on geometric singularities does not converge to a finite value under mesh refinement. Figure 5.7 shows this phenomenon happening on the L-Beam domain with homogeneous material distribution. Despite having exactly the same properties and boundary conditions, the maximum stress goes from 600Pa, to 900Pa, and then to 1300Pa, simply due to the mesh refinement. As it does so, it becomes increasingly more concentrated at the L-shape corner.
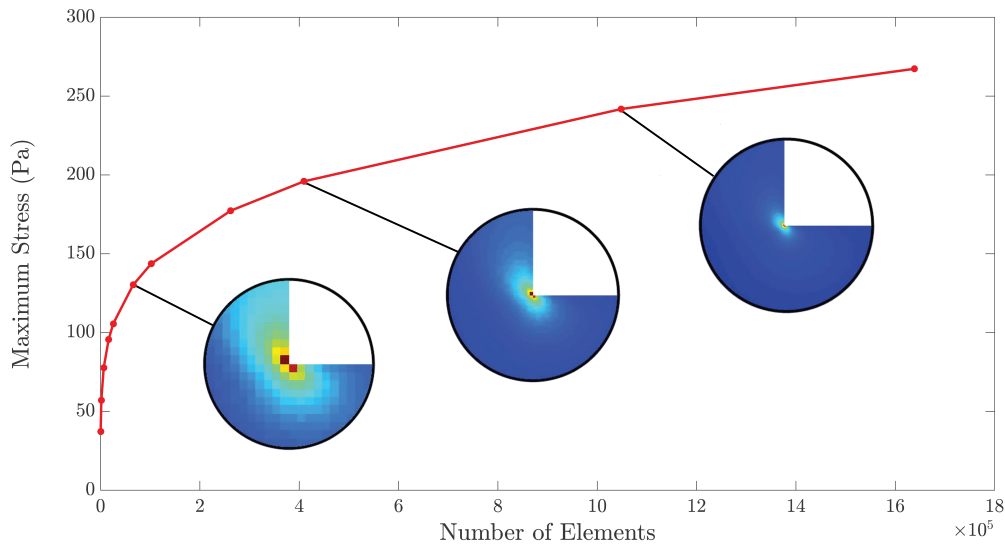


Figure 5.7: Plot of the maximum stress of the L-Beam domain with homogeneous material distribution as a function of the mesh size.

A sharp corner like the one present in the domain would not happen in nature because the stress in such regions is so high that it would deform (at least microscopically) to a rounded form or fracture completely. Nonetheless, the model predicts a stress tending towards infinity. Therefore, this numerical paradigm comes from a lack of consistency with the physical reality.

### 5.2.1
### Mesh Refinement and Filtering

The filter generates regions of intermediate densities around the borders of the structure even if the design variables depict a clear zero or one frontier for the distribution of material. This can be seen in Fig. 5.8 for different sized elements with the same filter radius. Consequently, there is a layer of weaker

material around the surfaces of the design. This in turn, leads to an unexpected complications.
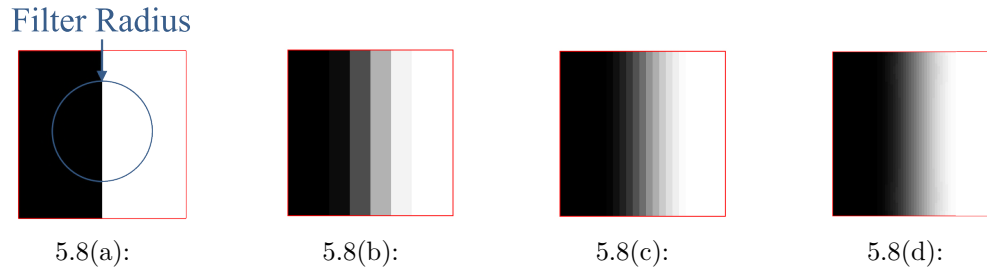
5.8(a):   5.8(b):   5.8(c):   5.8(d):

Figure 5.8: Effect of the filter on the density distribution for meshes of decreasing element size from (a) to (d).

It is well know that the highest stresses of a structure will be located at its surface when there are no body forces at play. Yet, these zones are precisely the ones with the lower stiffness, hence the high stress in these areas is aggravated. This is even more troublesome when dealing with fine meshes that have a large quantity of elements in these regions and are therefore, more capable of capturing the small-scale transition.

The issue can be alleviated using a polynomial filter instead of a linear one. The increase of the exponent "$s$" on Eq. (2.25) diminishes the extension of gray and allows a more abrupt transition between void and material as can be seen in Fig. 5.9. This allows a better representation of the material boundaries. Also, if the exponent is too high, it allows the appearance of small scale artifacts that might be undesirable.



5.9(a): Exponent = 1.0     5.9(b): Exponent = 2.0     5.9(c): Exponent = 4.0
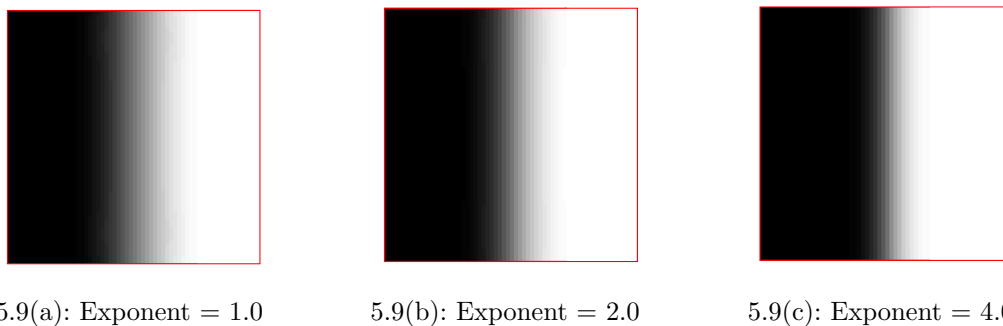
Figure 5.9: Stress map of the L-Beam domain with homogeneous material distribution and a mesh of (a) 16380 Elements (b) 160000 Elements (c) 1000000 Elements.

These effects can be seen in Table 5.4 where the final solution is displayed for various values of "s" and regular meshes of different sizes. The red frames indicate the optimim values for "s" for each mesh size. The evaluation was based solely on visual comparisons, meaning that there are some inherent

biases. However, there is a clear deterioration of the results for the 16,384 element mesh with the increase of "s", at the same time that the results of the larger meshes improved. Moreover, there is a very apparent deterioration of the structure after "s" exceeds a certain value.

Of course this increment also causes the appearance of smaller scale features that are somewhat undesirable. For this reason the value of "s" should be the smallest possible.

## 5.3
## Stress Constraint on Domains Without Geometrical Singularity

The main focus of the stress constrained topology optimization has been the generation of structures in domains with geometrical singularities as seen in the L-Beam case. Many authors have argued that there is a equivalence between the compliance minimization problem and the stress constrained one. In fact Christensen & Klarbring (2008) states that this is so for trusses. However, for topology optimization, it is more complicated.
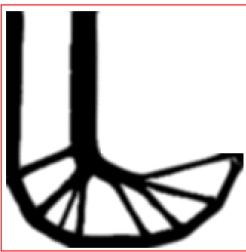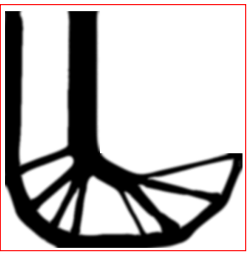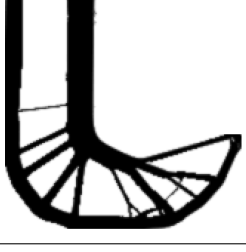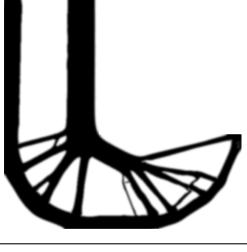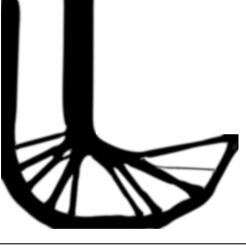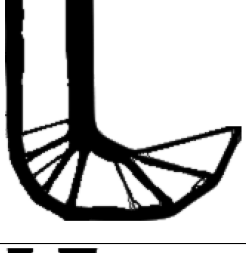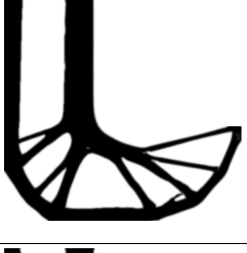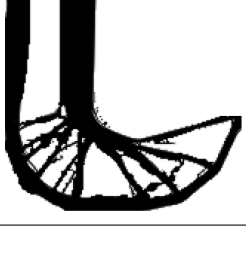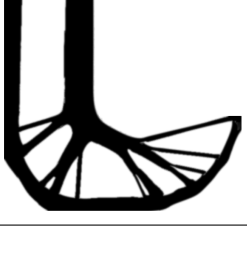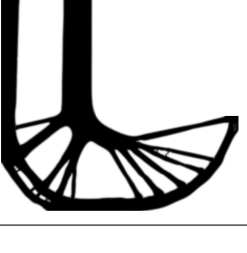
A common practice when dealing with stress constraints is to remove the elements around the supports and loads from the optimization, keeping them fixed throughout the whole process. The reason for keeping them fixed, is that they are regions of stress singularities, because of the boundary conditions, and would disrupt the optimization process. This habit is justified by claiming that this is a artificial phenomenon.

Here it is useful to make a clear distinction between stress concentration and stress singularities. The first one is a real phenomenon characterized by a high gradient in the stress within a small, local region. The second is a numerical consequence of unrealistic modeling and will not converge towards any value under mesh refinement. In stress constrained topology optimization problems, stress concentrations are the subject of interest, while stress singularities should be treated, so as not to disrupt the results.

Although point-applied loads characterize as stress singularities, it is important to understand that there is a real stress concentration around the application of forces. For this reason, the load should always be distributed throughout a large enough region, so as not to violate the stress constraint.

Another point of caution is that the end of a displacement constraint, such as fixed supports, generally behaves as a sharp corner, causing a stress singularity that masks another possible stress concentrati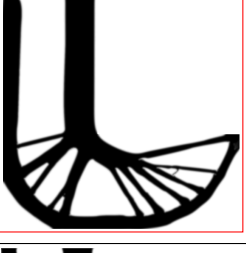on. The reason for this is that an infinitely stiff support is not a realistic model. An alternative is to use a spring like foundation in order to have a better physical representation.

Table 5.4: Influence of the filter power "s" on regular meshes with different number of elements.

| | 16,384 Elements | 160,000 Elements | 1,000,000 Elements |
|---|---|---|---|
| $s = 1$ | | | |
| $s = 2$ | | | |
| $s = 3$ | | | |
| $s = 4$ | | | |
| $s = 5$ | | | |

### 5.3.1
### MBB Beam

The MBB beam is a classical domain for topology optimization and is described in the Fig. 5.10. The load and supports are distributed through a small region to avoid stress singularity, as described in the previous Section.
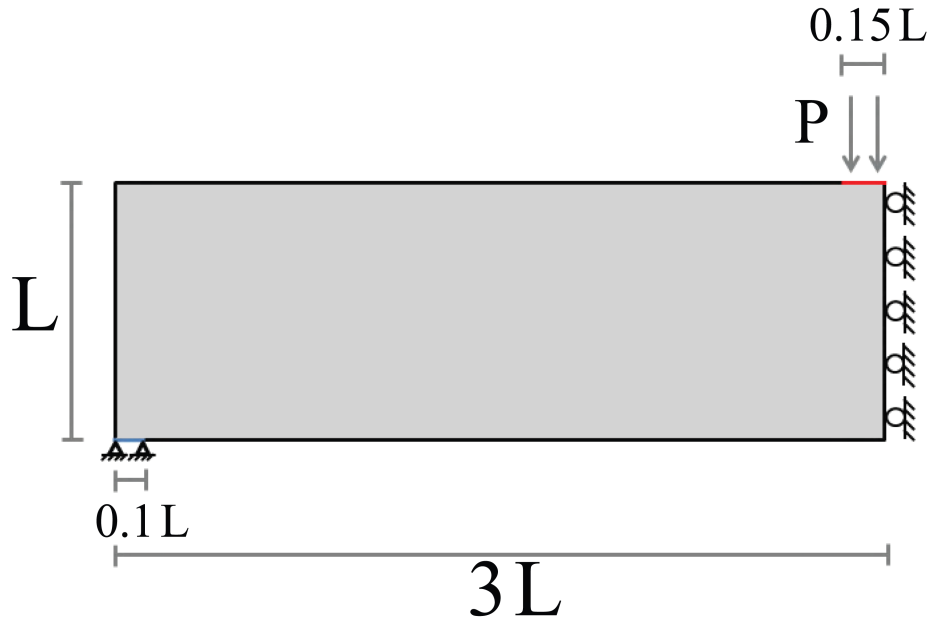


Figure 5.10: MBB beam Domain and boundary conditions.

Table 5.5: Physical parameter for the MBB problem.

| Physical Parameters | | |
|---|---|---|
| Parameter | Description | Value |
| $E_0$ | Young's Modulus | 1 Pa |
| $v$ | Poisson Ratio | 0.3 |
| $\sigma_{lim}$ | Stress Limit | 126 Pa |
| L | Characteristic Length | 1 m |
| t | Thickness | 1 m |
| P | Total Load | 5 N |
| r | Filter Radius | 0.045 m |

Figure 5.11 shows the result excluding the elements around the regions of load and support. Fig. 5.12 shows the result for the compliance minimization version of the problem, using a volume constraint equal to the final volume of the stress-constrained solution. The mesh used has 30,000 regular Q4 elements. The filter power used was $s = 2$. Both are pretty similar, insinuating some level

of equivalence between the two. However the analyses of the stress show that the pair presents stress concentrations much higher than the limit imposed, and that they behave quite differently. On a side note, the stress displayed in Figs. 5.11 and 5.12 was clamped to achieve a better image. The stresses in red are higher than the maximum value on the color map.
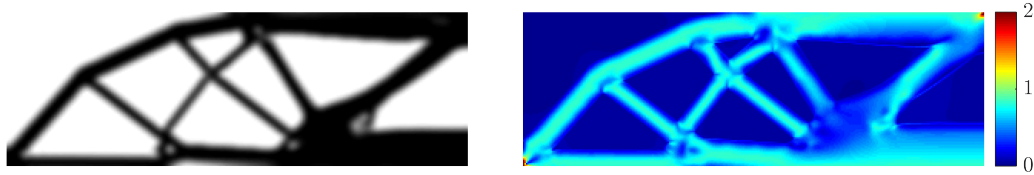


Figure 5.11: MBB beam solution removing the elements around the boundary conditions.
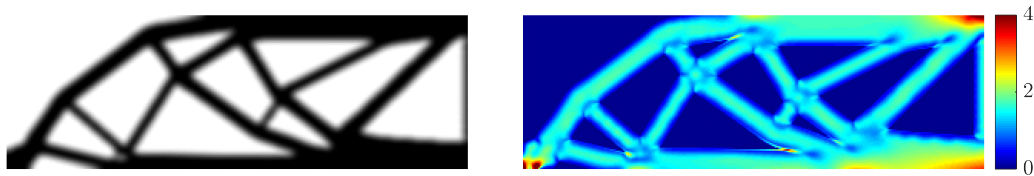


Figure 5.12: MBB beam solution for the minimization of compliance with a volume constraint equal to the Fig. 5.11.

The elements around the boundaries are then included in the optimization in order to see their influence in the final design. The results are displayed in Figs. 5.13 and differ significantly from the previous ones. The most prominent feature is the straight beam that eliminates the stress concentration over the support region.
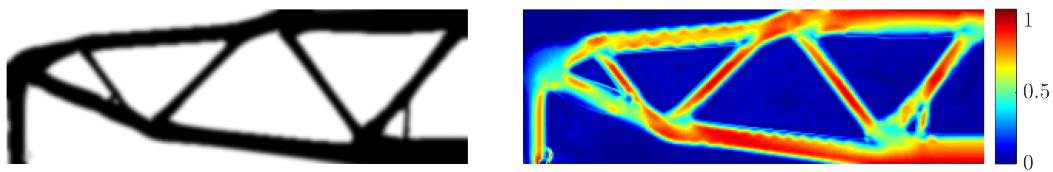


Figure 5.13: MBB beam solution for the stress constrained problem including the boundary elements. The final volume is 35% of the total volume.

The presence of the boundary elements dramatically changes the results and ensures a more realistic model of the structure. The design in Fig. 5.13 is more suitable for a real-life structure while the ones in Figs. 5.11 and 5.12 would probably fracture around the support and load regions.

### 5.3.2
### Wrench Domain

The wrench domain, shown in the Fig. 5.14, displays the versatility of the polygonal mesh as it has circles and lines that are neither parallel nor perpendicular. Two Load cases are applied and ensure symmetry.

Handling multiple load cases in the weight minimization stress constrained problem is much more straight forward than for the compliance minimization problem. In the latter the multiple load cases stem a multi-objective optimization which might be concerning. As for the problem of interest the multiple load cases only adds more constraints that are treated naturally with the Augmented Lagrangian method.
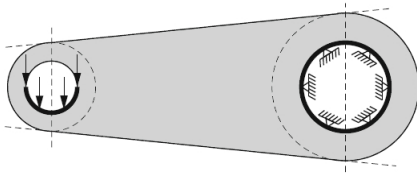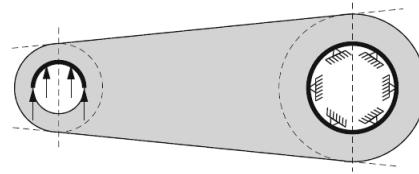


5.14(a): Load Case 1          5.14(b): Load Case 2

Figure 5.14: Wrench domain, Support and Load cases.

Table 5.6: Physical parameter for the Wrench domain problem.

| Physical Parameters | | |
|---|---|---|
| Parameter | Description | Value |
| $E_0$ | Young's Modulus | 1 Pa |
| $\upsilon$ | Poisson Ratio | 0.3 |
| $\sigma_{lim}$ | Stress Limit | 120 Pa |
| L | Characteristic Length | 2.8 m |
| t | Thickness | 1 m |
| P | Total Load | 4.70 N |
| r | Filter Radius | 0.035 m |

The mesh used has $15,000$ polygonal elements. The filter power used was $s = 1$. Despite not having stress singularities the results for the minimization of compliance, Fig. 5.15, and the stress constrained problem, Fig. 5.16, have some significant differences. Both of the final results have the same percentage of volume, however, in the stress constrained case the material is concentrated towards the middle of the tool while the compliance case has more material in the boundaries of the domain which leads to some stress concentration in specific regions.
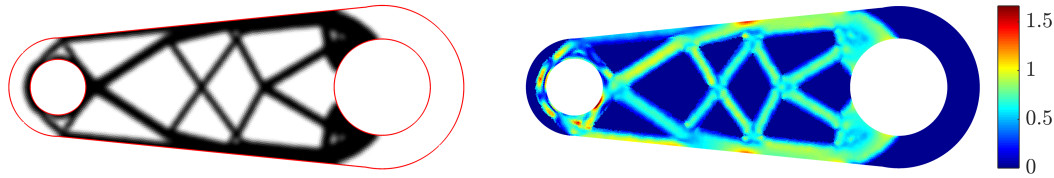
Figure 5.15: Wrench domain solution for the minimization of compliance with 34% of the total volume. The stress displayed is for the first load case.
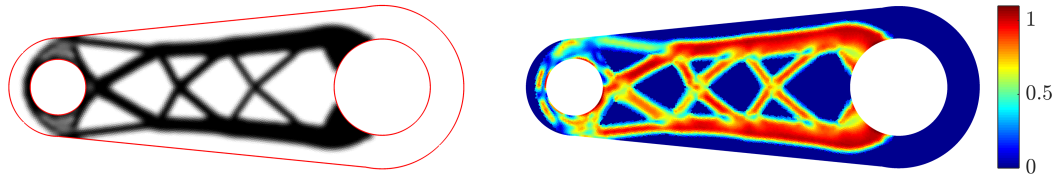


Figure 5.16: Wrench domain solution for the stress constrained problem with 34% of the total volume. The stress displayed is for the first load case.

## 5.4
## 3D Cases

Although 2D cases are useful for various reasons, ultimately one needs to do a 3D model for real-life applications. The main complication of adding an extra dimension is the increase of computational cost, both in memory and processing power. Not only does the size of the mesh have to grown to maintain the numerical precision and structure representation capability, but the cost of solving the equilibrium equations also greatly increases. Nevertheless, the formulation proposed worked well with the same parameter values described in Table 5.2. The only modification is the value of constant "c" in Eq. (5.1).

The 3D L-Beam problem was solved with the properties described in Table 5.7. The generation of a good polygonal mesh in 3D is more complicated. Hence, only regular hexahedral meshes were used.

Table 5.7: Physical parameter for the 3D L-Beam problem.

| Physical Parameters | | |
|---|---|---|
| Parameter | Description | Value |
| $E_0$ | Young's Modulus | 1 Pa |
| $v$ | Poisson Ratio | 0.3 |
| $\sigma_{lim}$ | Stress Limit | 420 Pa |
| L | Characteristic Length | 1 m |
| t | Thickness | 0.1 m |
| P | Load | 1 N |
| d | Load Distribution | 0.06 m |
| r | Filter Radius | 0.015 m |

The results for meshes of 64,000 and 265,000 Elements are displayed in Figs. 5.17 and 5.20, respectively, together with a iso-surface interpretation of the structures in Figs. 5.18 and 5.21. Despite having a lot of common features with the 2D solution, it is interesting to perceive the 3D artifacts that make the design more efficient.
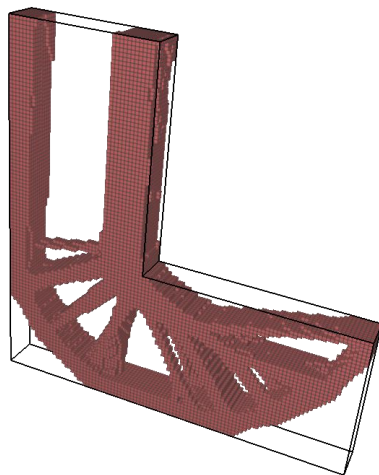


5.17(a): Isometric view          5.17(b): Side view
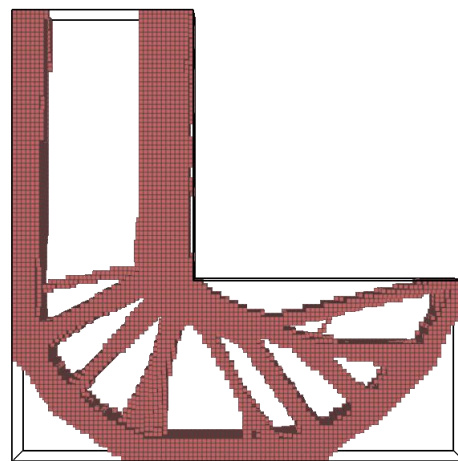
Figure 5.17: Results for the 3D L-Beam problem meshed with 64,000 elements. Displaying the elements with density above 0.5.
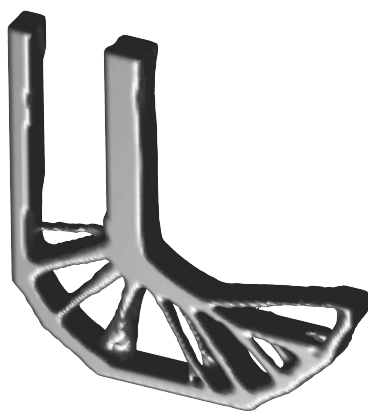


5.18(a): Isometric view          5.18(b): Side view
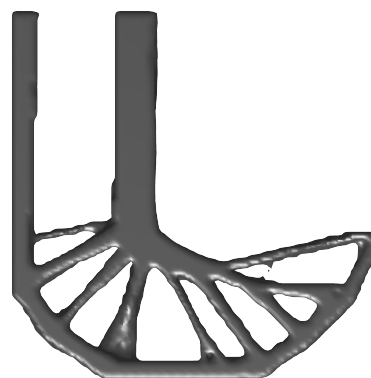
Figure 5.18: Iso-surface of the result displayed in 5.17 with a cutoff value of 0.5.
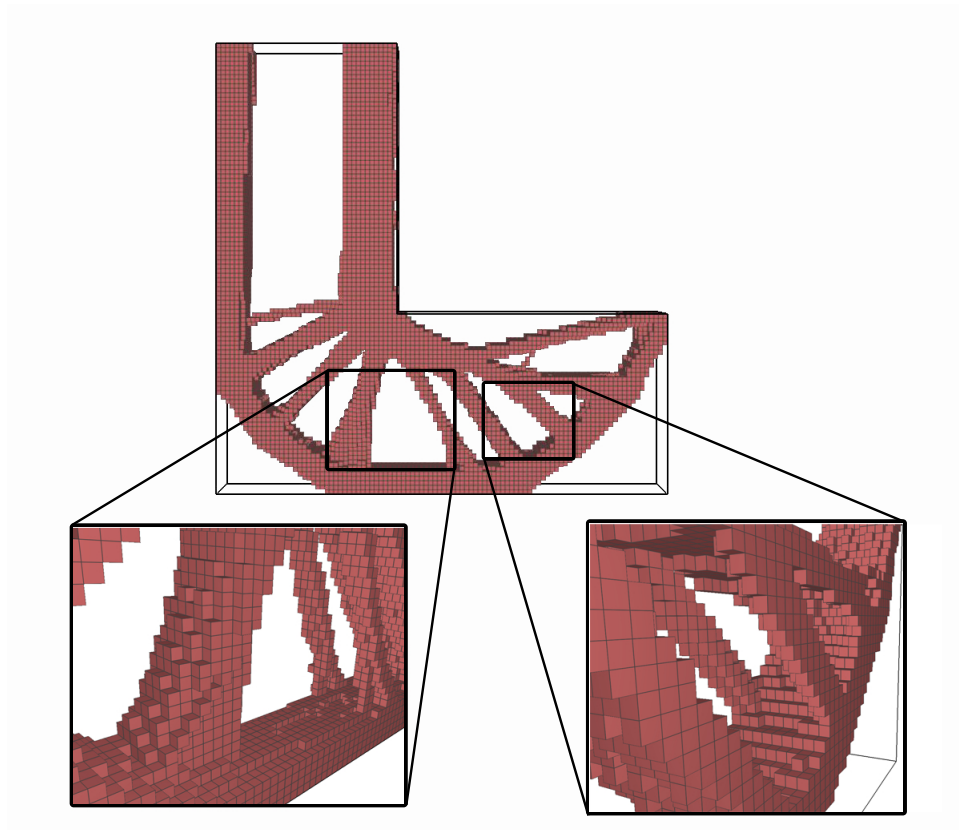
Figure 5.19: 3D details of the result in Fig. 5.17.
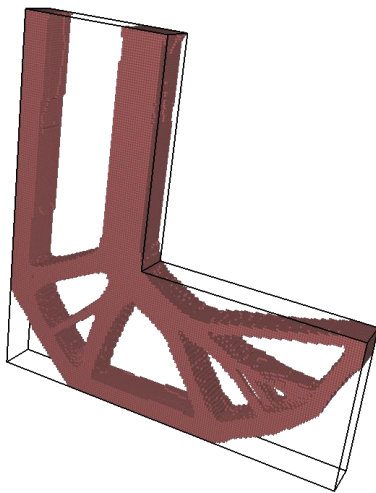


5.20(a): Isometric view
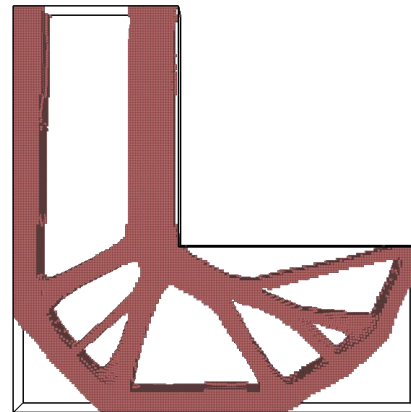
5.20(b): Side view

Figure 5.20: Results for the 3D L-Beam problem meshed with 64,000 elements. Displaying the elements with density above 0.5.
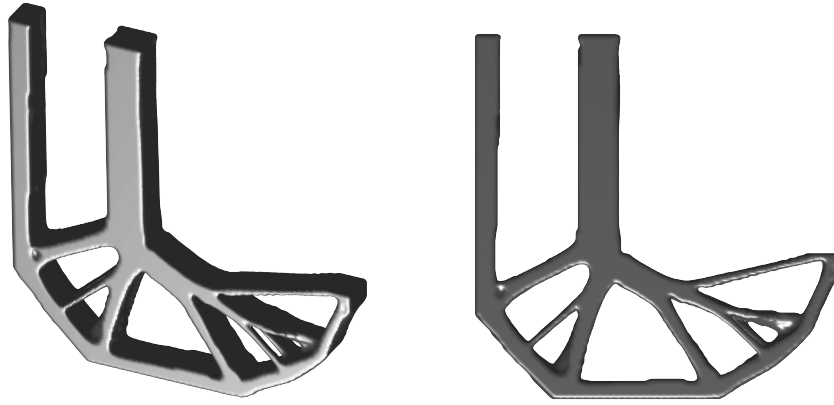
5.21(a): Isometric view          5.21(b): Side view

Figure 5.21: Iso-surface of the result displayed in 5.20 with a cutoff value of 0.5.
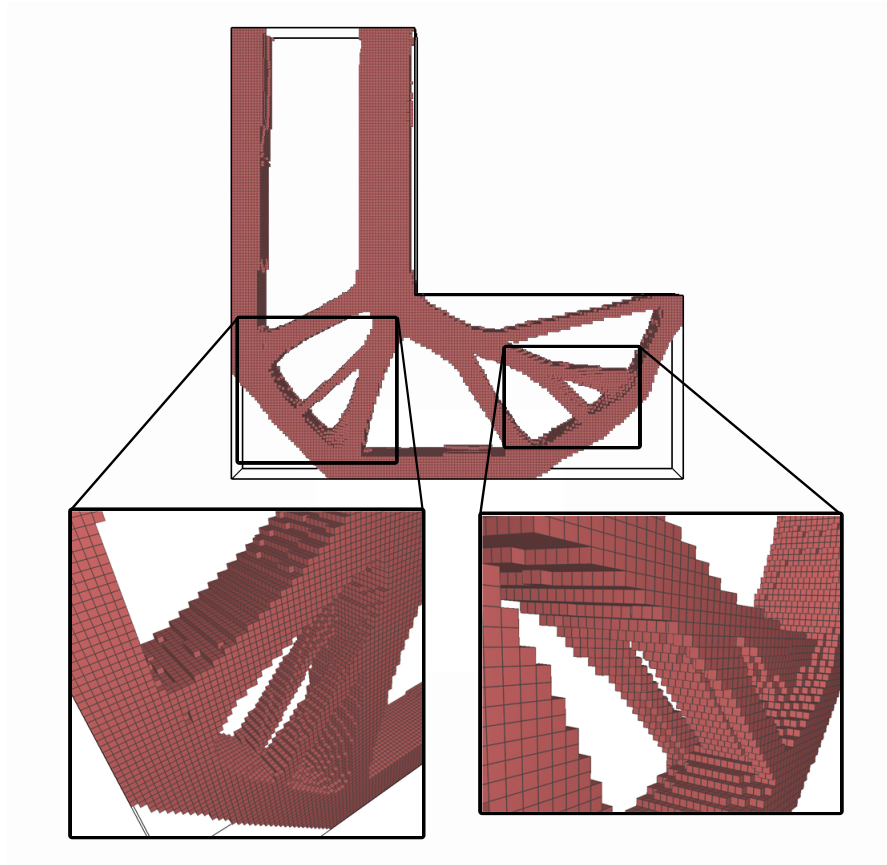


Figure 5.22: 3D details of the result in Fig. 5.20.

## 5.5
## Computational Efficiency

The stress-constrained problem is usually associated with a high computational cost. This Section attests to the efficiency of the proposed method, which requires only a small number of iterations to achieve the solution.

The bottleneck of the implementation is the solution of linear systems both for the equilibrium equations and for sensitivities' calculation.

The assembling of the stiffness matrix is also problematic and requires significant time. This was alleviated using a third-party implementation called MILAMIN, an efficient FEM implementation, for more information see Dabrowski *et al.* (2008).

All of the tests were conducted in two different machines due to memory requirements. The first denominated "Van Dyke" had an Intel Core i5-3330 CPU at 3.00 GHz and 8GB of RAM. The second, called "Ncc", had an i7-4930k CPU at 3.40 GHz and 64GB of RAM. Both were running on a 64-bit operating system.

Table 5.8: Table with the efficiency of the proposed method. The letter R indicates a regular mesh and P a polygonal mesh.

| Results | | | | | | |
|---|---|---|---|---|---|---|
| Problem | Mesh | Machine | Iterations | Time | Volume | Figure |
| 2D L-Beam | 16,380 P | Van Dyke | 153 | 215 s | 44 % | 5.2 |
| 2D L-Beam | 6,400 R | Van Dyke | 144 | 58 s | 43 % | 5.3 |
| 2D L-Beam | 16,380 R | Van Dyke | 145 | 56 s | 42 % | 5.4 |
| 2D L-Beam | 160,000 R | Van Dyke | 362 | 1.14 h | 45 % | 5.5 |
| 2D L-Beam | 1,000,000 R | Ncc | 564 | 8.84 h | 46 % | 5.6 |
| 2D MBB | 30,000 R | Van Dyke | 479 | 656 s | 35 % | 5.13 |
| 3D L-Beam | 64,000 R | Ncc | 150 | 1.5 h | 42 % | 5.17 |
| 3D L-Beam | 265,200 R | Ncc | 243 | 62.8 h | 41 % | 5.20 |

The computational time for the 2D case seems to follow a linear behavior over the number of elements as can be seen in Fig. 5.23. There is not enough results of 3D cases to make a similar claim. The number of iterations necessary also increases with the mesh size, but in a reasonable manner. This is probably because the finer meshes provide a better representation of the stress, making fine adjustments necessary in order to satisfy the increasing number of constraints.
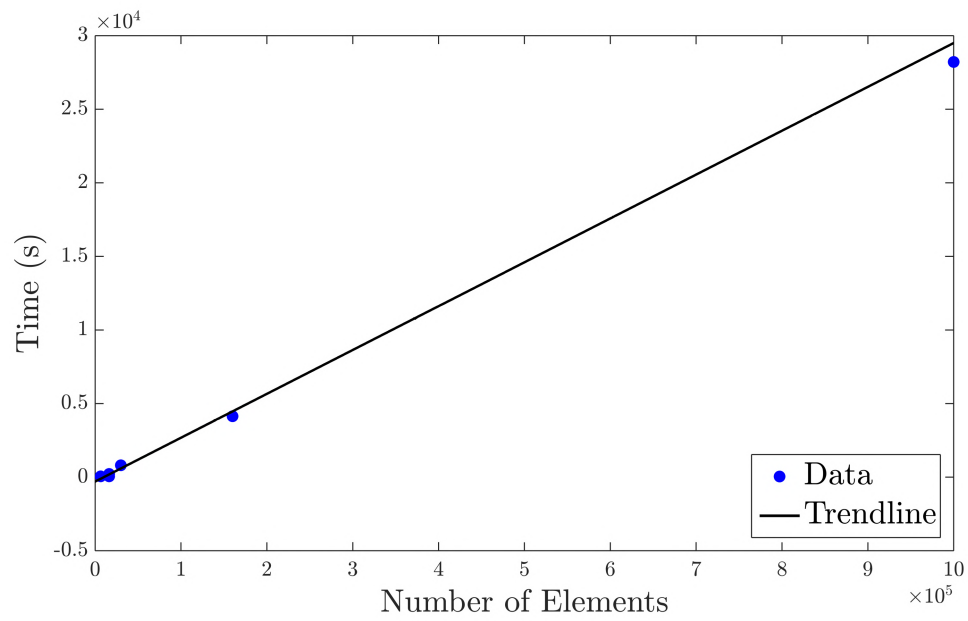
Figure 5.23: Computational time vs. the number of elements in the mesh for 2D cases.

# 6
# Conclusions and Future Work

Topology optimization with stress constraints poses remarkable complications. Hopefully, this text will offer the reader some relevant insights that lead to a better understanding of this problem.

## 6.1
## Conclusions

The two main concerns of the stress constraints, locality and singular optima, were discussed in detail. The high number of constraints, due to the local property of the stress, makes this inherently a large- scale problem. Therefore, efficiency is crucial to the solution. It was shown that the regions where the singular optima is presented were not only degenerated but also disconnected, making the problem remarkably complicated. Nonetheless, these two issues greatly interfere with each other, and anyone proposing a method to solve this problem, must take this in consideration.

The literature review of current techniques, meant to address these concerns brings some serious weaknesses of these techniques to our attention: Clustering techniques have too many numerical parameters to be adjusted for each case and do not scale well to large meshes, in addition to have severely questionable efficiency. The damage approach has weak control over the maximum stress on the result, and its formulation demands the solution of at least 3 linear systems for each iteration. As the size of the mesh increases, or as one handles 3D cases, the computational cost increases, undermining the efficiency. Finally, the traditional Augmented Lagrangian method has difficulty reaching the degenerated regions of the solution space where the optimal points are present. Thus, the final solution becomes more complicated and could require a much higher number of iterations.

The main contribution of this work was the technique proposed in chapter 4, which is based on the Augmented Lagrangian, and does not rely on clustering. The technique uses an adaptive parameter function of a measure of stress that allows the optimizer to reach the singular optima. This proved to be quite efficient, requiring only few iterations. It also scales well, as

it does not need many numerical adjustments, and maintains a reasonable computational time, which increases linearly with the number of elements. This work shows the technique to be easily extendable for 3D cases without any relevant modification.

This new method allows for the solution of large problems that reach one million elements. The larger problems revealed unfamiliar difficulties of the stress constraint problem. In particular, it revealed the paradoxical weak boundary of the material region, caused by the filter and the high stress, as described in Subsection 5.2.1. This was partially handled using a polynomial filter and varying its exponent.

Furthermore, it leads us to question the equivalence between the volume-constrained compliance minimization problem and the stress-constraint volume minimization problem for domains without geometrical singularities. The MBB example displayed drastically different solutions for the two problems when considering the boundary elements as part of the optimization. This, in turn, is essential for a more realistic modeling of the structure.

## 6.2
## Suggestions for Future Works

It is frustrating to leave unanswered questions, but due to limitations on time and energy, there was only so much that the author could realistically do. If the reader found the text relevant, and is interested in the subject, perhaps the following topics will incite your curiosity as they do mine:

– The stress constrained problem generally does not converge to the same solution over mesh refinement. This is a concerning issue that needs to be addressed urgently. It is necessary to find ways to control the minimum length scale of the result without compromising the material boundaries.

– The update of the factor $\gamma$ in the proposed method is completely heuristic and does not depend on the stress value. Finding a consistent adaptive formulation for it is not trivial and may considerably enhance the performance.

– The bottleneck of most topology optimization implementation is the finite element analyses. This is especially costly for 3D cases when it is necessary to have a considerably large mesh for a decent structure representation. The computational time can easily become prohibitive. Each iteration demands the solution of a different, but closely related,

linear system. The challenge is to use the information from the previous solution to solve the new system more quickly (Wang *et al.*, 2007).

– A realistic representation of stress demands a fine mesh which, as stated before, greatly increases computational time. However, the regions of high stress are the ones most crucial for the final result. It might be beneficial to refine the mesh locally in those regions during the optimization, so as to reduce the total number of necessary elements.

– Perform a non-linear Finite Element Anaylisis of the structure and do the topology optmization based on this criteria. Generally speaking the non-linear analysis tends to be more consistent with reality. It would be interesting to compare the results and see the influence that the non-linearity has on the solution.

# A
# Update of the $\gamma$ parameter

The $\gamma$ is a numerical parameter used in the proposed formulation in Chapter 4. Its value must be determined iteratively during the optimization based on the stress measure

The update must satisfy a straightforward condition, it must decrease the value of $\gamma$ if the stress measure is above a certain limit and increase otherwise. For the sake of simplicity this is done through a piecewise linear function based on the value of $\gamma$ and the stress measure. As it can be seen in Eq. (A.1) this translates to four parameter, $a_1$, $a_2$, $b_1$, $b_2$ which need to be adjusted, $\gamma_l$, $\gamma_u$ are lower and upper limits, respectively, for the value of $\gamma$.

$$
\gamma_i^{k+1} = \begin{cases} max(a_1\gamma_i^k + b_1, \gamma_l), & \text{if} \quad \rho_i^{0.5}\dfrac{\sigma_i^{VM}}{\sigma_{lim}} > 1.01 \\[2em] min(a_2\gamma_i^k + b_2, \gamma_u), & otherwise \end{cases} \tag{A.1}
$$

The required condition is quite loose and the set of values that satisfy it is infinity, so additional constrains are set based on reasonable requests:

– If the value of $\gamma$ is at its lowest and the stress measure is below the limit it is desirable that it would have a high increment which we set arbitrarily as 0.75.

– If the value of $\gamma$ is at its highest, $\gamma_u$, and the stress is below the limit we want it to stay the same.

– If the stress is above the limit and the value of $\gamma$ is decreasing we want that it jumps to the lowest value if it is within a certain range from it, choosing it to be $[\gamma_l, \gamma_l + 0.7]$ arbitrarily.

– If the value for $\gamma$ is high and the stress is above the limit it is desirable that the decrement be slow.

The empirical values in these items might leave the reader apprehensive. However their influence on the capability of the method is modest. The

algorithm is quite robust over the way the $\gamma$ update is performed, meaning that this procedure has little influence on its effectiveness. With this extra demands we obtain a system of linear equations:

$$\begin{cases} a_1(\gamma_u) + b_1 = \gamma_u - c \\ a_1(\gamma_l + 0.7) + b_1 = 0 \\ a_2(\gamma_u) + b_2 = \gamma_u \\ a_2(\gamma_l) + b_2 = \gamma_l + 0.75 \end{cases} \tag{A.2}$$

The variable $c$ is a small value to avoid stagnation in the case that $\gamma$ reaches $\gamma_u$. This system gives the solution:

$$a_1 = \frac{10.0\,(c - \gamma_u)}{10.0\,\gamma_l - 10.0\,\gamma_u + 7.0} \qquad b_1 = -\frac{(10.0\,l + 7.0)\,(c - \gamma_u)}{10.0\,\gamma_l - 10.0\,\gamma_u + 7.0} \tag{A.3}$$

$$a_2 = -0.25 \left[ \frac{3.0 + 4.0\,\gamma_l - 4.0\,\gamma_u}{\gamma_l - \gamma_u} \right] \qquad b_2 = 0.75 \left[ \frac{\gamma_u}{\gamma_l - \gamma_u} \right] \tag{A.4}$$

Setting $\gamma_u = 4$, $\gamma_l = 0$ and $c = 0.01$ which are typical values used for the numerical cases in this dissertation the plots on Figs. A.1 and A.2 are obtained and it is possible to clearly that this equations have the desirable behavior.
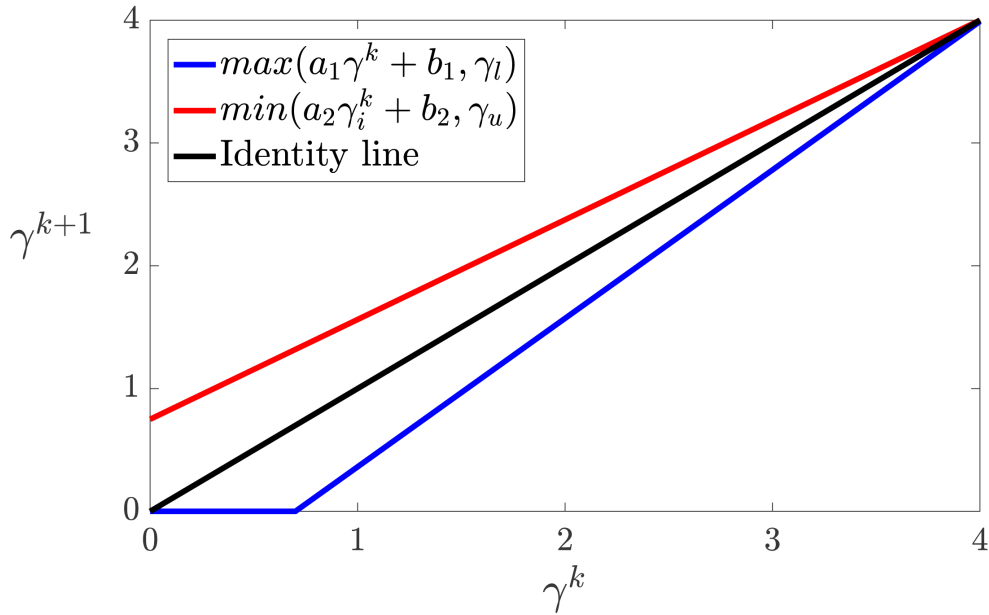


Figure A.1: Plot of the piecewise linear functions describe in Eq. (A.1) with $a_1$, $a_2$, $b_1$, $b_2$ defined as Eqs. (A.3) and (A.4) for $\gamma_u = 4$, $\gamma_l = 0$ and $c = 0.01$.
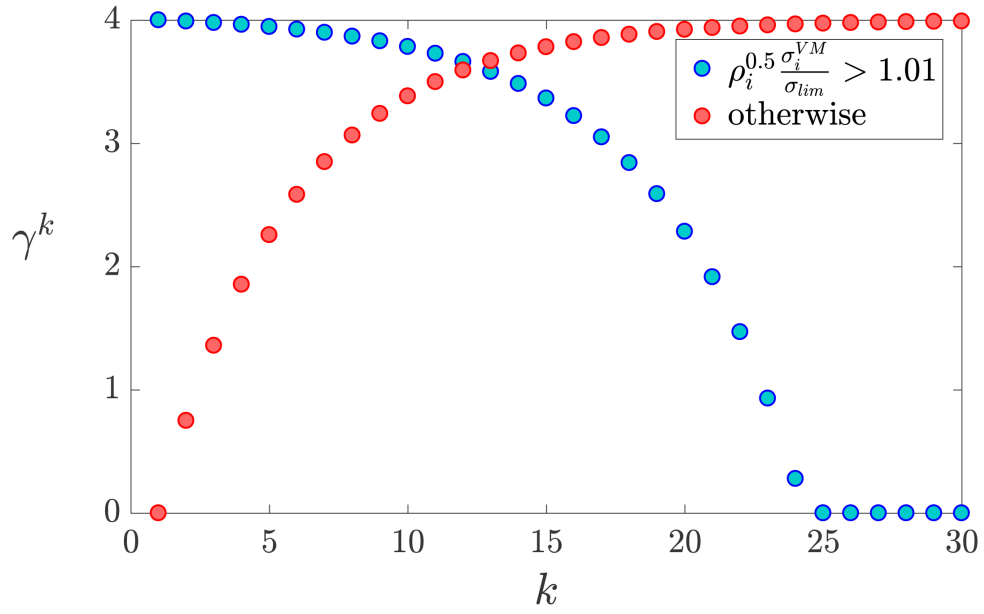
Figure A.2: Values of $\gamma^k$ for successive $k$ iterations in the two cases of stress measure below the limit and above it. The updates follow Eq. (A.1) with $a_1$, $a_2$, $b_1$, $b_2$ defined as Eqs. (A.3) and (A.4) for $\gamma_u = 4$, $\gamma_l = 0$ and $c = 0.01$.

# B
# Hashin-Shtrikman bounds

Hashin-Shtrikman bounds (Hashin & Shtrikman, 1963) impose limits on the possible isotropic material properties for composite two-phase materials as a function of the volume fraction. In this case, the two materials would be $E_0$ and $\epsilon = 0$. Requiring that $E$ satisfies these bounds provides some physical consistency to the formulation, giving the intermediate density regions a reasonable material behavior. For $E_0 = 1$, $\epsilon = 0$ and Poisson ratio $\nu = 1/3$, the bounds are reduced to Eq. (B.1). Figure B.1 shows that the final penalization should be at least $p = 3$ in Eq. (B.2) for this value of $\nu$.

$$E_{upper} = \frac{\rho}{3 - 2\rho} \qquad\qquad E_{lower} = \begin{cases} 0 & \text{if } \rho < 1 \\ 1 & \text{otherwise} \end{cases} \qquad\qquad \text{(B.1)}$$

$$E(\rho) = \epsilon + \rho^p(1 - \epsilon) \qquad\qquad \text{(B.2)}$$
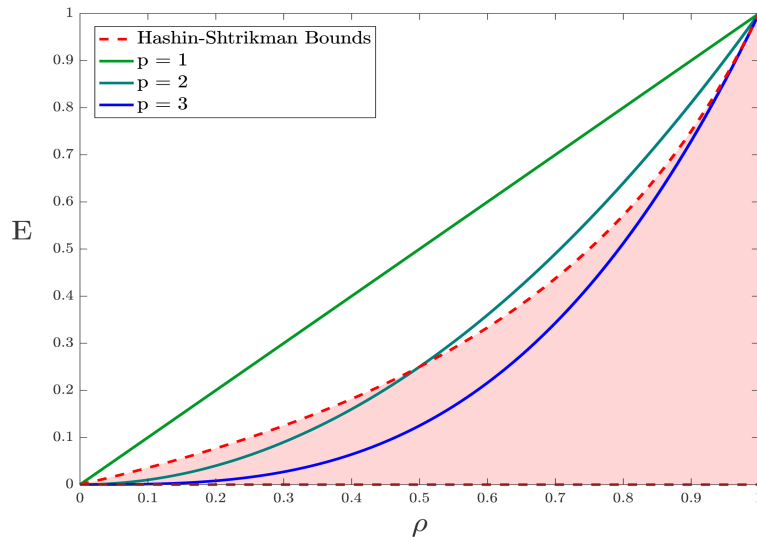


Figure B.1: Hashin-Shtrikman bounds and the material interpolation function (E) with different penalizations.

# C
# Simplified Damage Approach

The Damage approach proposed by Verbart *et al.* (2016a) in his doctorate thesis is yet another formulation to constrain the stress in the design. Although it is based on a physical phenomenon, this technique is simply a mathematical artifice and it is not intended to accurately reproduce the actual damage in the structure. It can be considered a clever way to aggregate the stresses into a global constraint.

The idea behind this approach is that high stresses will damage the structure making it more flexible. A damaged model of the domain is generated where the regions with stress above the limit have a lower stiffness when compared to the undamaged model as is shown in Fig. C.1. The damaged stiffness, $\widetilde{E}$, must then satisfy the conditions in the Eq. (C.1).



$$\Omega_\sigma := \{\ \Omega \mid \sigma > \sigma_{lim}\ \}$$

Figure C.1: Damaged model of the domain.

$$\begin{cases} \widetilde{E}(\mathbf{z}) < E(\mathbf{z}), & \forall \mathbf{z} \in \Omega_\sigma := \{\mathbf{x} \mid \sigma(\mathbf{x}) > \sigma_{lim}\} \\ \widetilde{E}(\mathbf{z}) = E(\mathbf{z}), & \forall \mathbf{z} \in \Omega \setminus \Omega_\sigma \end{cases} \tag{C.1}$$

Verbart *et al.* (2016a) proposes the following relation for $\widetilde{E}$ in agreement with Eq. (C.1):

$$\widetilde{E}(\mathbf{z}, \sigma) = \varepsilon + \beta(\sigma)(E(\mathbf{z}) - \varepsilon) \qquad (C.2)$$

where $\epsilon$ is the Erzats stiffness and $\beta$ is the piecewise function:

$$\beta(\sigma) = \begin{cases} 1, & \text{if } \sigma \leqslant \sigma_{lim} \\ e^{-\alpha(\sigma/\sigma_{lim}-1)^2}, & \text{otherwise} \end{cases} \qquad (C.3)$$

$\alpha$ is a numerical parameter that controls the steepness of $\beta$ as it is seen in Fig. C.2. A helpful interpretation is to think of $\alpha$ as a parameter that controls how much damage is caused by high stresses and $\beta(\sigma)$ as the damage factor.
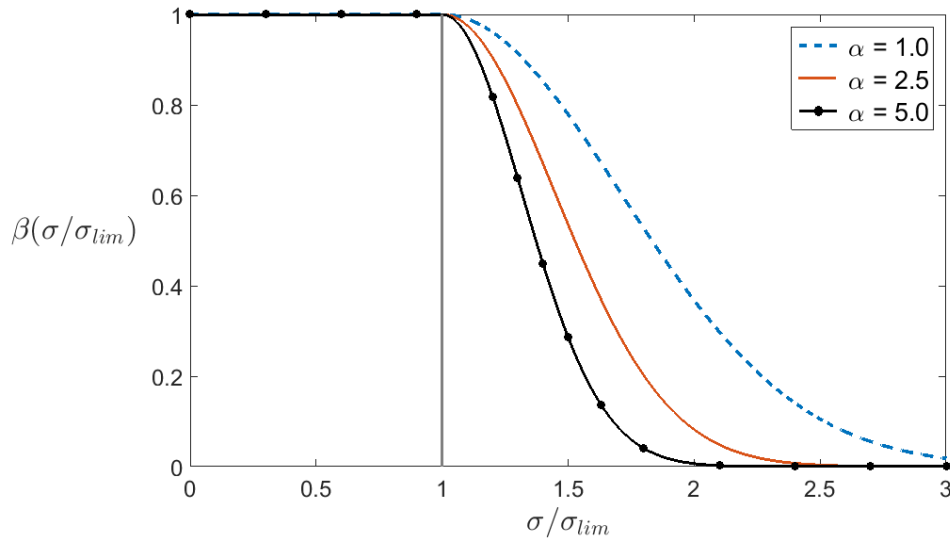
Figure C.2: Influence of the numerical parameter $\alpha$ in the function $\beta$.

$\widetilde{E}$ is then used to compute the global stiffness matrix $\widetilde{K}$ of the damaged model from which it is possible obtain the displacements $\widetilde{U}$ solving Eq. (C.4). All variables marked with a tilde ($\widetilde{\ }$) refer to the damage model.

$$\widetilde{\mathbf{K}}(\widetilde{E})\widetilde{\mathbf{U}} = \mathbf{f} \qquad (C.4)$$

Once $\widetilde{U}$ is obtained, it is possible to calculate the compliance of this model which is always going to be higher than or equal to the compliance of the undamaged one because the damaged regions only make the structure more flexible.

A constraint is then introduced to the problem, in the form of Eq. (C.5), requiring that the two compliances have the same value. This only happens if

the final structure has no damage, meaning that there is no stress above the established limit.

The scheme below summarizes the procedure:
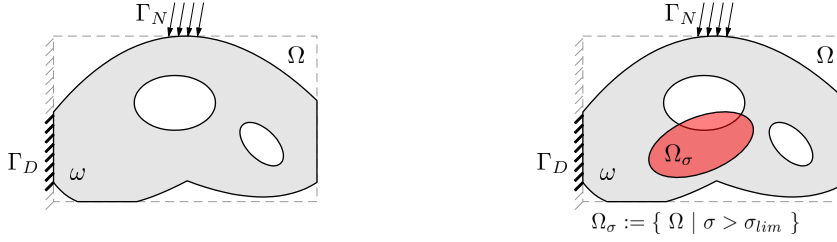


$$E(\mathbf{z}) = \varepsilon + \rho(\mathbf{z})^p(1 - \varepsilon) \qquad \geqslant \qquad \widetilde{E}(\mathbf{z}, \sigma) = \varepsilon + \beta(\sigma)(E(\mathbf{z}) - \varepsilon)$$

$$\mathbf{K}(\mathbf{E})\mathbf{U} = \mathbf{F} \qquad\qquad \widetilde{\mathbf{K}}(\widetilde{\mathbf{E}})\widetilde{\mathbf{U}} = \mathbf{F}$$

$$C = \mathbf{U^T F} = \mathbf{U^T K(E)U} \qquad \leqslant \qquad \widetilde{C} = \widetilde{\mathbf{U}}^{\mathbf{T}}\mathbf{F} = \widetilde{\mathbf{U}}^{\mathbf{T}}\widetilde{\mathbf{K}}(\widetilde{\mathbf{E}})\widetilde{\mathbf{U}}$$

$$g(\mathbf{z}) = \frac{\widetilde{C}}{C} - 1 \leqslant 0 \tag{C.5}$$

This constraint is, however, too strict for traditional optimization algorithms and makes it hard to achieve convergence to a satisfactory result. In order to mediate this, a numerical parameter $\delta > 0$ is introduced and so a relaxed version of the constraint is used:

$$g(\mathbf{z}) = \frac{\widetilde{C}}{C} - 1 - \delta \leqslant 0 \tag{C.6}$$

The equivalent version of the optimization problem using this formulation is described in Eq. (C.7). In the same fashion as the other aggregation techniques, the constraints in each element are replaced by a single constraint which makes the problem substantially more manageable.

Though, there is the additional cost of solving one extra linear system for the equilibrium equation of the damaged model in each iteration. Generally for normal size meshes in 2D examples, the benefits outweigh the costs, because this formulation tends to need fewer iterations to converge. However, one must consider that this might not be the case for large meshes or 3D examples where solving the equilibrium equations dominates the computational cost.

$$\begin{aligned}
\underset{\mathbf{z}}{\text{minimize}} \quad & M(\mathbf{z}) = \sum_{i}^{nElem} \rho_i(\mathbf{z}) v_i \\
\text{subject to} \quad & g(\mathbf{z}) = \frac{\widetilde{C}}{C} - 1 - \delta \leqslant 0 \\
& 0 \leqslant z_i \leqslant 1 \\
\text{with} \quad & \mathbf{K}(\mathbf{z})\mathbf{U} = \mathbf{F} \\
& \widetilde{\mathbf{K}}(\mathbf{z})\widetilde{\mathbf{U}} = \mathbf{F}
\end{aligned} \tag{C.7}$$

## C.1
## Influence of $\alpha$ and $\delta$

As with most formulations, the damage approach is dependent on the adjustment of some numerical parameter, which is mostly done empirically. Its values can greatly influence the final result, making the proper choice of this parameters crucial to the application of this method.

The $\delta$ relaxation of the constraint has severe theoretical consequences, as it allows for some extent of damage in the design. For instance, the stress can be higher than the limit in some regions of the final structure. The amount of damage allowed is also dependent of the value of $\alpha$. The choice of $\alpha$ and $\delta$ is then intertwined.

A high value of $\alpha$ and a low value of $\delta$ diminish the allowable damage but it is important to emphasize that this decreases the well posedness of the problem. The convergence is then impaired leading to unsatisfactory results. In the end, one must make a reasonable balance between accuracy and efficiency.

## C.2
## Damage Approach

The Damage approach naturally handles the singular optima in a theoretically elegant fashion. Although the stresses in void regions are high, they don't influence the optimization because damage in regions without material is irrelevant as they don't contribute to the overall compliance of the structure.

The damage approach acts as a relaxation on its own and the singular optimas are included as feasible points, however they can still be disconnected from the main feasible region.

The numerical parameter $\alpha$ and $\delta$ control the level of relaxation as displayed in the Figs. C.3 and C.4. For $\delta = 0$ the constraint resembles the original ones very closely and still includes the singular optima. Nonetheless these optimum points cannot be reached through traditional optimization.

Increasing the value of $\alpha$ has a similar effect. Lowering the value of $\alpha$ and increasing the value of $\delta$ allows for those points to be reached. But this also changes the global optimum of the problem, allowing solutions with a higher stress than is admissible.
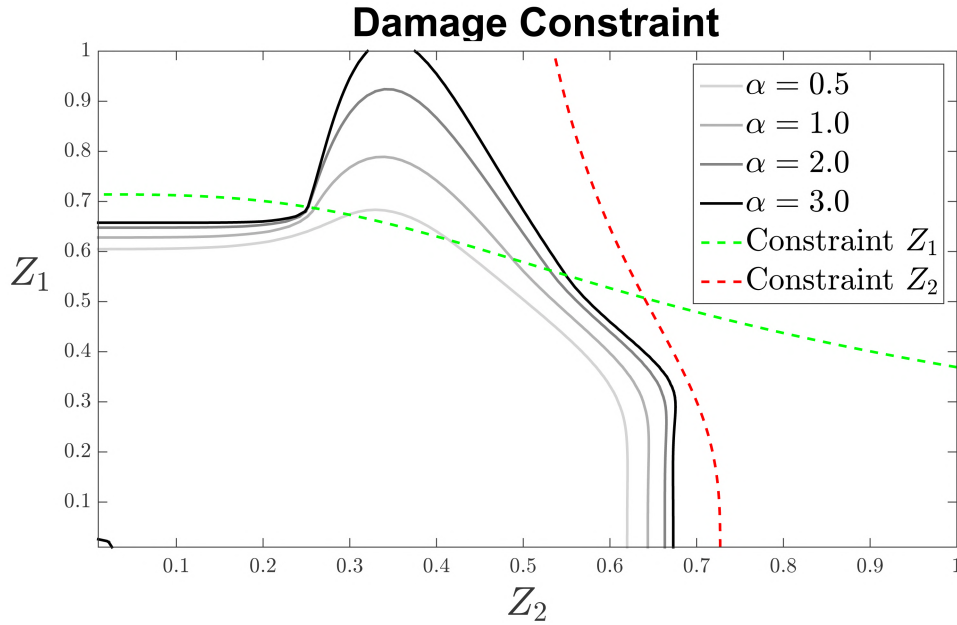
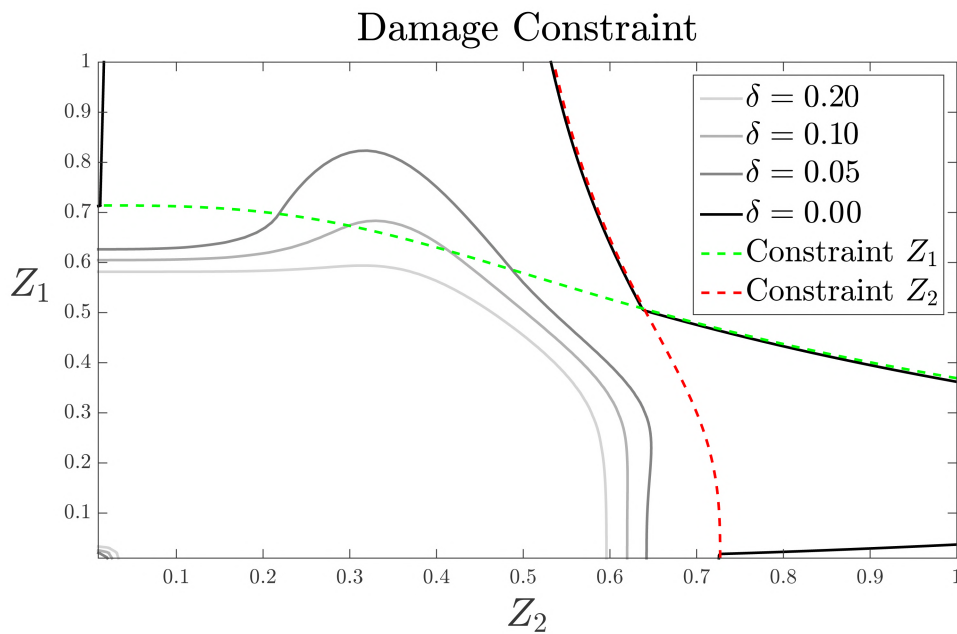Figure C.3: Variation of the damage constraint with the value of $\alpha$ with a fixed $\delta = 0.1$.



Figure C.4: Variation of the damage constraint with the value of $\delta$ with a fixed $\alpha = 0.5$.

# Bibliography

Amstutz, Samuel, & Novotny, Antonio A. 2010. **Topological optimization of structures subject to Von Mises stress constraints**. *Structural and Multidisciplinary Optimization*, **41**(3), 407–420.

Bathe, Klaus-Jürgen. 1996. ***Finite element procedures***. Englewood Cliffs, N.J. Prentice Hall. Éd. rev. de: Finite element procedures in engineering analysis. 1982.

Bendsøe, M. P. 1989. **Optimal shape design as a material distribution problem**. *Structural optimization*, **1**(4), 193–202.

Bertsekas, D.P. 1996. ***Constrained Optimization and Lagrange Multiplier Methods***. Athena scientific series in optimization and neural computation. Athena Scientific.

Bourdin, Blaise. 2001. **Filters in topology optimization**. *International Journal for Numerical Methods in Engineering*, **50**(9), 2143–2158.

Bruggi, Matteo. 2008. **On an alternative approach to stress constraints relaxation in topology optimization**. *Structural and Multidisciplinary Optimization*, **36**(2), 125–141.

Bruggi, Matteo, & Duysinx, Pierre. 2012. **Topology optimization for minimum weight with compliance and stress constraints**. *Structural and Multidisciplinary Optimization*, **46**(3), 369–384.

Cheng, G. D., & Guo, X. 1997. $\epsilon$-**relaxed approach in structural topology optimization**. *Structural optimization*, **13**(4), 258–266.

Christensen, P.W., & Klarbring, A. 2008. ***An Introduction to Structural Optimization***. Solid Mechanics and Its Applications. Springer Netherlands.

Dabrowski, M., Krotkiewski, M., & Schmid, D. W. 2008. **MILAMIN: MATLAB-based finite element method solver for large problems**. *Geochemistry, Geophysics, Geosystems*, **9**(4), n/a–n/a. Q04030.

Duysinx, P., & Bendsøe, M. P. 1998. **Topology optimization of continuum structures with local stress constraints**. *International Journal for Numerical Methods in Engineering*, **43**(8), 1453–1478.

Duysinx, Pierre, & Sigmund, Ole. 1998. **New Developments in Handling Stress Constraints in Optimal Material Distributions**. *Proceedings of 7th AIAA/USAF/NASA/ISSMO symposium on Multidisciplinary Design Optimization*, Paper 98–4906.

Emmendoerfer Jr., Hélio, & Fancello, Eduardo Alberto. 2014. ***A level set approach for topology optimization with local stress constraints***. Ph.D. thesis, Department of Mechanical Engineering, Federal University of Santa Catarina.

Guo, Xu, Zhang, Wei Sheng, Wang, Michael Yu, & Wei, Peng. 2011. **Stress-related topology optimization via level set approach**. *Computer Methods in Applied Mechanics and Engineering*, **200**(47–48), 3439 – 3452.

Haber, R. B., Jog, C. S., & Bendsøe, M. P. 1996. **A new approach to variable-topology shape design using a constraint on perimeter**. *Structural optimization*, **11**(1), 1–12.

Hashin, Z., & Shtrikman, S. 1963. **A variational approach to the theory of the elastic behaviour of multiphase materials**. *Journal of the Mechanics and Physics of Solids*, **11**(2), 127 – 140.

Hoheisel, Tim et al. 2009. ***Mathematical programs with vanishing constraints***. Ph.D. thesis.

Holmberg, Erik, Torstenfelt, Bo, & Klarbring, Anders. 2013a. **Global and clustered approaches for stress constrained topology optimization and deactivation of design variables**. *10th World Congress on Structural and Multidisciplinary Optimization*.

Holmberg, Erik, Torstenfelt, Bo, & Klarbring, Anders. 2013b. **Stress constrained topology optimization**. *Structural and Multidisciplinary Optimization*, **48**(1), 33–47.

Kirsch, U. 1990. **On singular topologies in optimum structural design**. *Structural optimization*, **2**(3), 133–142.

Kirsch, Uri. 1989. **Optimal topologies of truss structures**. *Computer Methods in Applied Mechanics and Engineering*, **72**(1), 15 – 28.

Kiyono, C.Y., Vatanabe, S.L., Silva, E.C.N., & Reddy, J.N. 2016. **A new multi-p-norm formulation approach for stress-based topology optimization design**. *Composite Structures*, **156**, 10 – 19. 70th Anniversary of Professor J. N. Reddy.

Le, Chau, Norato, Julian, Bruns, Tyler, Ha, Christopher, & Tortorelli, Daniel. 2009. **Stress-based topology optimization for continua**. *Structural and Multidisciplinary Optimization*, **41**(4), 605–620.

Nguyen, Tam H., Paulino, Glaucio H., Song, Junho, & Le, Chau H. 2010. **A computational paradigm for multiresolution topology optimization (MTOP)**. *Structural and Multidisciplinary Optimization*, **41**(4), 525–539.

Nocedal, J., & Wright, S. J. 2006. ***Numerical Optimization***. 2nd edn. New York: Springer.

París, J., Navarrina, F., Colominas, I., & Casteleiro, M. 2010. **Block aggregation of stress constraints in topology optimization of structures**. *Advances in Engineering Software*, **41**(3), 433–441.

Pereira, Anderson, Talischi, Cameron, Paulino, Glaucio H., M. Menezes, Ivan F., & Carvalho, Marcio S. 2016. **Fluid flow topology optimization in `PolyTop`: stability and computational implementation**. *Structural and Multidisciplinary Optimization*, 1–20.

Pereira, J.T., Fancello, E.A., & Barcellos, C.S. 2004. **Topology optimization of continuum structures with material failure constraints**. *Structural and Multidisciplinary Optimization*, **26**(1), 50–66.

Petersson, Joakim, & Sigmund, Ole. 1998. **Slope constrained topology optimization**. *International Journal for Numerical Methods in Engineering*, **41**(8), 1417–1434.

Rozvany, G.I.N. 2001. **On design-dependent constraints and singular topologies**. *Structural and Multidisciplinary Optimization*, **21**(2), 164–172.

Stolpe, M., & Svanberg, K. 2001. **On the trajectories of the epsilon-relaxation approach for stress-constrained truss topology optimization**. *Structural and Multidisciplinary Optimization*, **21**(2), 140–151.

Svanberg, Krister. 1987. **The method of moving asymptotes—a new method for structural optimization**. *International Journal for Numerical Methods in Engineering*, **24**(2), 359–373.

Sved, G., & Ginos, Z. 1968. **Structural optimization under multiple loading**. *International Journal of Mechanical Sciences*, **10**.

Takezawa, Akihiro, Nishiwaki, Shinji, & Kitamura, Mitsuru. 2010. **Shape and topology optimization based on the phase field method and sensitivity analysis**. *Journal of Computational Physics*, **229**(7), 2697 – 2718.

Talischi, Cameron, Paulino, Glaucio H., Pereira, Anderson, & Menezes, Ivan F. M. 2010. **Polygonal finite elements for topology optimization: A unifying paradigm**. *International Journal for Numerical Methods in Engineering*, **82**(6), 671–698.

Talischi, Cameron, Paulino, Glaucio H., Pereira, Anderson, & Menezes, Ivan F. 2012a. `PolyMesher`**: A general-purpose mesh generator for polygonal elements written in Matlab**. *Struct. Multidiscip. Optim.*, **45**(3), 309–328.

Talischi, Cameron, Paulino, Glaucio H., Pereira, Anderson, & Menezes, Ivan F. 2012b. `PolyTop`**: A Matlab implementation of a general topology optimization framework using unstructured polygonal finite element meshes**. *Struct. Multidiscip. Optim.*, **45**(3).

van Dijk, N. P., Maute, K., Langelaar, M., & van Keulen, F. 2013. **Level-set methods for structural topology optimization: a review**. *Structural and Multidisciplinary Optimization*, **48**(3), 437–472.

Verbart, Alexander, Langelaar, Matthijs, & Keulen, Fred van. 2016a. **Damage approach: A new method for topology optimization with local stress constraints**. *Structural and Multidisciplinary Optimization*, **53**(5), 1081–1098.

Verbart, Alexander, Langelaar, Matthijs, & Keulen, Fred van. 2016b. **A unified aggregation and relaxation approach for stress-constrained topology optimization**. *Structural and Multidisciplinary Optimization*, 1–17.

Wang, Shun, de Sturler, Eric, & Paulino, Glaucio H. 2007. **Large-scale topology optimization using preconditioned Krylov subspace methods with recycling**. *International Journal for Numerical Methods in Engineering*, **69**(12), 2441–2468.

Yang, R. J., & Chen, C. J. 1996. **Stress-based topology optimization**. *Structural optimization*, **12**(2), 98–105.